ESTIMATING SETTLEMENTS AND CAPACITIES OF PILED FOUNDATIONS WITH NON-LINEAR FINITE ELEMENT ANALYSES

by

DERRICK YAT BOND PANG

B.S. Civil and Environmental Engineering
University of California, Berkeley, 1997

Submitted to the
Department of Civil and Environmental Engineering in Partial Fulfillment of the
Requirements for the Degree of

MASTER OF ENGINEERING
in Civil and Environmental Engineering

at the

MASSACHUSETTS INSTITUTE OF TECHNOLOGY
June, 1998

©1998 Derrick Yat Bond Pang
All rights reserved

The author hereby grants to MIT permission to reproduce and to distribute publicly paper and electronic copies of this thesis document in whole and in part.

Signature of Author ....
Department of Civil and Environmental Engineering
May, 1998

Certified by ....
Andrew J. Whittle
Associate Professor of Civil and Environmental Engineering
Thesis Supervisor

Accepted by ....
Professor Joseph Sussman
Chairman, Departmental Committee on Graduate Studies

JUN 02 1998

LIBRARIES

ESTIMATING SETTLEMENTS AND CAPACITIES OF PILED FOUNDATIONS WITH NON-LINEAR FINITE ELEMENT ANALYSES

by
DERRICK YAT BOND PANG

Submitted to the Department of Civil and Environmental Engineering on May 22, 1998 in partial fulfillment of the requirements for the degree of Master of Engineering in Civil and Environmental Engineering.

ABSTRACT

Conventional foundation settlement calculation methods are performed assuming elastic soil behavior. However, soil exhibits non-linear stress-strain properties at relatively small shear strains. Therefore, large factors of safety are needed, such that the designed capacity is within the elastic zone of the soil, leading to inefficient designs and increased costs.

This thesis explores the use of non-linear finite element analyses, to predict the load settlement response of piled foundations. The accuracy of the non-linear analyses depends in large part, on the ability of soil models to describe the actual soil behavior. In order to check the validity, two cases studies are analyzed with finite element analysis using an elastic-perfectly plastic model to represent free draining, sands and silts, and Modified Cam Clay to describe soft clay behavior. In the first study, finite element analysis predicts the capacities and settlement responses of instrumented single piles tested at Northwestern University in 1989. The second case study considers the rate and extent of consolidation settlement of a heavy storage building supported by a piled raft in Oslo, Norway. Both FE and conventional analyses are performed, and the results are compared and evaluated with measured capacities and settlements.

Results show that the finite element analysis predict consistent and reliable results. In the first case, the predicted capacities of driven piles are within one percent of the measured capacity. For the second case, the predicted rate and extent of settlement are also in good agreement with measured data. However, FE predictions for the stiffness and capacity of drilled shafts are much too conservative. Results can be improved with more accurate soil parameters for the models, better understanding of the installation effects of piles, and more advanced soil models.

Thesis Supervisor: Andrew J. Whittle
Title: Associate Professor of Civil and Environmental Engineering

Acknowledgments

I would like to thank Professor Whittle for spending hours and hours of time helping me in my analyses and getting me through this painful process. Although I didn't get much sleep in April and May, I have learned a great deal from the thesis and you; and without you, this would not have been possible. Thank You.

I would also like to thank Professor Ladd for being such a great professor and teaching me a whole lot more than just geotechnical engineering.

For my parents, thank you for always being there even though you are many miles (I don't know how many) away.

To my brother and sisters, thank you for helping me out whenever I needed it, and please continue!

To my friends, thanks for keeping my company and take care.

Table of Contents

List of Figures

List of Tables

Chapter 1 Introduction

Conventional pile foundation designs focuses mainly on satisfying the ultimate capacity criteria, while settlement calculations are performed assuming elastic soil behavior. Neither methods account for the progressive mobilization of the shaft resistance as the load level increases, nor the settlements associated with consolidation in low permeability clay soils. Design loads based on ultimate capacity are adequate when settlements are not the limiting criterion. However, there are many applications where piles are used to minimize settlements of raft foundations (e.g. Randolph, 1994). In these cases, accurate predictions of pile-soil interactions become important in designs, in order to optimize the number and sizes of piles. In the case of piled rafts, the load is at least partially supported by the raft and; therefore, bearing capacity is no longer the parameter controlling the number of piles required. In order to reduce the costs of pile foundations, a reliable analysis that can predict the complete load-deformation response of piles is needed. This will lead to the development of settlement based design method, that can determine the number of piles required to satisfy the settlement criteria. The settlement-based approach can reduce the number of piles required and ultimately the cost of the foundation system.

Current settlement analyses are based on solutions that assume linear stress-strain properties of the soil. However, soils behave non-linearly, and more advanced effective stress soil models are needed for such analyses. Therefore, this thesis will evaluate the settlement results of piles and pile group systems analyzed with non-linear soil models. Models are created and analyzed using a finite element analysis program. Results from the finite element models are also compared with two case studies. In chapter 2, a general description of the finite element program and the background information about the soil models used in the analysis are given. Chapter 3, describes finite element analyses of the pile loading tests performed at the National Geotechnical Experiment Site in Northwestern University (Finno, R.J. 1989). Chapter 4 describes further analyses of a piled raft foundation for a storage building in Oslo, Norway (Anderson, K.H., & Clausen. 1974). The summary and conclusions based on these two case studies are presented in chapter 5.

Chapter 2 Background and Development of Finite Element Model

2.1 Background of Finite Element

The finite element method (FE) provides a powerful numerical framework for analyzing pile foundation systems. In contrast to current design methods, which make major simplifying assumptions for representing pile-soil interactions (e.g. using equivalent pier representation of pile groups, Fleming et al. 1992). The finite element method is capable of discretizing the pile (or pile group) soil profile and properties (including deformation and flow) and pile-soil interface properties. The individual components (pile-soil) can be modeled by a variety of constitutive laws and hence, enable detailed study of complex time-dependent interactions (relating to consolidation and creep of the surrounding soil). In a pile foundation system analysis, elements are used to represent the different properties of soil layers, piles and pile cap. In order for the model to represent the system accurately, continuity must be maintained throughout the system, and the governing equations (equilibrium, constitutive laws and stress-deformation) are solved while simultaneously satisfying the boundary and initial loading conditions. Instead of considering only the overall system response, the finite element method enables engineers to examine the stress-strain behavior at specific locations of the foundation system in detail. The corresponding disadvantages are

1) FE analyses require large computational power
2) Experience is needed to control the accuracy of the non-linear solution
3) Approximations are necessary to define the FE model for a given site condition (site properties, models…etc., must all be selected to capture main aspects of project)

2.2 Description of PLAXIS Program

PLAXIS (acronym for PLasticity AXISymmetric) is a 2-D finite element program designed to solve axisymmetric and plane strain geotechnical design problems involving groundwater flows, consolidation, foundation engineering, and tunnel construction. This thesis uses version 6.31 (PLAXIS, 1997), which runs in the MS-DOS operating system. The program discretizes the soil mass using triangular elements with either 6-displacement nodes (quadratic displacement interpolations) or 15-nodes (cubic-strain triangles after Sloan & Randolph, 1981). For 15-noded triangular elements, PLAXIS calculates cubic distributions of stress and strain, resulting in smooth and accurate stress-strain distributions using relatively coarse meshes. These high order elements are especially reliable in modeling undrained incompressible clay behavior. PLAXIS provides a library of different types of elements for modeling geotechnical problems:

i) Soil Elements (soils and solids)
ii) Interface Elements
iii) Walls, plates & shells
iv) Geotextiles
v) Anchor elements

The program incorporates 5 different constitutive models to define stress-strain properties of the soil. They are Elastic, Mohr-Coulomb (Elastic-Perfectly Plastic), Soft Soil, Hard Soil, and Modified Cam-Clay models. In the thesis, only Elastic, Mohr-Coulomb, and Modified Cam-Clay models are used for the modeling piles and soil strata. These models will be explained in detail in the following sections. The program has a simple mesh generator to define the distribution of elements for each problem. This particular version has a maximum number of 200 15-noded triangular elements.

Interface Elements are used to describe the contacting surface between two different types of materials. These elements allow the user to define reduced/increased strength parameters and/or hydraulic conductivity between the two different types of elements. Interface elements are especially useful when modeling the pile-soil interactions

Wall, plate and shell elements are designed to model elastic wall and beam structures. The flexural rigidity and axial stiffness are used to define the elastic properties of the beam or wall. Mindlin beam theory is used to estimate the shear deformation of the beam elements. The advantage of these elements (instead of soil elements) is that mesh lines do not need to be defined according to their placement, leading to more efficient and compact solutions. The shell elements are equivalent to walls in plane strain problems and are used in the modeling of pile groups.

Geotextiles and anchor elements are not used in the current modeling of foundation systems, and are ideal in modeling materials like geomembranes and tieback systems respectively.

In this thesis, all stress curves are plotted using effective stress invariants, **p'** and **q'**, where **p'** is the mean effective stress, and q is the second invariant of deviatoric stress which is a measure of the total shear stress within the soil.

$$p' = \sigma'_{oct} = \frac{1}{3}(\sigma'_1 + \sigma'_2 + \sigma'_3);$$

$$q = \frac{1}{\sqrt{2}}\sqrt{(\sigma_1 - \sigma_2)^2 + (\sigma_1 - \sigma_3)^2 + (\sigma_2 - \sigma_3)^2}$$

This thesis uses standard soil mechanics sign convention with stresses in compression.[1]

[1] The PLAXIS Code uses positive stresses in tension, consistent with other fields of solid mechanics

2.3 Clay Models

In the pile foundation analyses, the following three soil models are used to model soil and structural elements:

i) Linear Elastic Model
ii) Mohr-Coulomb Model
iii) Modified Cam-Clay Model

The linear elastic model has linear stress-strain relationship, and is therefore ideal for modeling structural elements where no failure is expected. The elastic modulus, E, and the Poisson's ratio, ν, govern the stress-strain relationship of this model.

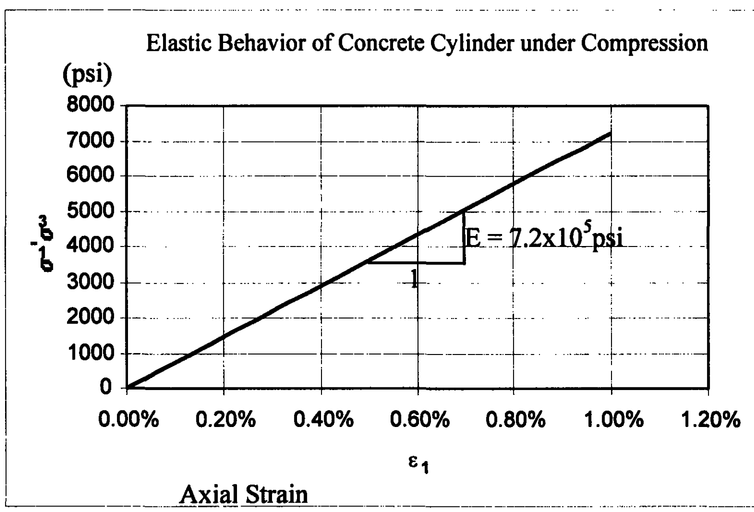

FIGURE 2.1 STRESS-STRAIN RELATIONSHIP OF A CONCRETE CYLINDER WITH ELASTIC MODEL

The Mohr-Coulomb Model is a linear elastic and perfectly plastic model (see Figure 2.2). The user can specify the strength, and stress-strain properties of the element through the input of internal friction angle (ϕ'), cohesion (c'), elastic modulus (E), and Poisson's ratio (ν). The shear modulus can be obtain through ν and E.

$$G = \frac{E}{2(1+\nu)} \quad ;Shear\ Modulus$$

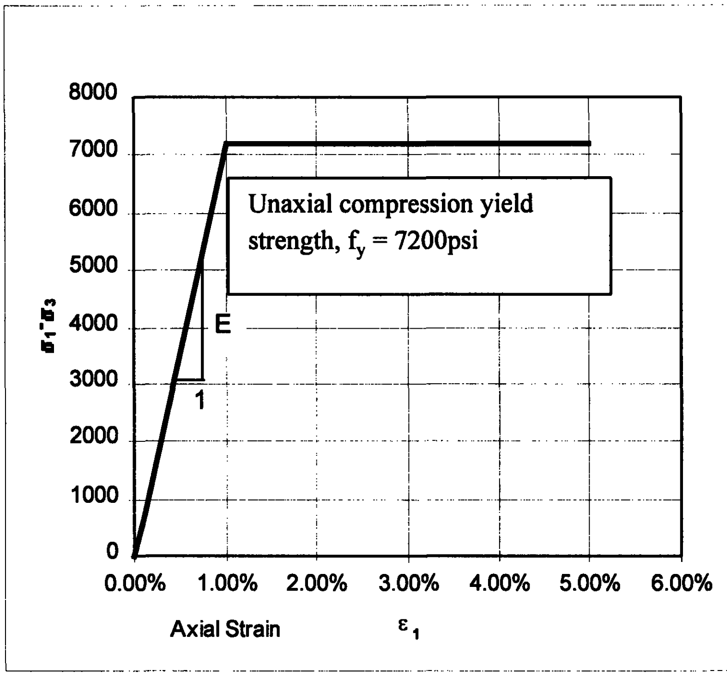

FIGURE 2.2 ELASTIC-PERFECTLY-PLASTIC MODEL FOR A CONCRETE CYLINDER

The relationship of the failure shear stress can be modeled with the Mohr-Coulomb Criterion and described with Mohr-circles, as shown in Figure 2.3. In order to verify the results from PLAXIS, **p'-q** curve of simple isotropic consolidated triaxial undrained compression model analyzed with PLAXIS is compared with the theoretical results. The result of a Mohr-Coulomb model (ϕ'=33°, c'=0, σ'_c=1ksf) is shown in Figure 2.4. In addition to the strength parameters, the hydraulic conductivity both in the vertical and horizontal directions must be specified for consolidation analyses.

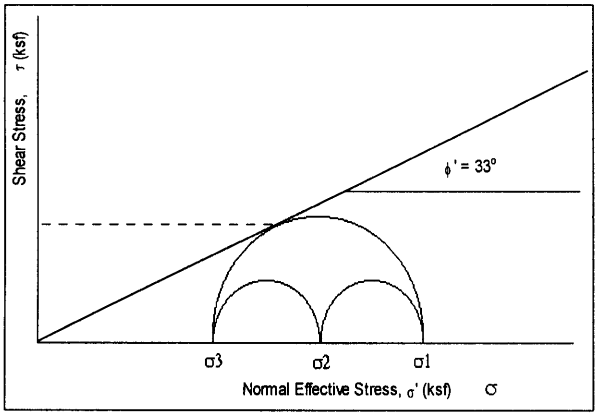

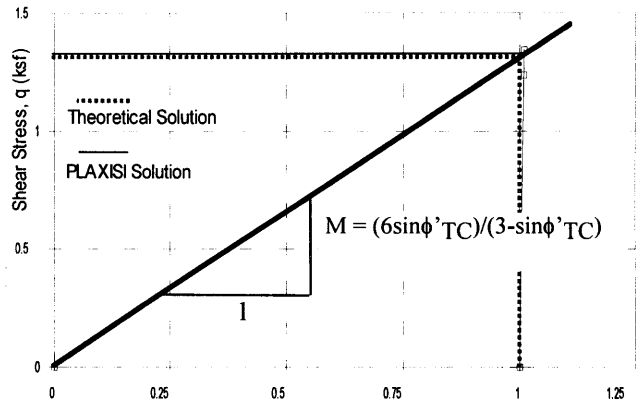

FIGURE 2.3 MOHR-COULOMB MODEL

FIGURE 2.4 MOHR-COULOMB MODEL FROM PLAXIS

The Modified Cam-Clay Model, developed by Roscoe and Burland in 1968, is one of the first generalized, effective stress, soil models. In order to use the Modified Cam-Clay (MCC) model for finite element analyses, the following input parameters are required:

i) M $= 6\sin\phi'/(3-\sin\phi')$
ii) κ^* $= C_s/(2.3*(1+e_o))$
iii) λ^* $= C_c/(2.3*(1+e_o))$
iv) ν = Elastic Poisson's Ratio
v) K_o $= \sigma'_{h\ initial}/\sigma'_{v\ initial}$ (for specifying the initial stress)
vi) $\mathbf{p'_m}$ = The initial yield stress

Where e_o is the initial void ratio

A brief explanation of the MCC model is given using the undrained shearing of an isotropically consolidated soil element as an example. In Figures 2.5, and 2.6, the effective stress path **(p'-q)** and the e vs. log **p'** for a soil with an initial OCR = 1.5 are shown. The failure shear strength of this model is governed by the Critical State Line (slope, M= $\tan^{-1}$ **q/p'**). In the Modified Cam-Clay model, the soil behaves elastically and exhibits recoverable volumetric strains at all points within the Yield Surface. In the e-log p' plane, the Loading and Reloading Line (URL) represents all attainable volumes under elastic loading and unloading with $\mathbf{p'_m}$ obtained from the maximum past pressure. The shape of the Yield Surface (YS) is defined as an ellipse in the p'-q plane, and its location is determined by the maximum past pressure of the soil. (Since the maximum past pressure can vary from zero to infinity, there are an infinite number of Yield Surfaces that can be generated.) The relationship of the YS is given below:

$$\frac{\mathbf{p'}}{\mathbf{p'}_m} = \left(\frac{M^2}{M^2 + R^2}\right); \qquad R = \frac{\mathbf{q}}{\mathbf{p'}};$$

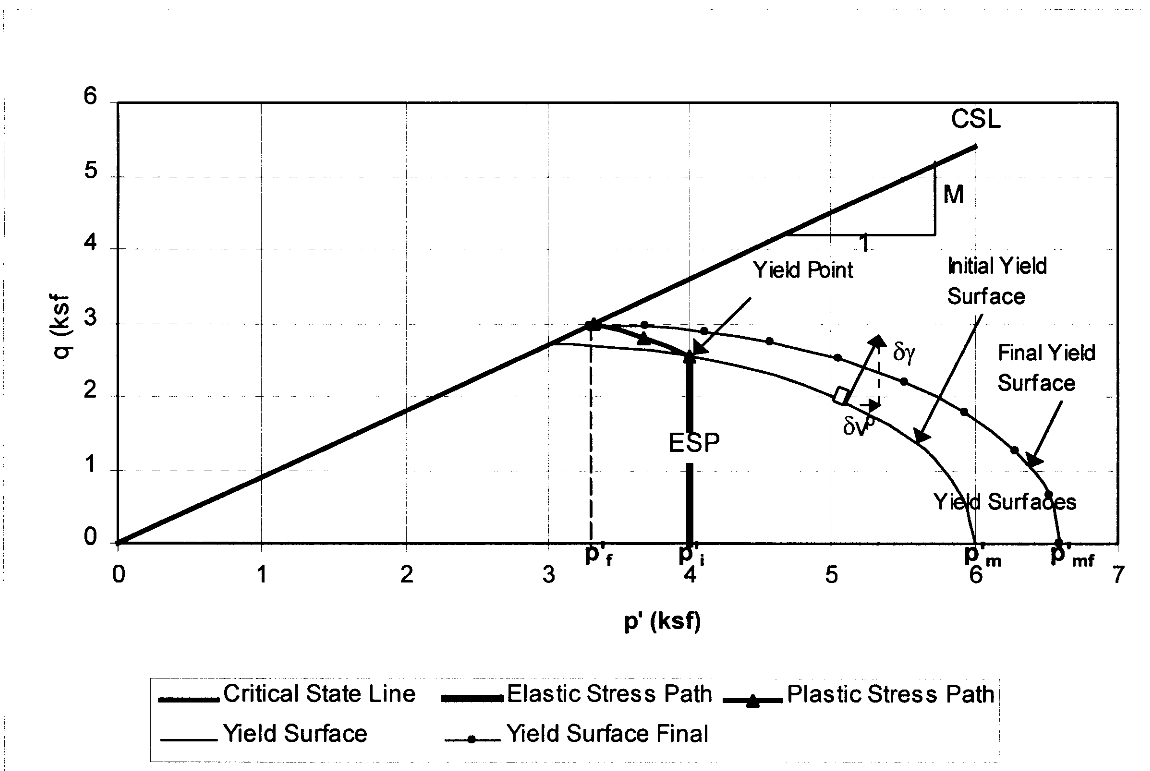

FIGURE 2.5 UNDRAINED TRIAXIAL SHEARING OF ELEMENT AT INITIAL OCR =1.5 WITH MCC MODEL

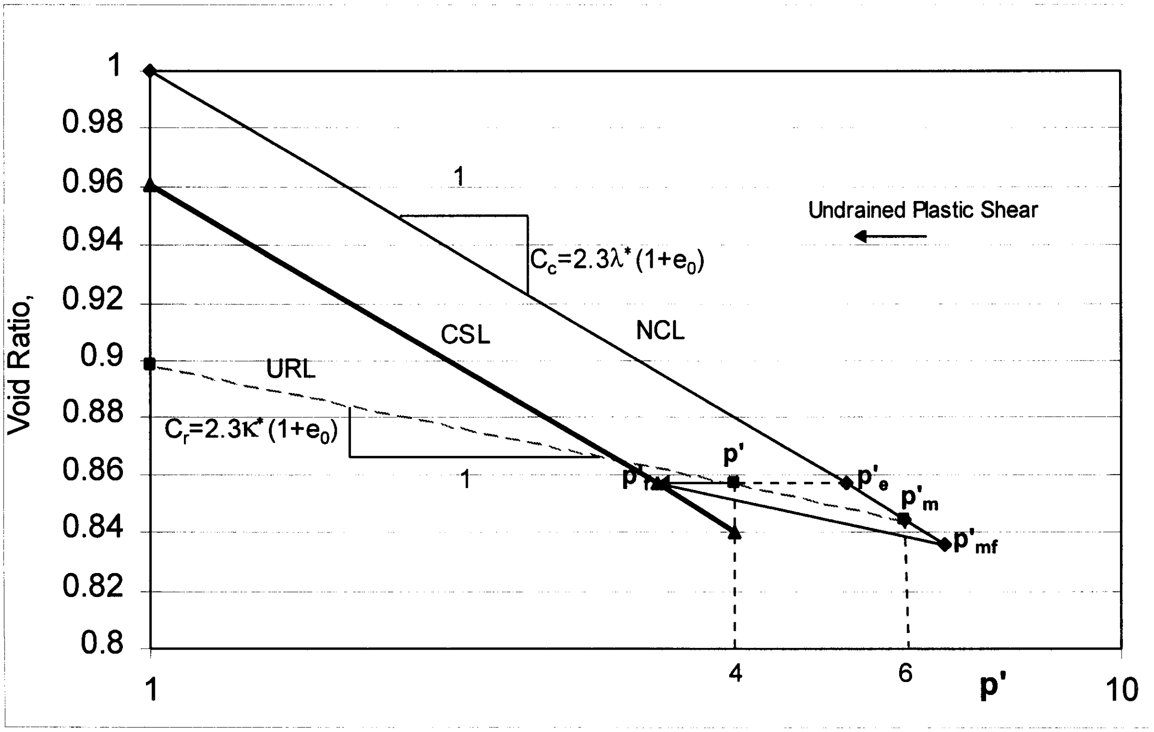

FIGURE 2.6 VOID RATIO VS. LOG P'

During undrained shearing at the elastic range, both **p'** and void ratio (e) remain constant. This shearing is represented by the vertical stress path (**p'**= 4ksf) in Figure 2.5. In Figure 2.6, since both e and **p'** remain constant in the elastic region, point **p'**$_i$ in the log **p'**-e plane represents the entire course of undrained shearing within the YS. In the elastic region, the stress-strain behavior of the soil is described by the following elastic properties:

$$E = \frac{3(1-2\nu)\mathbf{p'}}{\kappa^*}; \quad G = \frac{3(1-2\nu)\mathbf{p'}}{2\kappa^*(1+\nu)}$$

However, no elastic straining is generated due to undrained staining. After yielding, undrained shearing causes the soil to undergo both plastic and elastic straining. The

Normal Consolidation Line (NCL) in Figure 2.6 shows the amount of plastic deformation undergone. In order to maintain constant volume during undrained shearing, an equal but opposite amount of elastic deformation must occur.

For Undrained Shearing:

$$\Delta\varepsilon = \Delta\varepsilon^{elastic} + \Delta\varepsilon^{plastic} = 0; \quad \varepsilon = \frac{e}{1+e_0}$$

$$\Delta\varepsilon^{elastic} = -\kappa * \ln\left(\frac{\mathbf{p'}_i}{\mathbf{p'}_f}\right); \quad \Delta\varepsilon^{plastic} = -\lambda * \ln\left(\frac{\mathbf{p'}_m}{\mathbf{p'}_{mf}}\right)$$

The fraction of plastic volumetric deformation, δv^p, to plastic shear deformation, $\delta\gamma^p$, is governed by the (associated) flow rule as the gradient of the yield surface (see Figure 2.5). The stress path during plastic deformation follows the State Boundary Surface (SBS) from $\mathbf{p'_i}$ to $\mathbf{p'_f}$, which has constant volume throughout shearing (see Figure 2.6). As the soil undergoes plastic deformation, the maximum past pressure increases from $\mathbf{p'_m}$ to $\mathbf{p'_{mf}}$ at failure. Therefore, the yield surface expands as plastic deformation occurs reaching a final position $\mathbf{p'_m}$ for shearing to critical state conditions. The location of the SBS for normal-consolidated (NC) soil is characterized by $\mathbf{p'_c}$ (consolidation stress) which is equal to $\mathbf{p'_m}$. However, for over-consolidated (OC) soil, the SBS is characterized by an equivalent pressure, $\mathbf{p'_e}$ (shown on Figure 2.6). In Figure 2.6, one can view the undrained shearing of the OC soil at $\mathbf{p'_i}$, as part of the undrained shearing of the NC soil with $\mathbf{p'_m}$ equals to $\mathbf{p'_e}$. The following equations define the SBS in the **p'-q** plane.

$$\frac{\mathbf{p}'}{\mathbf{p}'_e} = \left(\frac{M^2}{M^2 + R^2} \right)^{1-m} \quad ; \quad m = 1 - \frac{\kappa^*}{\lambda^*}$$

In order to show how the MCC models behave in PLAXIS, a model is set up to simulate an isotropic consolidated triaxial undrained compression test. A confining stress of 1ksf is applied to clay prior to undrained shearing. In Figure 2.7, the effective stress (**p'-q**) path shows that yielding occur at the beginning of the loading and follows the SBS until failure occur when **q** is approximately equal to 0.745ksf.

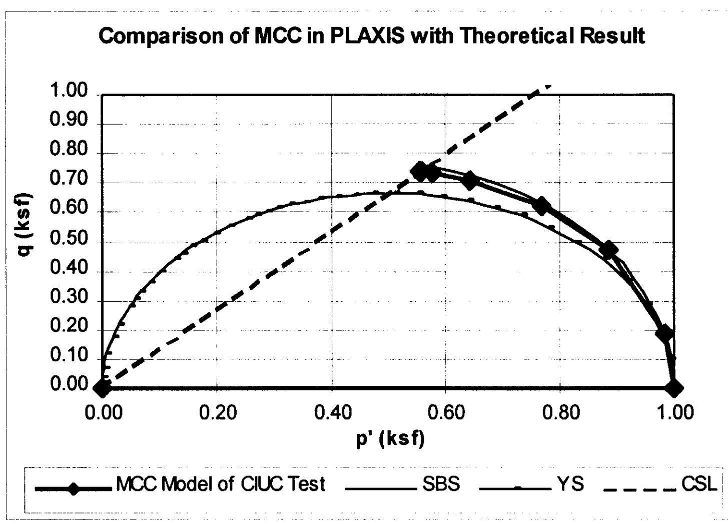

FIGURE 2.7 UNDRAINED BEHAVIOR IN CIU TEST ON NORMALLY CONSOLIDATED CLAY USING MCC.

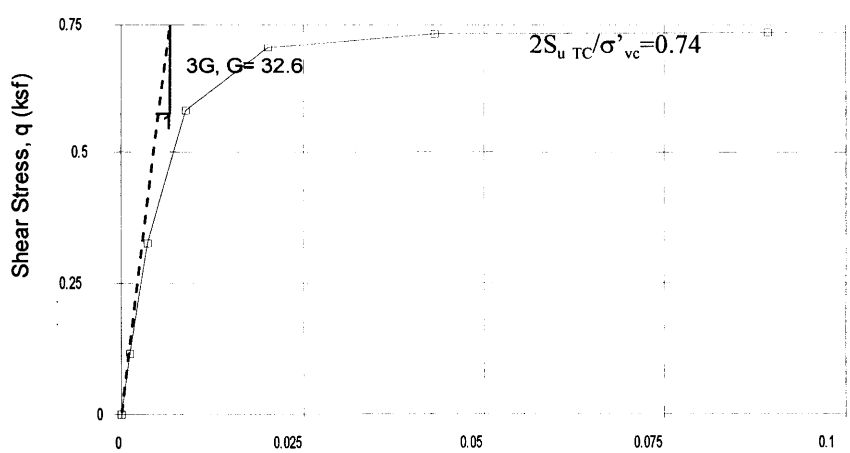

FIGURE 2.8 STRESS-STRAIN BEHAVIOR IN CIU TEST ON NORMALLY CONSOLIDATED CLAY USING MCC

The results from PLAXIS follow closely the analytical equations of the MCC SBS, with undrained shear strength mobilized at large shear strains (as the stress state asymptotes towards critical state conditions). The non-linear stress-strain response is also shown in Figure 2.8. From the graphs, one can check the results by back calculating the parameters. The input and back calculated parameters are summarized in Table 2.1.

Summary of MCC Parameters for CIUC	
M (ϕ' =33°)	1.3307
λ^*	0.08679
κ^*	0.01604
ν	0.277
Theoretical $G_{initial}$ (ksf)	32.7
Back Calculated Parameters	
M	1.331
$G_{initial}$ (ksf)	32.6

Table 2.1 Input and back calculated parameters for CIUC in MCC.

2.4 Validation of Finite Element Modeling Methodology

In order to validate the results on the FE model, trial analyses are first performed on problems that have published solutions. This section compares the analyses for an axially loaded pile in an elastic soil with solutions from the load-transfer method proposed by Randolph & Wroth (1978). Figure 2.9 summarizes the Load Transfer analyses. Figures 2.10 shows the finite element model used to analyze the behavior of axially loaded axisymmetric concrete and steel piles in an elastic soil.

$$\frac{Q_T}{w_T r_0 G_L} = \left(\frac{\frac{4}{(1-\nu)B_f} + \frac{2\pi}{\xi} R_s \frac{\tanh(\mu L)}{(\mu L)} \frac{L}{r_o}}{1 + \frac{4}{(1-\nu)B_f} \frac{1}{\pi\lambda} \frac{\tanh(\mu L)}{(\mu L)} \frac{L}{r_o}} \right)$$

$$\xi = \log_e (0.25 + (2.5 R_s (1-\nu) - 0.25) B_f) \frac{L}{r_o})$$

$$\mu L = \sqrt{\frac{2}{\xi\lambda}} (\frac{L}{r_o})$$

$$B_f = \frac{G_L}{G_b}$$

$$R_s = \frac{\overline{G}}{G_L}$$

$$\overline{G} = G_{avg} = \frac{1}{2}(G_o + G_L)$$

$$\lambda = \frac{E_{pile}}{G_L}$$

$$\xi = \log_e \left\{ (0.25 + (2.5 R_s (1-\nu) - 0.25) B_f) \frac{L}{r_o} \right\}$$

$$\eta = r_b / r$$

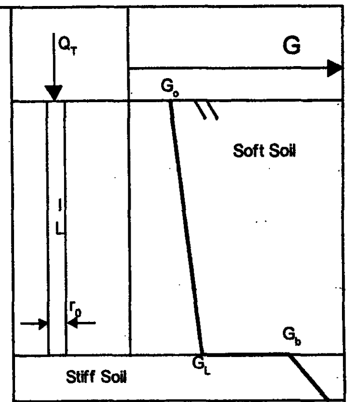

η = underream ratio

ν = possion's ratio of soil

FIGURE 2.9 SOLUTION OF THE LOAD TRANSFER METHOD (RANDOLPH & WROTH 1978)

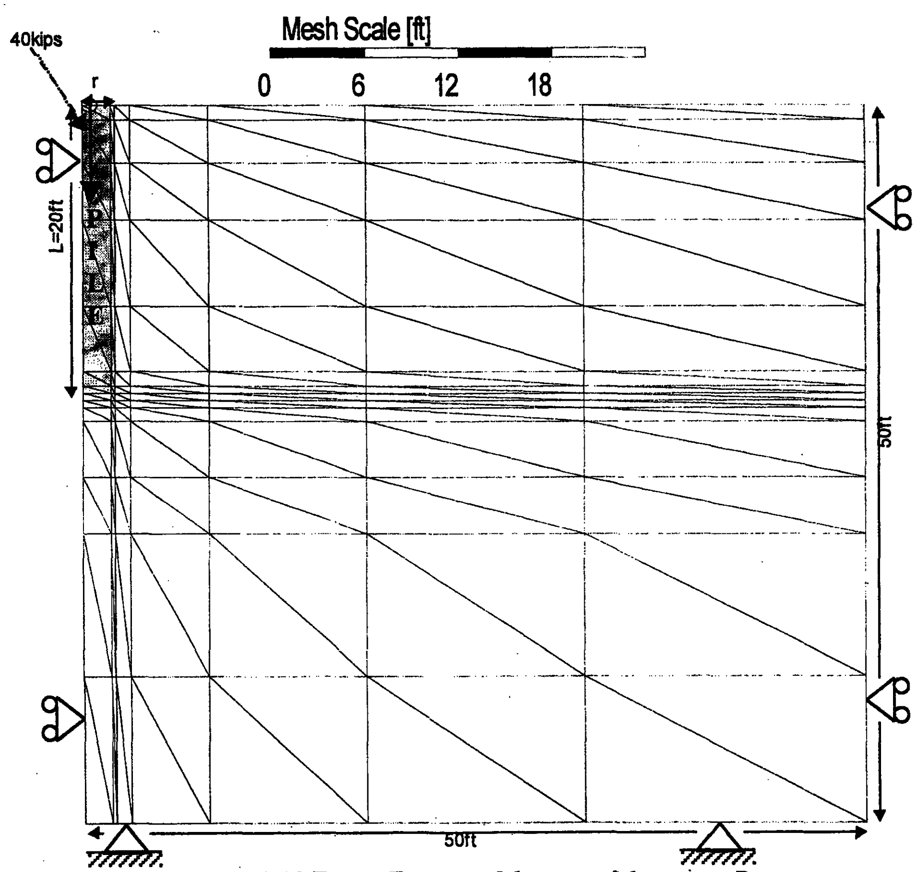

FIGURE 2.10 FINITE ELEMENT MESH FOR MODELING PILES

Figures 2.11 and 2.12 compare the pile head stiffness concrete and steel piles of different radii with the Load-transfer solutions. The results show very good agreement (within 1% of differences) between the finite element calculation of normalized pile head stiffness ($Q_T/(w_T r_o G_L)$, where Q_T is the load at the tip; w_T is the pile head displacement, r_o is the radius of the pile, and G_L is the shear modulus of the soil at the pile tip) and results of the Load-transfer analyses, for a wide range of pile aspect ratio, L/r_o. These results confirm the ability of the FE analyses to predict behavior of piles in elastic soil

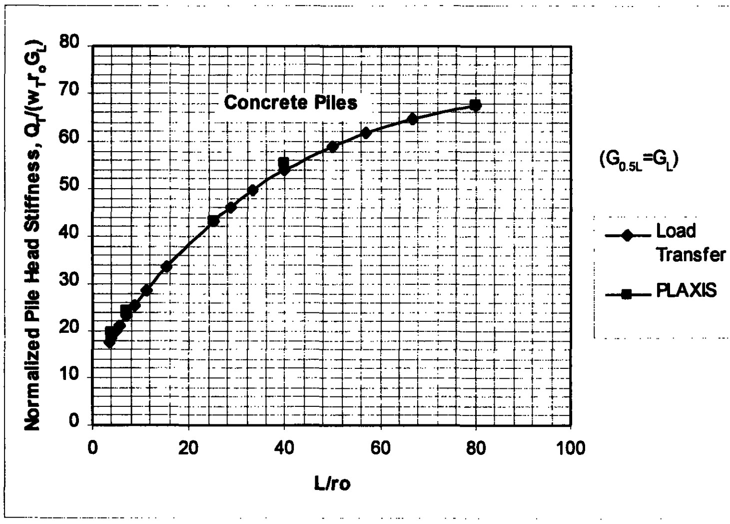

FIGURE 2.11 COMPARISON OF LOAD TRANSFER RESULT WITH PLAXIS FOR CONCRETE PILES

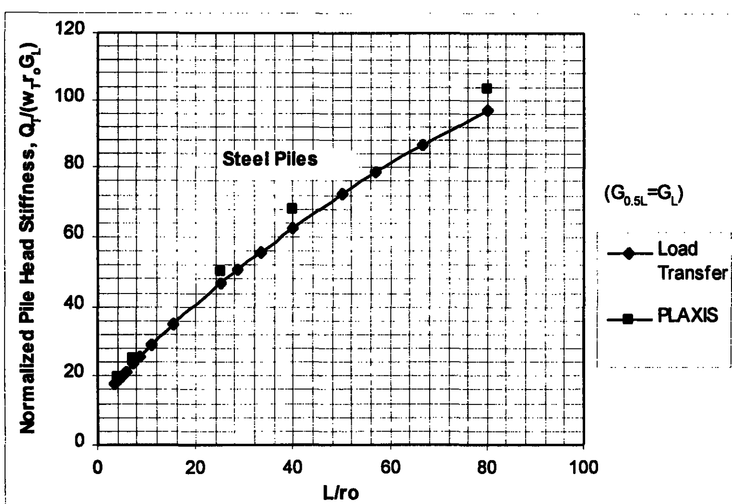

FIGURE 2.12 COMPARISON OF LOAD TRANSFER RESULT WITH PLAXIS FOR STEEL PILES

2.5 Pile Response in an Elastic-Plastic Soil

This section compares pile response in an element of elastic-plastic soil at a confining pressure, σ_c=1ksf. The calculations compare two cases: 1) soil is characterized by the Elastic Perfectly Plastic (EPP) Mohr-Coulomb model with G = 32.7ksf, ν=0.277, and ϕ'=33°; and 2) soil is modeled as normally consolidated clay with MCC model. The parameters used for the MCC model are listed below:

i) M = 1.331 (for ϕ'=33°)
ii) $\lambda^* = 0$
iii) $p'_m = p'_c$ = 1ksf
iv) $\kappa^* = 0.0848$
v) $\nu = 0.277$

With constant $\mathbf{p'_m}$ throughout the MCC model, the stiffness and the strength are homogeneous at all points. The piles used in the models have length of 20ft and radius of 1.75ft and self-weight stresses are neglected. Loads are then applied under undrained condition (i.e. no change in void ratio, Δe= 0) at the pile head until failure occurs. Figure 2.13 and 2.14 show the effective stress paths of the EPP and the MCC models, respectively at a point X adjacent to the pile shaft with depth to pile length ratio, z/L, = 0.725.

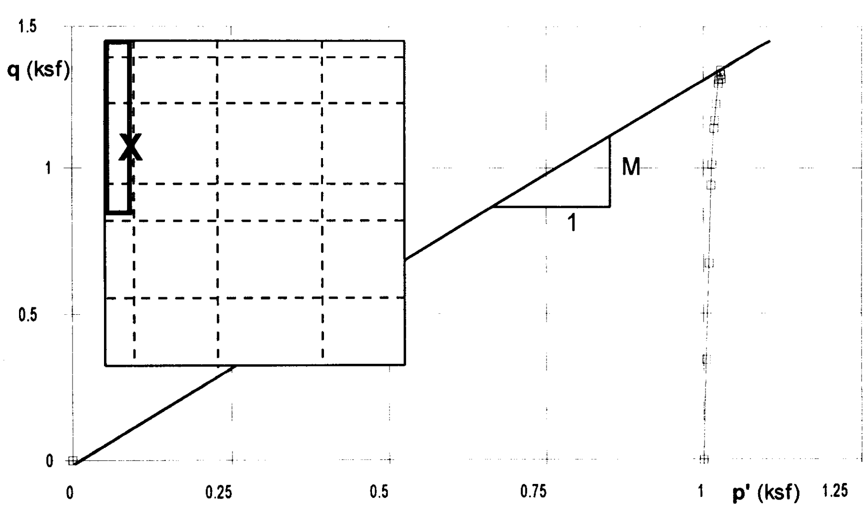

FIGURE 2.13 FAILURE FOR ELASTIC-PLASTIC MODEL

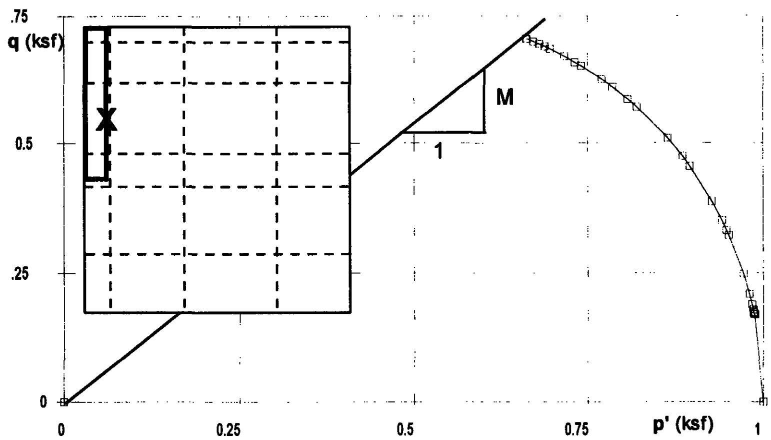

FIGURE 2.14 FAILURE FOR MMC MODEL

In Figure 2.13, **p'**, the mean effective stress, remains almost constant throughout shearing. In Figure 2.14, the MCC model exhibits plastic behavior and follows the SBS during undrained shearing. Both plastic and elastic deformations take place during shearing in this model because the soil is normally consolidated (initial state of stress is located at the YS), hence the changes in **p**' correspond to shear induced pore pressure. Both models have been set up to have a constant shear modulus of 32.7ksf throughout the depth of the soil. Figure 2.15 shows the stress-strain response of the EPP model at point X. The shear modulus remains constant until failure occurs. Figure 2.16 shows the stress-strain relationship of the MCC model, the modulus decreases as plastic deformation takes place.

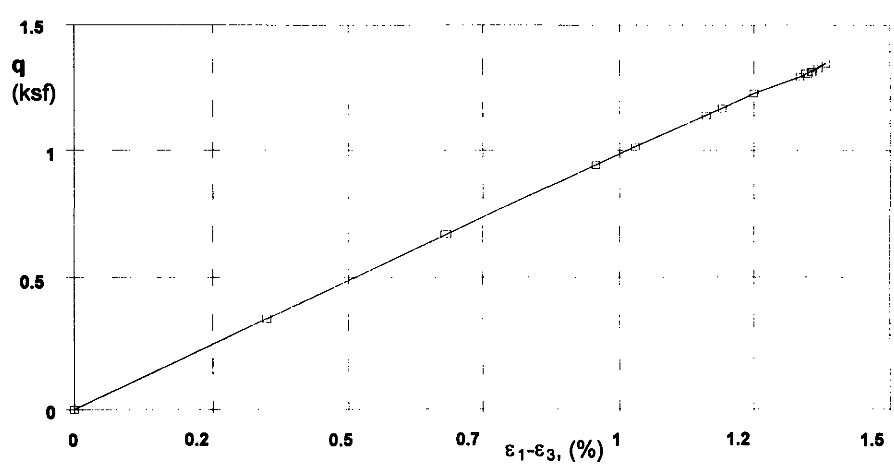

FIGURE 2.15 STRESS-STRAIN RELATIONSHIP FOR MOHR-COULOMB

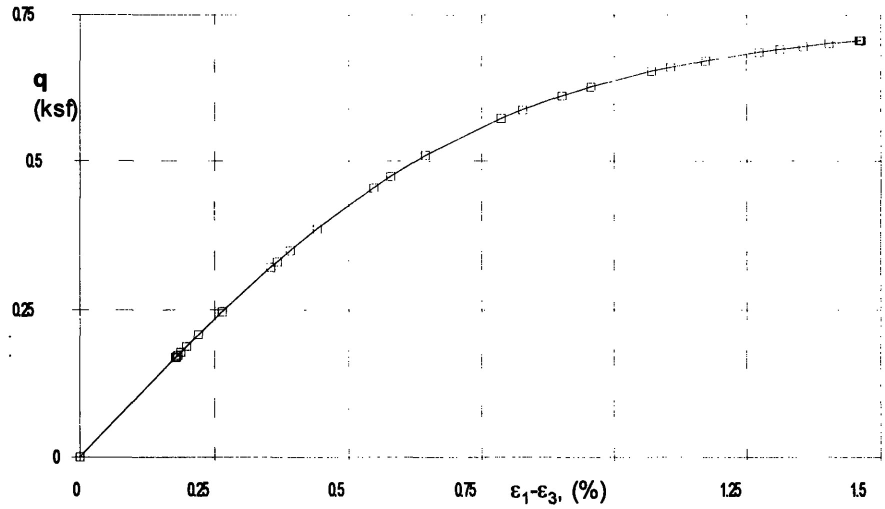

FIGURE 2.16 STRESS-STRAIN RELATIONSHIP FOR MCC MODEL

Nevertheless, the initial shear moduli of the two models have nearly identical values. Since both models have analogous modulus in the beginning of the loading throughout the soil, the pile head stiffness of the two models should also match at the beginning of the loading. As loading increases, however, the MCC model should have a lower pile head stiffness caused by plastic deformation. These type of pile head responses are verified by Figures 2.17 and 2.18, where the settlement of the pile head is plotted against the applied load on the pile head.

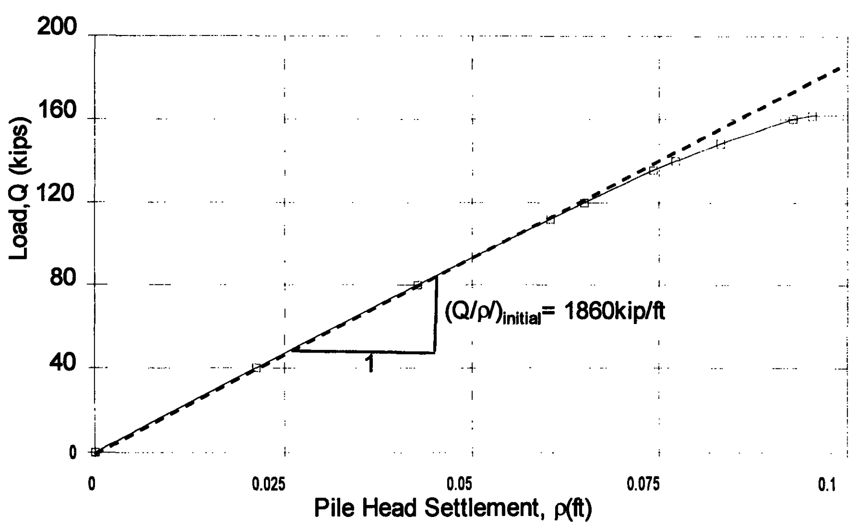

FIGURE 2.17 PILE HEAD STIFFNESS FOR MOHR-COULOMB MODEL

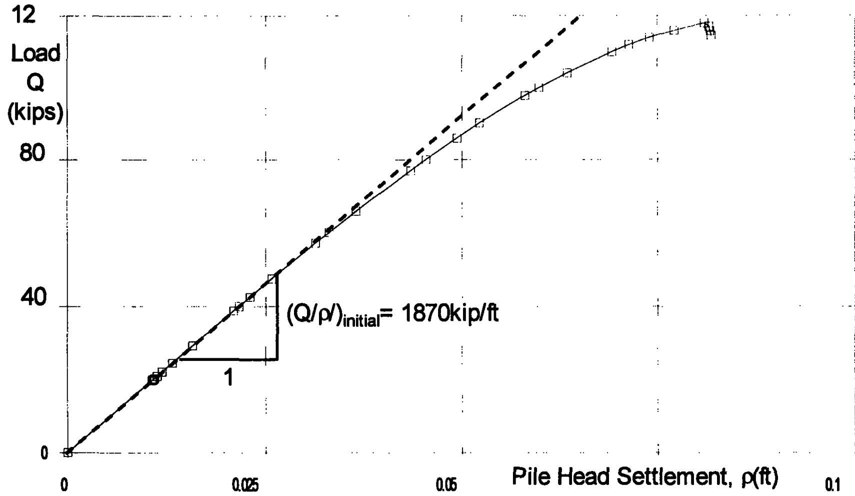

FIGURE 2.18 PILE HEAD STIFFNESS FOR MCC MODEL

A further calculation has been carried out for the pile in a normally consolidated clay layer (using MCC model) with gravity stresses controlled by the buoyant weight. The mesh is identical from the previous model. The initial stress condition is summarized in Table 2.2.

Summary of Initial Condition		
Depth of clay layer	50	(ft)
Depth to water table	0	(ft)
Surcharge Load, q	0.2	(ksf)
K_o: (σ'_h/σ'_v)	0.5	

Table 2.2 Initial Conditions for the Pile in NC MCC Model

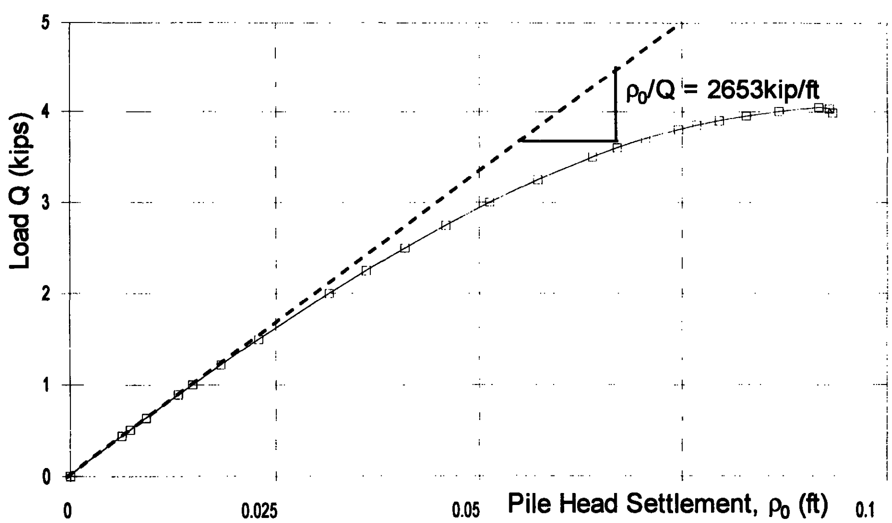

FIGURE 2.19 LOAD VS. DISPLACEMENT FOR NORMALLY CONSOLIDATED CLAY IN MCC MODEL

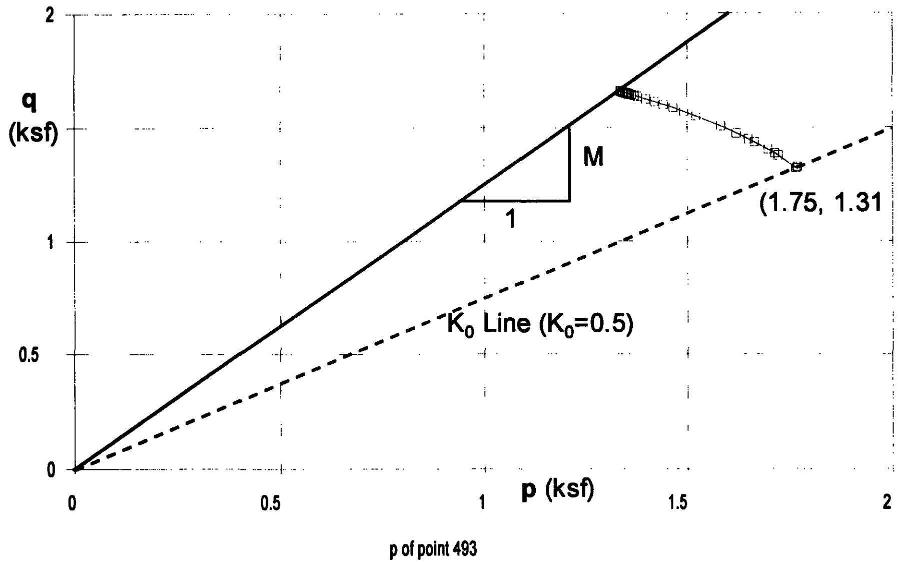

FIGURE 2.20 UNDRAINED FAILURE IN MCC WITH K_0 CONDITION

In this model, the modulus of the soil changes linearly with depth due to gravity stresses. The pile head stiffness of this model (Figure 2.19) is much more non-linear than the pile head stiffness in Figure 2.18. Note that the initial stress condition of this model is different from previous models. The stress path starts at K_o= 0.5 (see Figure 2.20) instead of **q**= 0 (K_o= 1) from the previous example.

In addition to examining the pile head stiffness of the pile, the capacities are also checked and compared with convention calculation method. Conventional calculation estimates capacity as the sum of skin friction capacity and tip resistance capacity. The estimated parameters for the conventional calculation are shown below:

$Q_{total} = Q_{bf} + Q_{sf}$; $\quad Q_{bf} = q_b A_b$ = tip resistance ; $\quad Q_{sf} = f_s A$ = side resistance

$q_b = N_c s_u + p$; $\quad N_c \approx 9$; $\quad p = \frac{1}{3}(1+2K_o)\sigma'_{vo} + u_0$

$f_s = \alpha S_u$; $\quad \alpha \approx 0.3 \, to \, 1.1$

A_b = area of the pile tip; $\quad$ A = Area of the pile shaft

Table 2.3 shows conventional calculations of design capacity (assuming a rigid pile) of the three piles mentioned above. The values of α depend on Su, and are selected from three different design curves. The undrained shear strength is based on the theoretical value of the models. For the first two cases where the pile is embedded in a soil element, the undrained shear strength is constant throughout, and can obtained from the input parameters. For the pile embedded in the NC MCC model, the undrained strengths at different depths are obtained from the equations (given in section 2.3) that define MCC model. In general the calculated design capacities are slightly higher but they are within a good range of one another. Table 2.4 shows the comparison of the capacities calculated from conventional design methods to the ones estimated by FE analysis.

Pile Properties	radius	Length	A_t	A							
	(ft)	(ft)	(ft^2)	(ft^2)							
	1.8	20.0	9.6	219.9							
	For σ'_c = 1ksf										
	Tip Resistance			***Skin Friction***					***Capacity***		
	Nc	p	q_b	Su	α	α	α	α_{avg}	Q_{bf}	Q_{sf}	Q_{total}
		(ksf)		(ksf)	Tomlinson	API 1981	O & S		(kips)	(kips)	**(kips)**
EPP Model	9.0	1.0	7.0	0.67	0.8	0.9	0.8	0.8	67.2	119.9	**187.1**
MCC Model	9.0	1.0	4.3	0.37	1.0	1.0	1.0	1.0	41.7	81.4	**123.0**
	For Normally Consolidated MCC Model, K_o= 0.5										
Skin Friction											
Depth	p_c	p_e	q	Su	Depth	α	α	α	α_{avg}	$Su_{avg.}$	Q_{sf}
(ft)	(ksf)	(ksf)	(ksf)		(ft)	Tomlinson	API 1981	O & S		(ksf)	(ksf)
0.0	0.2	0.3	0.2	0.09							
5.0	0.6	0.8	0.6	0.28	0 - 5	1.0	1.0	1.0	1.0	0.19	10.4
10.0	1.0	1.3	0.9	0.47	5 - 10	1.0	1.0	1.0	1.0	0.38	20.8
15.0	1.4	1.8	1.3	0.66	10 - 15	0.8	1.0	1.0	0.9	0.57	25.9
20.0	1.8	2.3	1.7	0.85	15 - 20	0.8	0.9	0.7	0.8	0.76	33.2
Tip Resistance									***Capacity***		
Nc	Su	q_b							Q_{bf}	$Q_{sf\,tot}$	Q_{total}
	(ksf)	(ksf)							(kips)	(kips)	**(kips)**
9.0	0.9	9.5							91.1	90.4	**181.5**

Table 2.3 Capacities Design Calculations for Piles in Three Types of Soil Model

	Capacity$_{design}$	Capacity$_{FE}$	% Difference
	(ksf)	(ksf)	(ksf)
EPP w/ σ'_c =1ksf	123.0	117.0	**4.9**
MCC w/ σ'_c =1ksf	187.1	164.0	**12.4**
NC MCC	181.5	163.0	**10.2**

Table 2.4 Comparison of Design Capacities with FE Capacities

2.6 1-D Consolidation

In addition to verifying the soil models in PLAXIS, consolidation predictions have also been checked. Results from a one-dimensional consolidation analysis on an elastic soil are compared with Terzaghi's solution. The model in PLAXIS is set up with the properties listed in Table 2.3. The FE mesh for the model is shown in Figure 2.21. To replicate 1-D consolidation, an axisymmetric model is used. The left, right and bottom boundaries do not allow any horizontal displacement, and the bottom boundary does not allow any vertical displacement. Both the top and the bottom allow the dissipation of excess pore pressure; therefore, the drainage height, H_d, is half of the total height of the model.

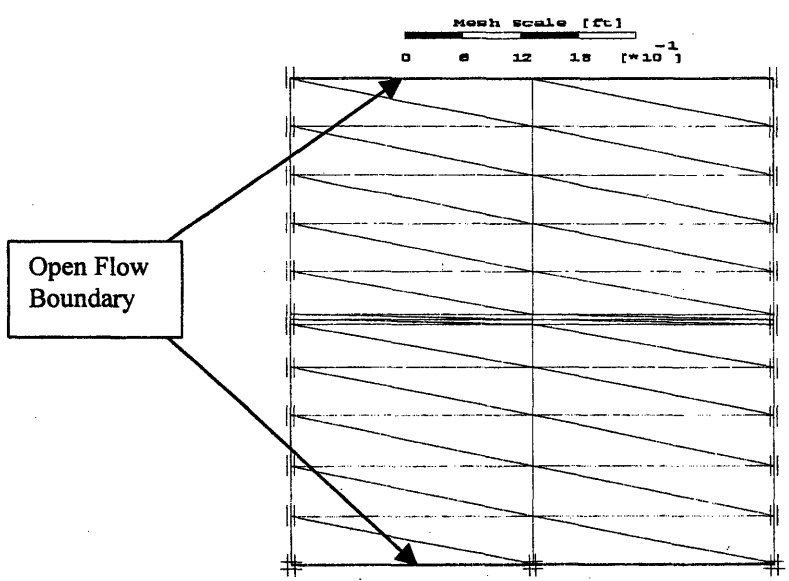

FIGURE 2.21 FE MESH FOR 1-D CONSOLIDATION ANALYSIS.

Consolidation Model Properties		
u_o, Initial excess pore pressure	1	(ksf)
k_v	0.0003	(ft/day)
γ_w	0.0624	(kips/ft^3)
H_d, Drainage Height	2.5	(ft)
G	32.7	(ksf)
ν	0.3	

Table 2.5 Consolidation Parameters for One Dimensional Analysis

From the properties of the model given above, m_v, the coefficient of volume change, can be obtained, and consequently, the equivalent Terzaghi's consolidation solution can be set up. The solutions of the Terzaghi's 1-D consolidation solution with double drainage are listed below.

$$u_e = \sum_{m=0}^{\infty} \frac{2u_o}{M}(\sin MZ)e^{-M^2T}$$

$$M = \frac{\pi}{2}(2m+1)$$

$$Z = \frac{z}{H_d} = \frac{depth}{drainage\ height}$$

$$T = \frac{C_v t}{H^2}$$

$$C_v = \frac{k_v}{m\,\gamma_w}; \quad m_v = \frac{\Delta\varepsilon_v}{\Delta\sigma_v}$$

For Axisymmetric Elastic Model:

$$m_v = \frac{(1+\nu)(1-2\nu)}{E(1-\nu)}$$

First, the displacement of a point located at the top of the mesh is computed (see Figure 2.22). The results are similar to the published Terzaghi's solution. In addition the excess pore pressure along the depth of the model is computed at different time gaps. The solution (see Figure 2.23) shows that the initial excess pore pressure (0.965ksf) deviates from the known solution (1ksf). In undrained condition, the initial excess pore pressure should equal to the applied load. However, the FE analysis shows the initial excess pore pressure is less than the applied load. Therefore, excess pore pressures at mid height from PLAXIS are also compared with Terzaghi's solution throughout the consolidation process to examine the degree of deviation. Although the results (see Figure 2.24) from the two solutions do not match exactly, PLAXIS provides a reasonable estimate of the pore pressure dissipated within an error of 6% of the initial excess pore pressure. The discrepancies between computed results and Terzaghi's are caused by the limitations of modeling incompressible response using finite elements. The maximum Poisson's ratio allowed in PLAXIS is 0.495, and therefore initial conditions do not match the Terzaghi's solution (where $\nu = 0.5$). The computed excess pore pressure at time,$t = 0$ is less than the applied load. In addition, PLAXIS can not model drainage at the edges of the consolidation boundary precisely, causing the rate of consolidation to differ slightly from the theoretical solution. According to the software developer, a finer mesh near the top and bottom drainage boundaries can improve these results.

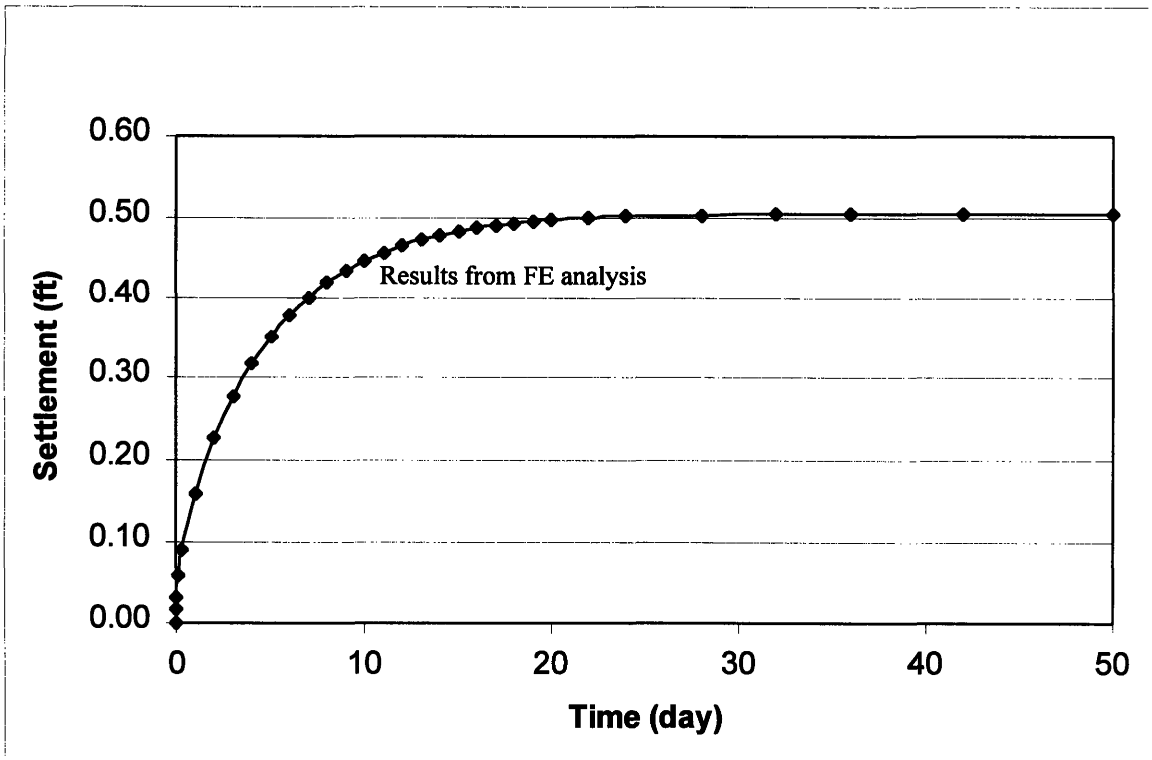

FIGURE 2.22 SETTLEMENT VS. TIME AT THE TOP OF THE MESH

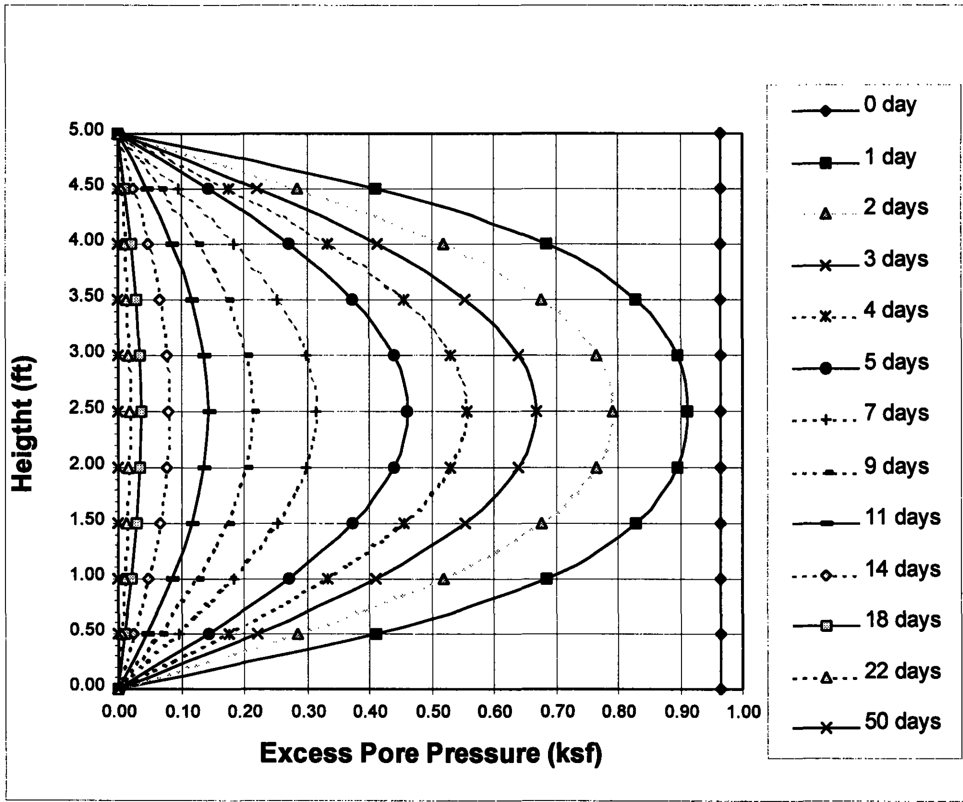

FIGURE 2.23 ISOCHRONES OF EXCESS PORE PRESSURE AT DIFFERENT TIMES

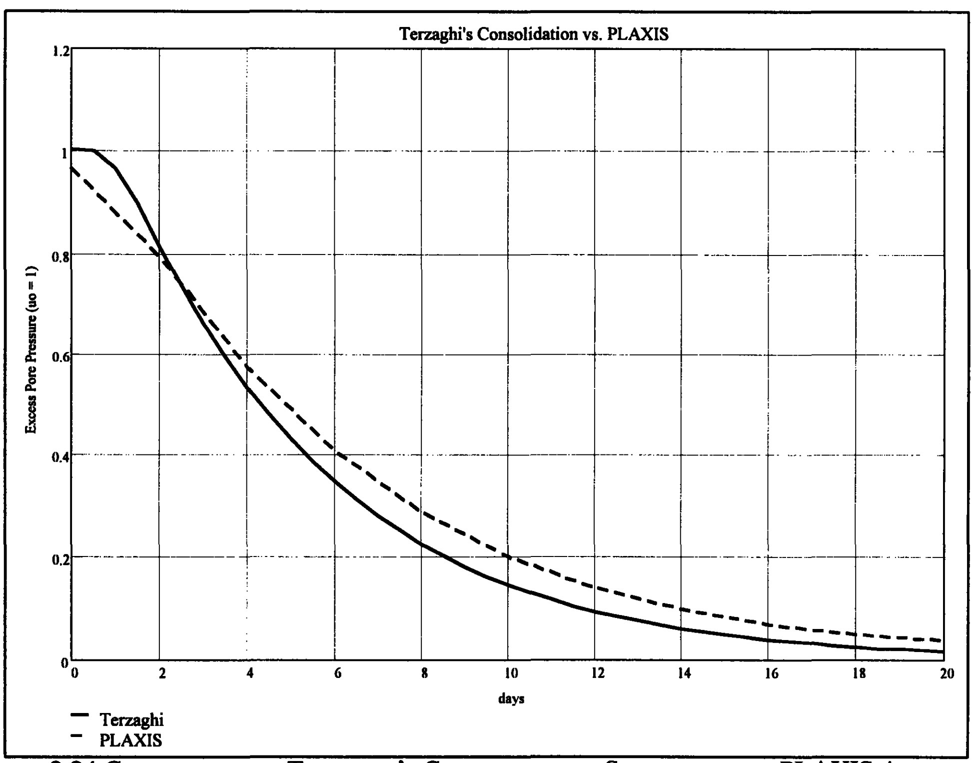

FIGURE 2.24 COMPARISON OF TERZAGHI'S CONSOLIDATION SOLUTION WITH PLAXIS ANALYSIS

Chapter 3 Analysis of National Geotechnical Experiment Site, Northwestern

3.1 Background and Detail of Testing Program

A series of pile load were performed on four different types of piles at the Evanston Campus of Northwestern University (Finno et al, 1989). The test piles included 1) HP 14x73 steel pile; 2) 18"-diameter, closed-ended, pipe pile; 3) 18"-diameter drilled pier installed using the slurry method; and 4) 18"-diameter drilled pier installed with temporary casing. All four-test piles are approximately 50ft long, and the layout of the piles is shown in Figure 3.1. A summary of the activities performed in the Northwestern site is listed in Table 3.1.

Date	Activity
24-May-88	Pre-auger 12-in.-diameter hole for 18-in.-diameter pipe pile; drive pipe pile and HP 14x73 test piles; drive 2 anchor piles (HP 10*42)
25-May-88	Drive remaining 7 anchor piles (HP 10*42)
26-May-88	Install 2 drilled piles
7-Jun-88	Perform 1st load test on HP 14*73
8-Jun-88	Perform 1st load test on 18-in.-diameter pile
9-Jun-88	Perform 1st load test on drilled pier (slurry method)
10-Jun-88	Perform 1st load test on drilled pier (cased method)
26-Jun-88	Begin 2nd set of load tests
29-Jun-88	Complete 2nd set of load tests
12-Jun-88	Begin 3rd set of load tests

Table 3.1 Summary of Pile Load Test Activities.

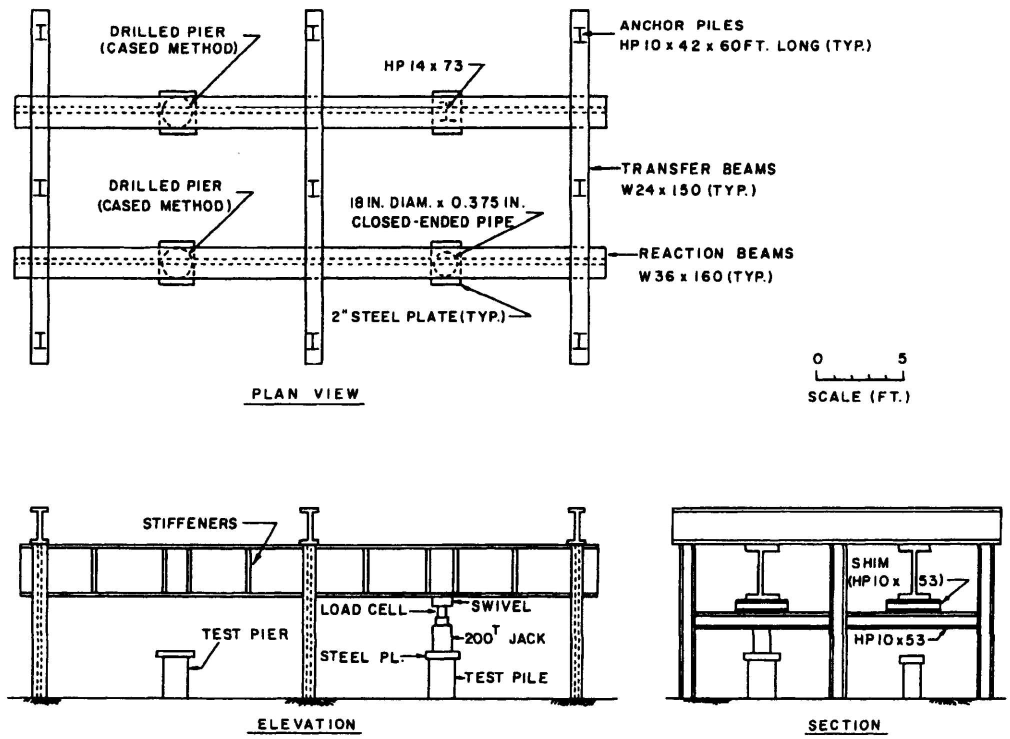

FIGURE 3.1 LAYOUT OF TEST PILES

The load tests were performed in three different phases according to the standard procedures suggested by ASTM D-1143-81 (ASTM, 1994). The first load sequence was applied two weeks after installation of the piles; a second series at five weeks; and a third series of load tests were carried out forty-three weeks after installation. The loading is applied to the piles using a hydraulic jack supported by the loading frame, which in turn is supported by another nine HP 10*42 anchor piles. Incremental loading is applied to the pile tip, and the pile is considered to have reached failure when the rate of settlement exceeds 0.015" per hour and continuous pumping of the jack is required to maintain a constant load. Therefore, strain gauges are installed along the pile to monitor movements during loading. Figure 3.2 shows the cross section and the location of the strain gauges for the driven piles.

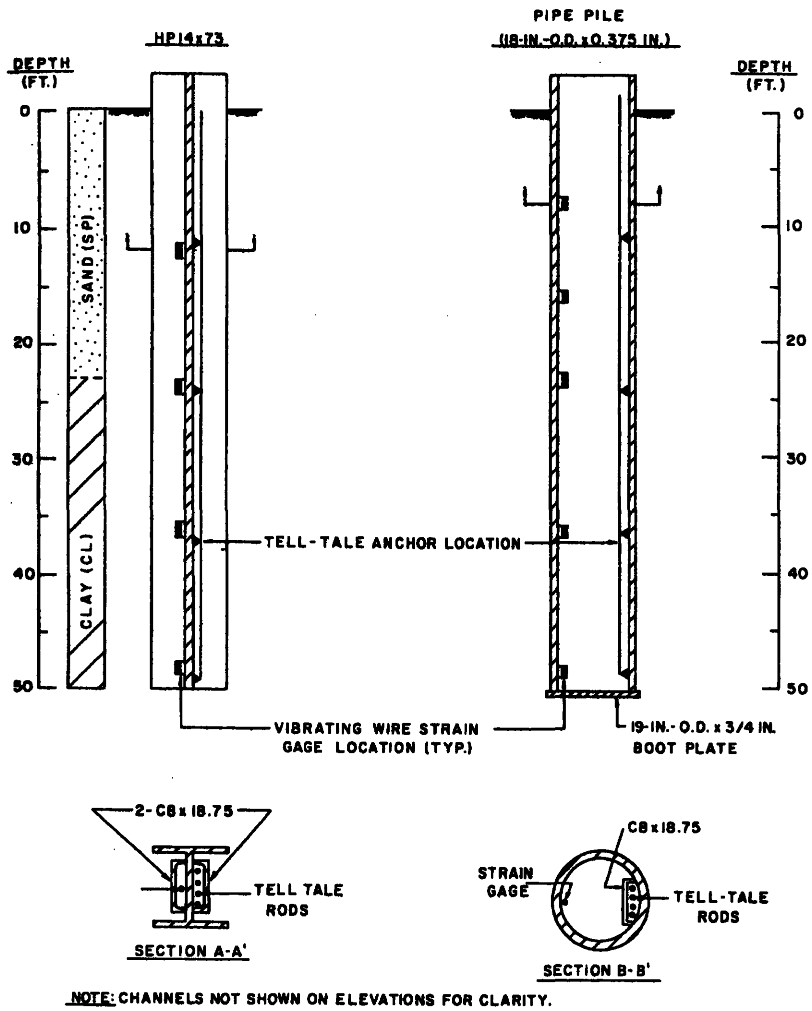

FIGURE 3.2 DETAILS OF DRIVEN PILES

3.2 Subsurface Characteristics and Engineering Properties

The upper twenty-three feet of the soil profile comprise a fine-grained sand (SP) that was bottom-dumped from barges in 1966 by the University to raise the ground above the elevation of an adjacent lake. Clamshells were also used to place the sand, but no standard compaction procedures were performed on the sand. Approximately thirty-seven feet of NC soft to medium clay (CL) lies underneath the sand. As suggested by

Finno, (1989), water contents of the soil are a few percents above the plastic limit which suggest that the clay was originally OC. Nevertheless, placing the sand over the clay in1966 appears to re-load the (soft to medium) clay back to a normally or very lightly over-consolidated. Below the NC clay, twenty feet of OC stiff clay (CL) is underlain by ten feet of hard silt (ML), and the Niagaran dolomite bedrock is beneath the hard silt. The water table is located at a depth of 13ft and pressures are essentially hydrostatic.

The sand and NC clay stratum have the most influence on the behavior of the piles, and therefore, extensive site investigations were performed from the top of the sand stratum down to a total depth of seventy feet. A series of in-situ tests were performed, including standard penetration test, field vane tests (FV) cone penetration tests (CPT), piezocone soundings, dilatometer tests (DMT), and Ménard pressuremeter tests (PMT) are performed throughout the site. Figure 3.2 indicates the location of the tests, and the results are included in the Appendix A.

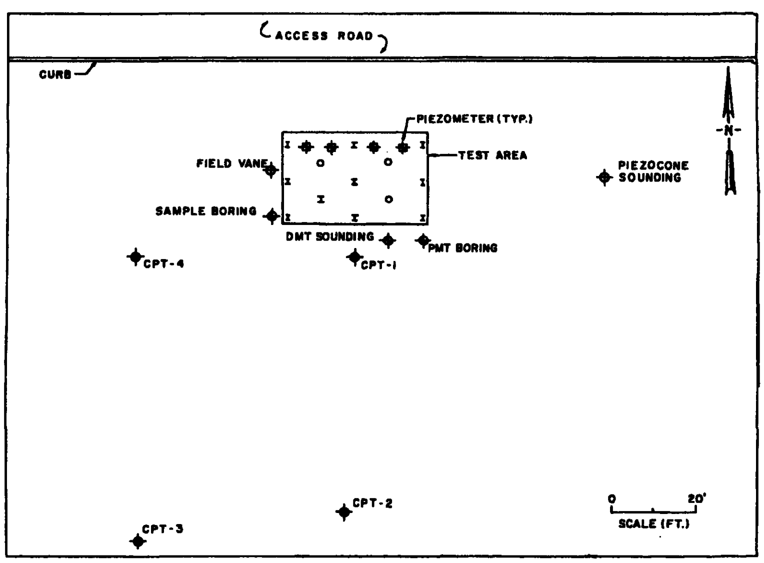

Fig. 1. Location Plan

FIGURE 3.3 LOCATION OF IN-SITU TESTS AND SITE INVESTIGATIONS

In addition to in-situ tests, laboratory tests were also conducted on samples of the soft to medium clay to obtain the pertinent engineering properties. These include consolidation tests, unconsolidated-undrained (UU) triaxial compression tests, direct shear tests, and K_o-consolidated, undrained (CK_oU) triaxial compression and extension tests. All test results are also included in the Appendix A.

In order model the strength of the clay correctly, the maximum past pressure of the clay stratum must be determined. From the consolidation test data, the maximum past pressure (σ'_p) profile was obtained (by Casagrande construction) together with information on the compression ratio (CR), and recompression ratio (RR) for the clay. The in-situ stresses and maximum past pressure profile are shown in Figure 3.4. The best estimated line (Finno, 1989) is used in the following calculations to represent the OCR because the measured maximum past pressures from oedometer tests were lower than the in-situ effective stresses (σ'_{vo}). Most of the data for maximum past pressure are lower than the vertical effective stress profile. This suggests that the samples originally have maximum past pressures close to the in-situ effective stresses, and sample disturbances reduce the estimated maximum past pressures below the in-situ vertical effective stresses. Therefore the over-consolidated ratio is estimated as OCR ≈1.1.

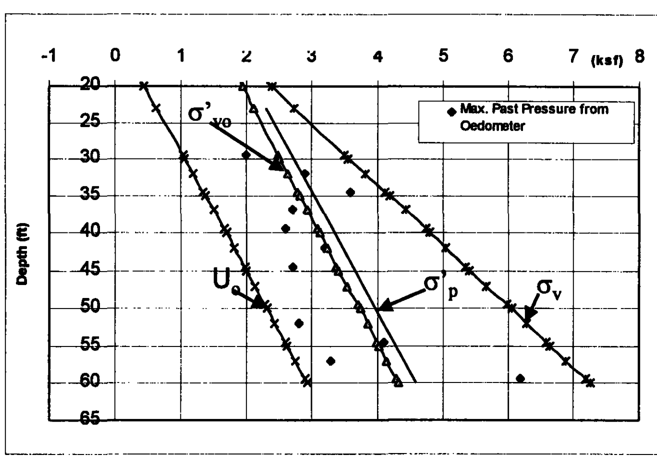

FIGURE 3.4 APPROXIMATE STRESS PROFILE AT NORTHWESTERN NGES

For the stiff clay the stress history profile is back calculated from undrained field vane strength tests using SHANSEP normalized strength parameters. The relationship between the undrained shear strength ratio, (S_u/σ'_{vc}), and OCR is described by the following relation (Ladd & Foott, 1974):

$$\frac{Su_{FV}}{\sigma'_v} = S(OCR)^m$$

For the soft to medium clay, both OCR and Su_{FV} profiles have been obtained (hence S= $(S_u/\sigma'_{vc})_{NC}$ = 0.216). However, the OCR profile for the stiff clay layer is not available because minimal consolidation data were obtained on samples from this stratum. Assuming m = 0.8 for typical CL clay, the stiff clay has the same normalized parameters (S and m) as the overlying soft clay, the OCR profile for the stiff clay stratum can also be determined. Table 3.2 presents the OCR calculation, and Figure, 3.5 illustrates the estimated OCR profile for NC and OC clay and OCR inputs for the MCC model.

Depth	Su_{FV}	Estimated σ'_v		S	
(ft)	(ksf)	(ksf)			
Soft to Medium Clay					
29.5	0.66	2.47		0.248	
34.4	0.82	2.78		0.277	
37.7	0.66	2.98		0.208	
41	0.74	3.17		0.220	
44.3	0.8	3.36		0.224	
47.6	0.82	3.58		0.217	
50.8	0.76	3.79		0.191	
54.1	0.86	3.97		0.206	
57.4	0.68	4.17		0.155	
			S_{avg}	**0.216**	
Stiff Clay					
			Back Calculated σ'_p	**Estimated OCR**	**Su/σ'_{vc}**
60.7	1.56	4.37	8.18	1.9	0.357
64	1.42	4.56	7.19	1.6	0.312
66.3	3.58	4.69	22.69	4.8	0.764
__ γ_t is assumed to be 120pcf					

Table 3.2 Summary of Using SHANSEP to Estimate OCR Profile for Stiff Clay.

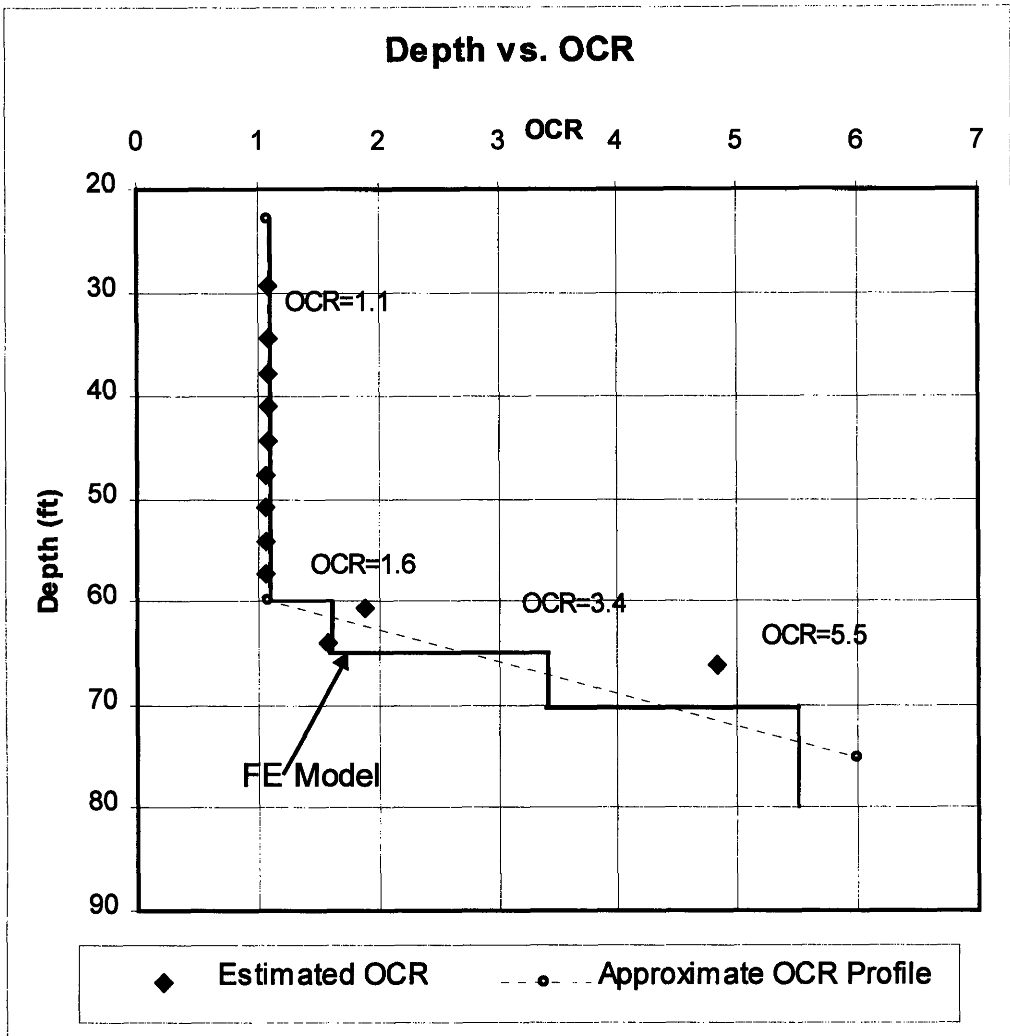

FIGURE 3.5 APPROXIMATE OCR PROFILE OF THE NORTHWESTERN NGES

In addition to strength properties of the soil, consolidation parameters and elastic and plastic properties are also obtained from consolidation tests. The hydraulic conductivities at different depths of the NC soil are back-calculated from the oedometer test data assuming constant m_v for each load increment. Void ratio is assumed to vary linearly with log k_v (hydraulic conductivity in the vertical direction) and the in-situ k_v is interpolated from the best-fit line. The calculations of k_v at different depths are included in the Appendix B, and the k_v profile for the soft to medium clay is shown in Figure 3.6.

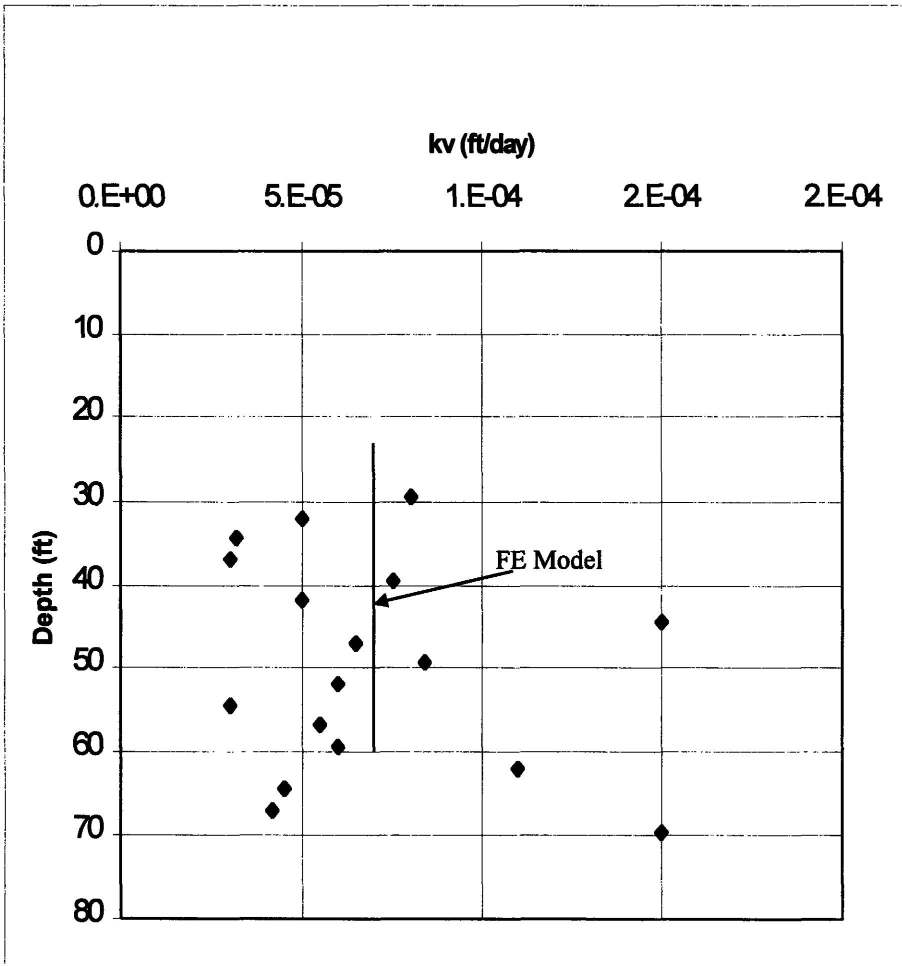

FIGURE 3.6 VERTICAL HYDRAULIC CONDUCTIVITY PROFILE AT TEST SITE

Since only a few consolidation tests are performed on the OC clay, k_v for OC clay can be interpolated from the best fit line of water content vs. log k_v. The water contents are obtained from boring samples from OC clay. The best-fit line is plotted in Figure 3.7, which shows the empirical correlation between water content and hydraulic conductivity. Finally, elastic and plastic stress-strain parameters of the MCC model are determined by κ^* and λ^* respectively. These parameters are obtained from the average RR and CR values from the consolidation tests and are assumed constant for soft and stiff clay layers.

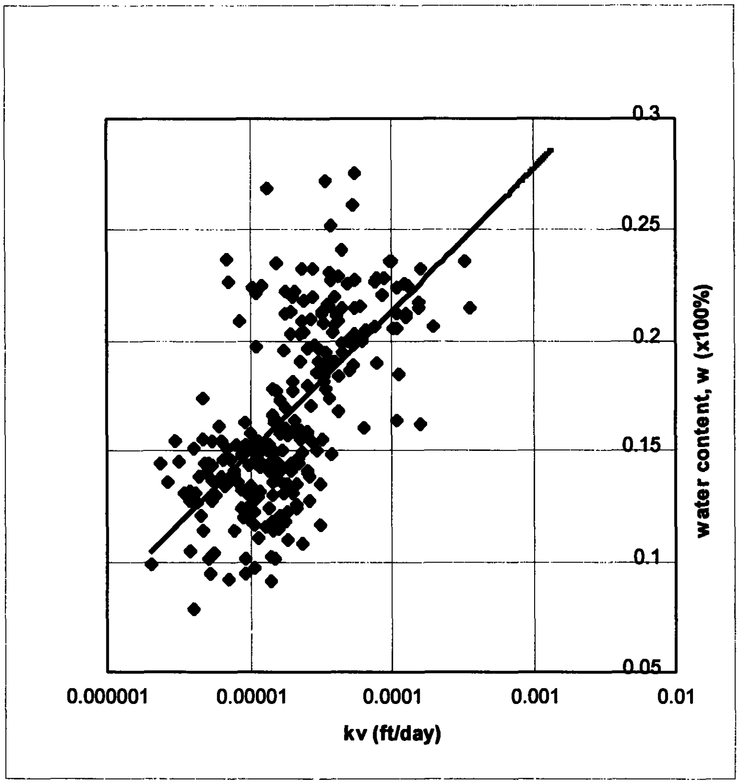

FIGURE 3.7 CORRELATION OF HYDRAULIC CONDUCTIVITY WITH WATER CONTENT

For other soil strata, either correlations from geotechnical publications or in-situ tests results are used to estimate properties. The elastic modulus of the sand layer is determined from dilatometer tests, and the sand layer is assumed to be free draining. The internal friction angle for the sand layer is interpreted from standard penetration tests performed by Woodward Clyde and STS consultants. The SPT data are corrected from N to $N_{1\,60}$ (Skempton, 1986) with published correlations, leading to a friction angle, $\phi' = 37^{\circ}$. The calculations are shown in the Appendix B. For the hard silt stratum, the elastic modulus , the internal friction angle and the hydraulic conductivity are obtained from correlations (Hasaab, 1951; Hough, 1957; Lambe & Whitman, 1969). The dolomite bedrock is assumed to have infinite stiffness and free draining. Finally, the soil profile of the Northwestern site with all the relevant properties is shown in Figure 3.8.

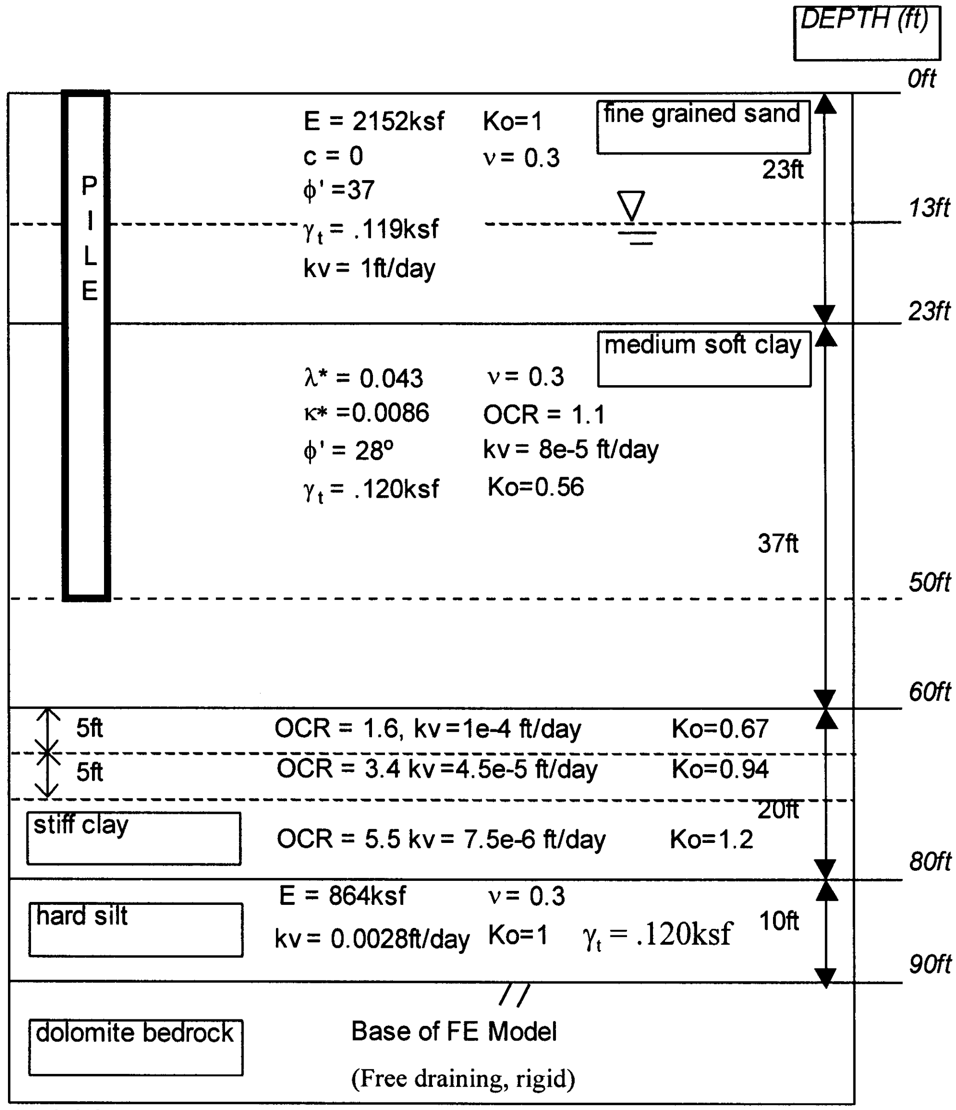

FIGURE 3.8 SOIL PROFILE AND PROPERTIES OF THE NORTHWESTERN TEST SITE

3.3 Analyzing the Pile Load Test of the Northwestern Site

In modeling the pile load tests at NGES, the following steps are taken to fully understand the how the solutions from current design procedure and FE modeling with MCC model differ from the actual monitored data:

1) Comprehensive capacity designs are performed on all tested piles.

2) Elastic solutions for single pile are used to estimate initial pile stiffness.

3) A FE model is set up to estimate the capacity and load-settlement response of all tested piles.

4) More in-depth analyses are performed to estimate the distribution of stress.

5) Compare design and FE results with monitored data.

3.3.1 Properties of Tested Piles

Since the design and modeling methods used in this thesis are based on solid cylindrical pile geometries, all properties of non-solid cylindrical piles must be transformed to represent the equivalent axial stiffness. For the 18" hollow steel pipe pile, the axial stiffness is much lower than the stiffness of a solid pile therefore the elastic modulus of steel is multiplied by (area of steel pipe/area of a solid steel pipe). For the 14*73 H pile, the failure mode is assumed to be rectangular, as shown by the dotted lines in Figure 3.9.

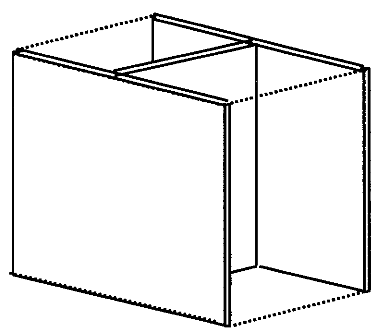

FIGURE 3.9 EXPECTED FAILURE MODE OF H PILE

The H pile is assumed to mobilize the soil between the webs during failure, and therefore, the soils within provide no addition capacity. Then an equivalent diameter, ϕ, of the H pile can be obtained by setting perimeter of the dotted rectangle equal to $\pi\phi_{eq}$. The equivalent axial stiffness of the H pile is obtained using the same method for the hollow pipe pile. For the concrete drilled piles, no modification is needed since both piles are solid and cylindrical. The modified pile properties are listed in Table 3.3.

Pipe Pile			H Pile 14*73					Drilled (cased/slurry)		$E_{concrete}$ (ksf)	
ϕ (ft)	Thick-ness (ft)	$E_{eq.}$ (ksf)	ϕ_{eq} (ft)	Tip Area (ft^2)	Width (ft)	depth (ft)	$E_{eq.}$ (ksf)	ϕ (ft)	E (ksf)	$7.2X10^5$	Tested Piles Length (ft)
										$E_{concrete}$ (ksf)	
1.50	0.03	$3.6X10^5$	1.50	0.15	1.22	1.13	$3.6X10^5$	1.50	$7.2X10^6$	$4.3X10^6$	50

Table 3.3 Properties of Piles Tested in Northwestern NGES.

3.3.2 Piles Capacity Analyses with Current Design Procedure

In order to obtain an approximate understanding of the capacity and the settling behavior of the pile, and evaluate pile design procedure, the four test piles are analyzed with current design methodologies. Both capacity and settlement analyses are performed, and they will be described respectively. The capacity of a single pile can be separated into two components, 1) skin friction and 2) end bearing. Since all pile tips are located in the soft to medium NC clay, the bearing capacity of a pile with 0.75 ft radius is relatively small compared to skin friction capacity[2]. Therefore, end-bearing capacity is neglected in the analyses for all four piles.

Skin friction capacities, f_s, for driven and drilled piles are estimated with the same methods but different parameters. However, no distinction is made between H and pipe-section piles and between the cased drilled or the slurry installed drilled piles since they all have equal equivalent diameter. For skin friction in the top 23 ft of sand, skin friction for driven and drilled piles can be estimated with the following procedure proposed by Poulos & Davis (1980):

$$fs = \sigma'_{vs} K_s \tan\delta'; \quad \phi^* = 0.75\phi'+10°\,(driven\,pile); \quad \phi^* = \phi'-3°\,(drilled\,pile)$$

$$d_c / \phi = critical\,embedment\,ratio; \quad d_c = critical\,embedment\,depth;$$

2 $9S_uA_b = Q_b = 9(3.5ksf)(0.21)(.44ft2) \approx 3kips$

The critical depth can be obtained using the design chart (Poulos & Davis, 1980) with the corrected friction angle, ϕ^*. For depth above the critical depth, d_c, σ'_{vs} is equal to the effective vertical stress, and depth greater than dc has σ'_{vs} equal to the effective vertical stress at the critical depth. $K_s \tan\delta$ can be obtained using the uncorrected friction angle and the design chart for either driven or drilled piles. Other methods in estimating f_s are suggested by, Vesic (1970), and Tomlinson (1973) and the relative density of the sand is used in obtaining f_s from the design charts.

Skin friction within the clay stratum is estimated using α and β methods. Nevertheless, it is commonly known that the α methods produce better estimates of f_s for OC clays while the β methods produce better estimates for NC clay. The α method uses the undrained shear strength of the soil to estimate f_s, while β method uses the pile penetration length, L, in the clay and the in-situ effective vertical stress to estimate f_s. For driven piles, design charts from Tomlinson (1971), API (1981), Peck (1961), and Dennis & Olson (1983) are used for the α method. For the β method, design charts suggested by Meyerhof (1976) and Burland (1973) are used for the driven piles. For drilled piles, skin frictions in clay are only estimated with the average β factor suggested by Kulhawy & Jackson (1989). The following equations summarize α and β method for estimating skin frictions.

$\underline{\alpha \, Method}$	$\underline{\beta \, Method}$
$fs = \alpha Su$	$fs = \beta\sigma'_{vo}$
$\alpha = f(Su)$	$\beta = f(L)$

Results from different design charts are averaged for both α and β methods to give an average capacity for the α method and an average capacity for the β method. Finally, the skin friction capacities for the sand and clay layers are added together, as shown in Table

3.4, to determine the overall capacity of the piles. Details of capacity calculations are provided in Appendix C.

Driven Piles	$Q_{fs\ low}$ (kip)	$Q_{fs\ avg}$ (kip)	$Q_{fs\ high}$ (kip)	Drilled Piles	$Q_{fs\ low}$ (kip)	$Q_{fs\ avg}$ (kip)	$Q_{fs\ high}$ (kip)
Method	*Vesic*		*Poulos*		*Poulos*		*Vesic*
sand	98	115	132	sand	39	47	54
Method	α		β		β		β
clay	58	89	119	clay	317	317	317
Total	156	204	251	**Total**	356	364	371

Table 3.4 Capacities for Pile Design Using Various Methods.

Although same methods were used to estimate skin friction for driven and drilled piles, but the empirical parameters have values that are quite different from one another. For driven piles, skin friction in sand is much higher when compared to drilled piles, as drilling causes densification of the sand during pile driving. On the other hand, the parameters for driven piles account for the loosening of sand during drilling; therefore, the capacity of skin friction in sand is reduced. The shaft resistance of drilled piles is much higher than for driven piles. This result reflects a bias associated with installation effects of driven piles (large excess pore water pressure are measured during installation).

3.3.3 Settlement Analysis with Load Transfer Method

Elastic stiffness solutions for single piles, given in section 2.3, are used to estimate settlements for the tested piles. The original solution for single layer of soil is modified to incorporate two soil layers, (top sand and the clay layers). The load transfer method predicts that pile head settlement increases linearly with load, (constant pile head stiffness). The shear modulus for the two layers are taken from the average results of the dilatometer tests, and the shear modulus profile is shown in Figure 3.10. Due to the differences in equivalent axial stiffness, the load transfer solutions for the drilled concrete piles are slightly different from the driven pile; however, steel pipe and H piles have nearly identical pile head stiffness. The solutions are presented in Figure 3.11, and detailed calculations are included in Appendix C.

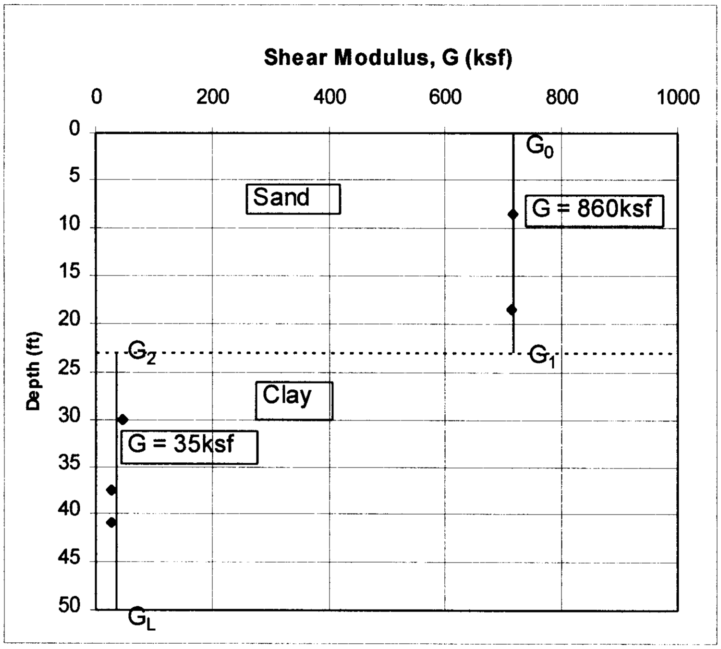

FIGURE 3.10 SHEAR MODULUS PROFILE FOR LOAD TRANSFER METHOD

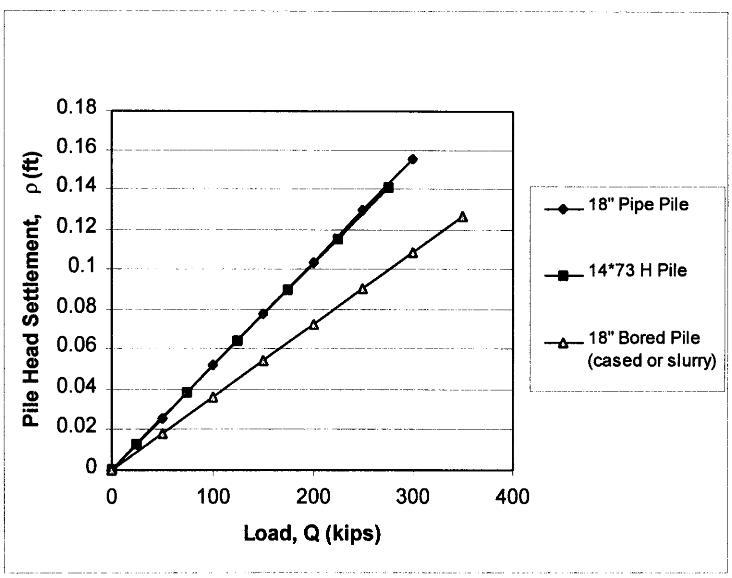

FIGURE 3.11 SETTLEMENT ANALYSIS WITH LOAD TRANSFER METHOD

3.3.4 Finite Element Analysis

In setting up the axisymmetric model for the FE analysis, the mesh is first created with several considerations in mind. The mesh extends to a depth of 90ft and laterally to 150ft, in order to minimize the effects of boundary conditions on predicted load-displacement results. The selected boundary conditions do not permit any lateral displacement at far field lateral boundaries (or centerline) while radial and vertical displacements are prevented at the base of the mesh. Horizontal mesh lines are created at the transitions from one soil to the other. Mesh lines are also denser around the pile due to the high concentration of stresses around that region, and one would also predict failure to occur close to the pile shaft.

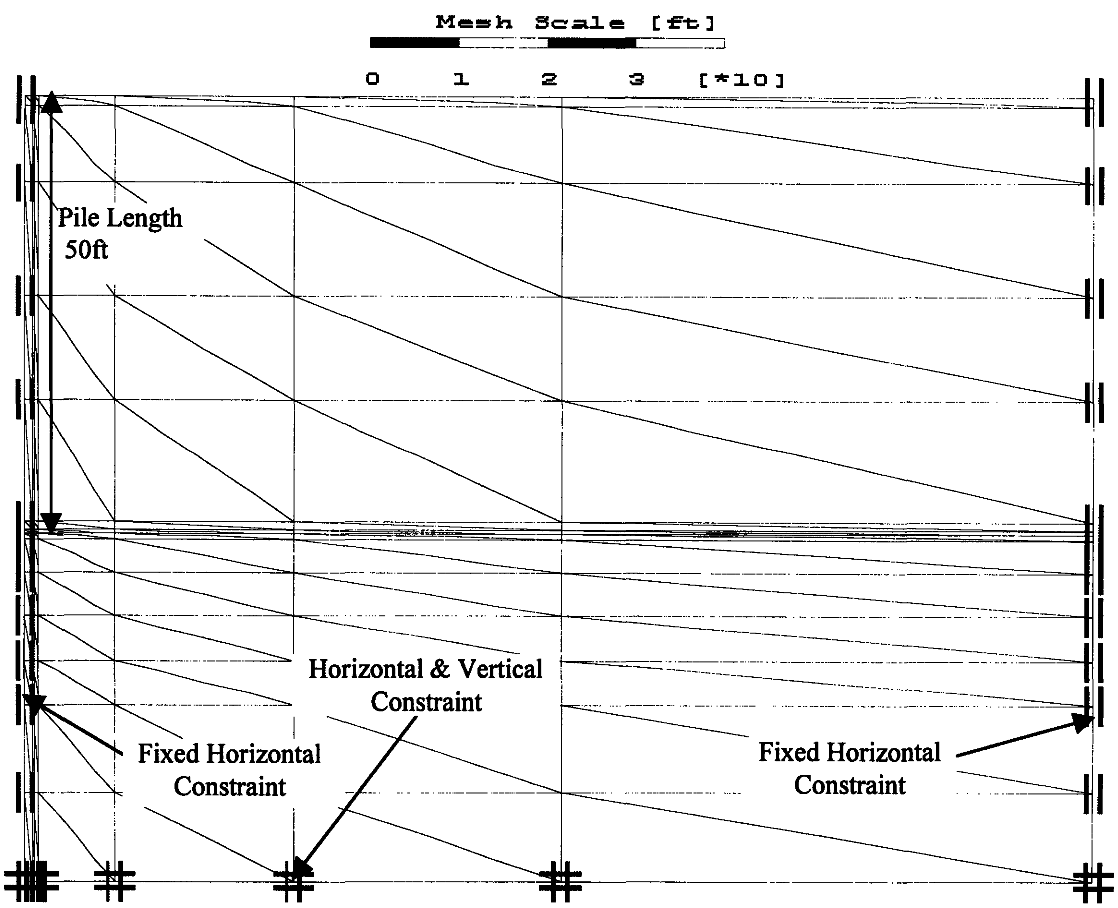

FIGURE 3.12 FINITE ELEMENT MESH FOR THE NORTHWESTERN PILE LOAD TEST ANALYSIS

The pile is represented by a linear elastic model with equivalent stiffness parameters (Table 3.3). The Mohr-Coulomb model is used to model the top sand and the hard silt at the base. The clay stratum is divided into four layers with increasing OCR, and all layers are modeled with the MCC model (Figure 3.8). The initial stress condition is also required for the FE model. For the sand, and silt layers, it is assumed that $K_o = 1$. For the clay layers, the initial condition is derived from empirical equations shown below (Mayne & Kulhawy, 1982):

$$K_o = (1 - \sin\phi')(OCR)^{\sin\phi'}$$

Once the model is constructed, loading is applied in increments until failure occurs. Different loading time rate are also applied to explore the effect of consolidation on the pile head settlement. Table3.5 summarizes the capacities and the settlements at maximum loading for the piles. More detailed comparison are presented in the next section.

	Pipe Pile	H Pile	Drilled Piles
Load Capacity (kip)	232	234	235
Pile Head Settlement (in)	0.439	0.383	0.339

Table 3.5 Capacities and Settlements of Piles from FE Analyses

3.4 Comparison of Analyzed Results with Measured Data

The capacities and settlements of the piles from the two types of analyses are first compared with the monitored data. Then the stress distributions from the FE analyses are compared with data measured along the pile.

3.4.1 Comparison of Pile Capacities

Different predicted capacities are compared with the actual measured short and long-term capacities in Figure 3.13.

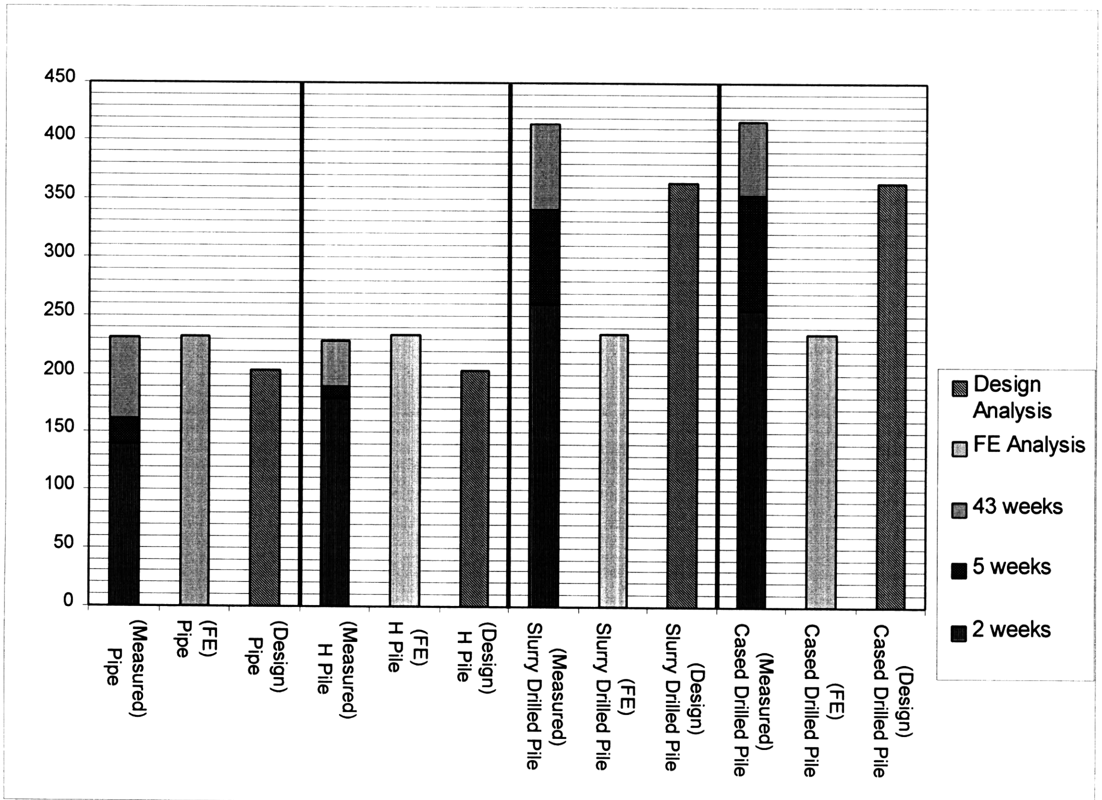

FIGURE 3.13 COMPARISON OF ESTIMATED PILE CAPACITIES WITH MEASURED CAPACITIES

The measured data shows that the long-term capacities both between the driven piles and between the drilled piles are within 1% of one another. Nevertheless, the capacities of drilled piles are 80% higher than the capacities of driven piles. The vast difference between the capacities of the drilled and driven piles is possibly caused by installation disturbance. The results in Figure 3.12 also show that FE analysis estimates the capacities of the driven piles very close to the measured long-term capacity. However, the FE analyses underestimate the measured capacities of the drilled piles by more than 40%. The capacities for drilled shafts and driven shafts estimated by FE analyses are almost identical because the FE model is unable to distinct the pile installation procedures, and the only difference between drilled shaft model and the driven shaft model is the modulus of the pile. This parameter should only influence the settlement of the pile head. For design analysis, the capacities of both driven and drilled piles are underestimated. For driven piles, the design calculations underestimate the measured capacity by about 15%. However, the empirical design calculations do distinguish differences in installation between driven and drilled piles using empirical correlations. This leads to a decrease in skin friction in the sand and an increase in skin friction in clay with the β method. The overall effect is an 80% increase in total capacity from the design capacity of driven. Nevertheless, the design capacity is 13% below the actual measured capacity.

3.4.2 Evaluating Pile Settlement Results

Settlements are recorded in the 2, 5, and 43 weeks pile loading tests, and the results of the monitored data are shown in Figures 3.14,15 and 16 respectively. In all cases, the pile head stiffness reduces as loading increases (due to progressive mobilization of the shear resistance along the pile shafts), and all of the tested piles are expected to have similar initial stiffness at the beginning of loading, with only slight variations due to differences in the axial stiffness of the piles. The Figures show that the initial pile head stiffness (from about 0 to 50 kips of loading) of the tested piles are indeed similar to one another in all tests performed. However the data for the 43 weeks (after installation) tests are much more consistent than those obtained at 2 and 5 weeks.

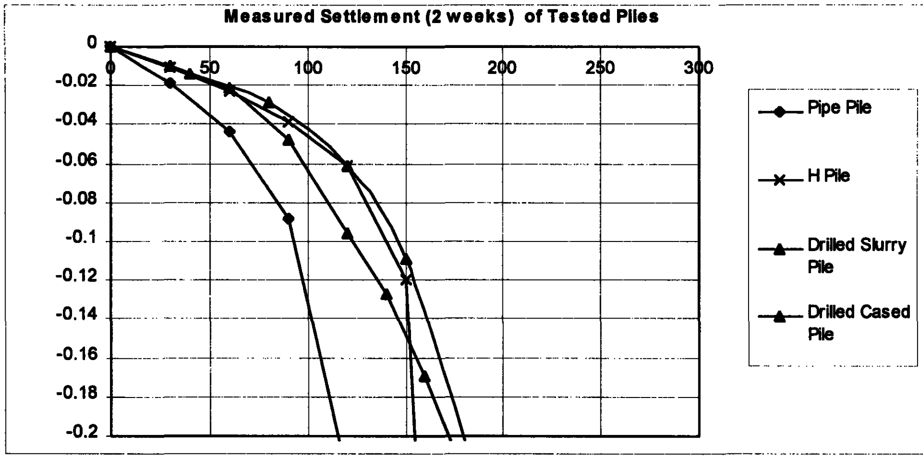

FIGURE 3.14 MEASURED SETTLEMENT OF PILE LOAD TEST PERFORMED 2 WEEKS AFTER INSTALLATION

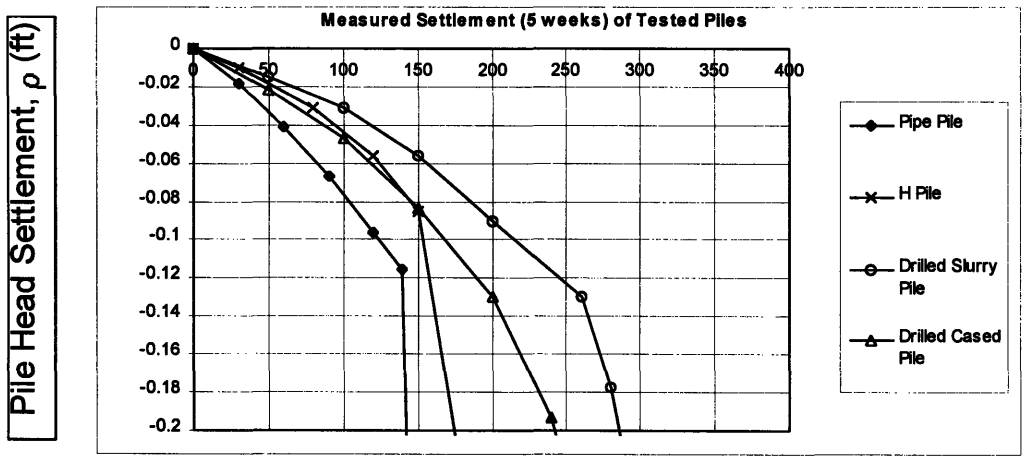

FIGURE 3.15 MEASURED SETTLEMENT OF PILE LOAD TEST PERFORMED 5 WEEKS AFTER INSTALLATION

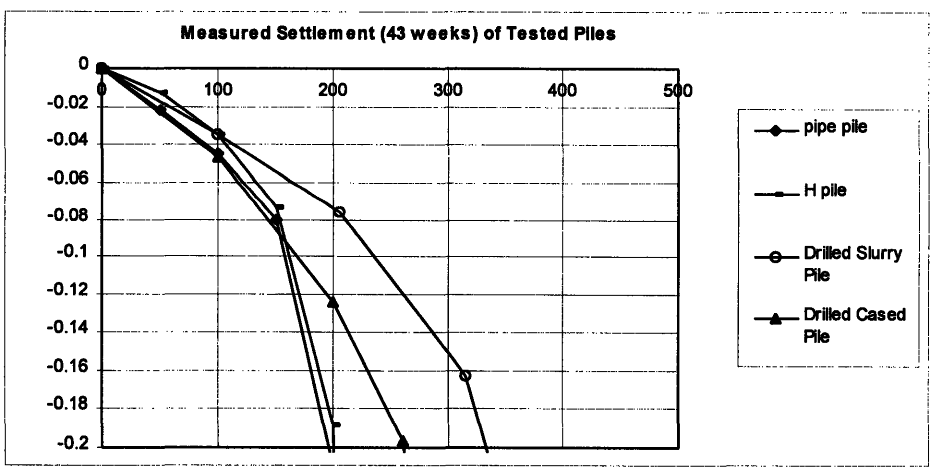

FIGURE 3.16 MEASURED SETTLEMENT OF PILE LOAD TEST PERFORMED 43 WEEKS AFTER INSTALLATION

The differences between the initial pile head stiffness of the tested piles are mainly caused by installation. For driven piles, pile driving causes excess pore pressure to build up within the clay layer and hence, reduce the stiffness of the surrounding clay. Therefore, the initial stiffness for driven pile is lower than the drilled piles. The reduction of the stiffness is controlled by the amount of soil displaced by the pile. Table 3.7 shows total volume of soil displaced by the pile.

Amount of Displaced Soil				
	ϕ (ft)	Drilled ϕ (ft)	Length (ft)	Displaced Vol. (ft^3)
Pipe Pile	1.5	1	50	49.1
Slurry Drilled Pile	1.5	1.5	50	n/a.
Cased Drilled Pile	1.5	1.5	50	n/a.
	H Area (ft^2)	**Drilled ϕ (ft)**	**Length (ft)**	**Displaced Vol. (ft^3)**
H Pile	0.15	0	50	7.5

Table 3.6 Volume of Soil Displaced by the Tested Piles

The hollow pipe pile with a cover plate displaces the most amount of soil even when the pile is installed in a 1ft diameter pre-augured hole. Results in Figure 3.14 clearly show that the pipe pile has the softest stiffness in the load test performed 2 weeks after installation.

In the FE analysis, an attempt is made to simulate the actual loading schedule in the test sites. Therefore, loading is applied in increments with a fixed time gap separating each increment. The FE model analyzes three configurations, which include load rates that are 1) instantaneous loading, 2) 50kips per 2 hours, and 3) 50kips per 4 hours, of loading rate. Results for the H pile and the drilled pile (cased or slurry) are shown in Figure 3.17 and 3.18. Both Figures show that the consolidation settlement is relatively insignificant with loading less than 100kips, 40% of the failure load of the model predicts. Significant settlements are generated after the pile is loaded to 150kips and

200kips. Nevertheless, consolidation increases the mean effective stress, **p'**, of the soil, which in turn increases the stiffness of the soil.

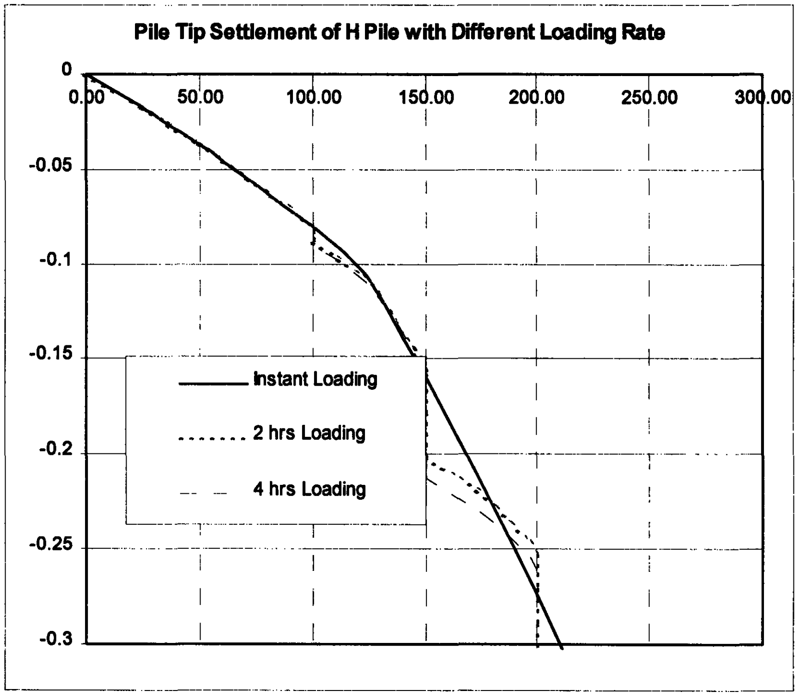

FIGURE 3.17 SETTLEMENT OF H PILE WITH DIFFERENT TIME RATE LOADING

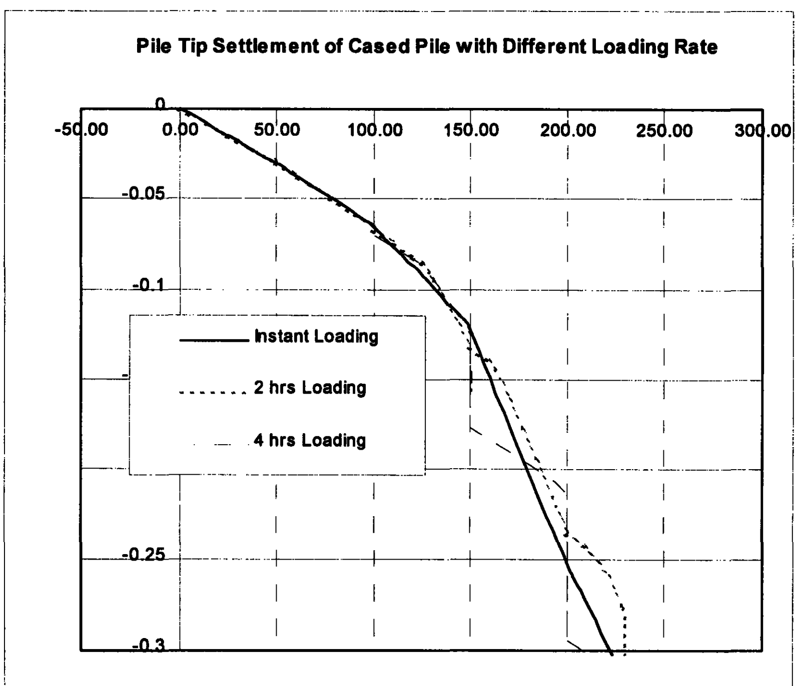

FIGURE 3.18 SETTLEMENT OF DRILLED PILE WITH DIFFERENT TIME RATE LOADING

As mention earlier, both elastic and shear moduli of the soil are a function of **p'**. When time gaps are increased, both consolidation settlement and the mean effective stress also increase. Therefore, when two models' pile head stiffness are compared at the same load increment, the model with larger time gap between each load increment has a higher stiffness. The results from the model also show that the increased pile head stiffness helps to compensate for the large increased settlement at the end of each load increment. Therefore, the final settlement of two different models may not differ significantly. The actual amount of difference in settlement will depend on the specific time frame. Since all settlement curves with time rate loading retains the shapes and also the amount of settlements of the instantaneous loading curves, the settlement comparison between different analyses will only include the settlement curves from instantaneous loading.

In comparing the settlement results from different analyses, all settlement curves for the same test pile are plotted on the same axes. Figures 3.19 to 3.22 show the settlement vs. load curves for pipe, H, slurry and cased piles respectively. In all four Figures, the load transfer method gives an excellent estimation of the initial pile head stiffness for the 43 weeks test. For most cases except for the cased drilled pile, the predicted pile head stiffness is too high for the 2 and 5 weeks load tests. Since the load transfer method does not take installation disturbance into consideration. However, the initial pile head stiffness from 2, 5, and 43 weeks tests match extremely well with the estimated value from load transfer, and the close match is contributed by the low level of disturbance. First of all, the installation does not displace any soil. In addition, before installing the concrete pile, a steel casing is installed before concrete is tremied to reduce the amount of disturbance.

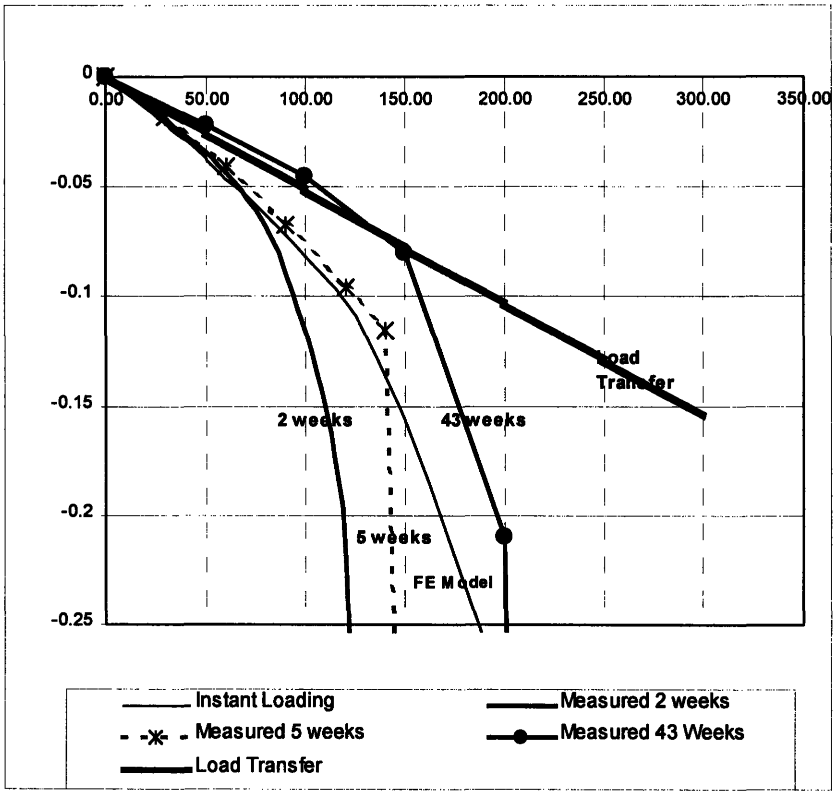

FIGURE 3.19 COMPARISON OF SETTLEMENT ANALYSES WITH MONITORED DATA FOR PIPE PILE

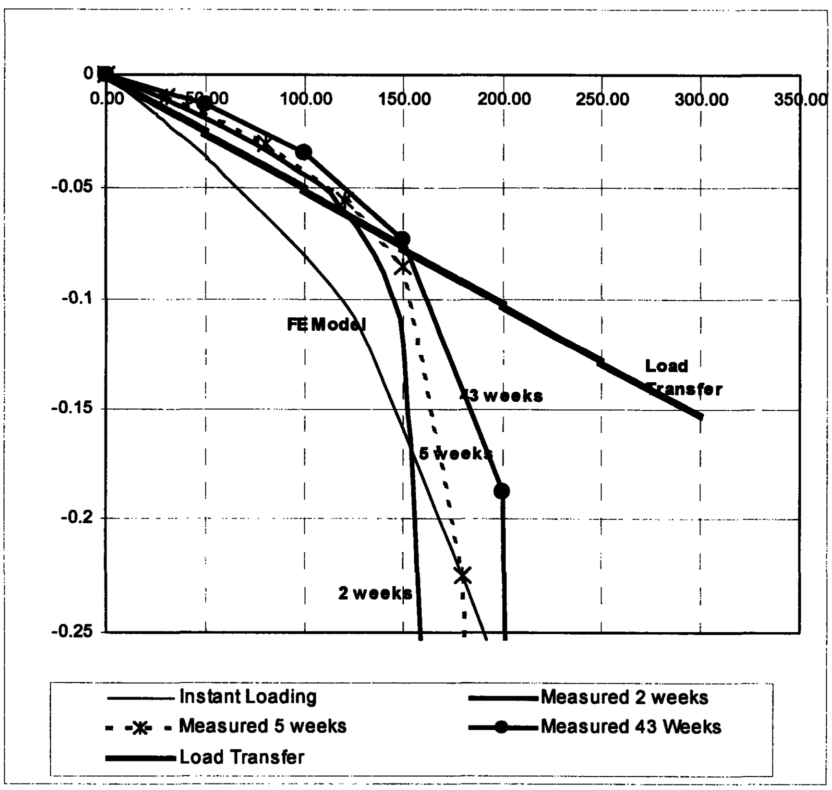

FIGURE 3.20 COMPARISON OF SETTLEMENT ANALYSES WITH MONITORED DATA FOR H PILE

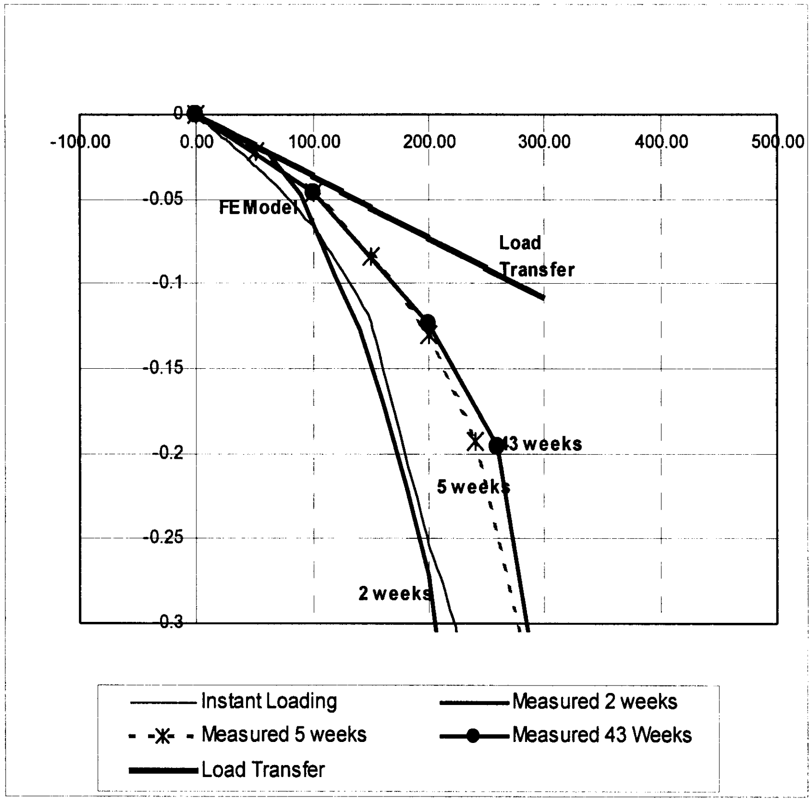

FIGURE 3.21 COMPARISON OF SETTLEMENT ANALYSES WITH MONITORED DATA FOR DRILLED SLURRY PILE

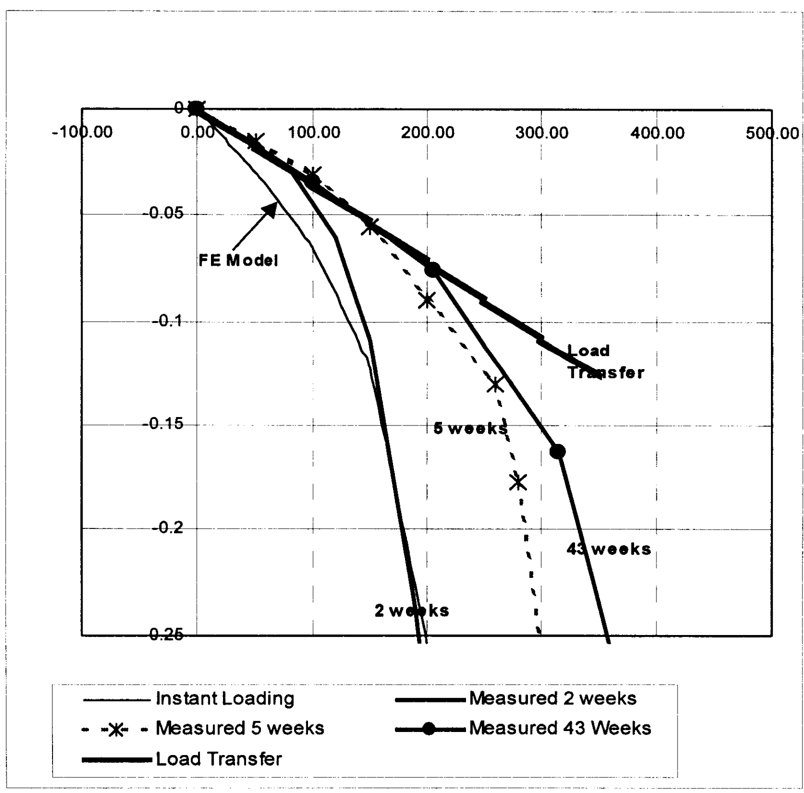

FIGURE 3.22 COMPARISON OF SETTLEMENT ANALYSES WITH MONITORED DATA FOR DRILLED CASED PILE

On the other hand, results show that settlements estimated by FE analysis seem to over predict the amount of settlement. With the MCC model for the NC clay, PLAXIS predicts load-settlement curves that match better with the 2 and 5 weeks load tests than 43 weeks load test. The low pile head stiffness predicted by FE analysis is mainly caused by how the MCC model estimates elastic straining. The MCC model uses the parameters, κ^* and ν, to estimate elastic strains, and the former is obtained from unload-reload data in 1-D oedometer tests. The value of κ does not represent closely the elastic shear stiffness of clay and may then cause an underestimate of pile stiffness. Since the initial pile head stiffness is mainly determined by the elastic deformation of the soil, which in turn is governed by κ^* in the MCC model, more attention is paid towards the applicability of κ^*. From the input κ^* for the MCC model, the shear modulus to undrained shear strength ratio, G/Su, can be estimated. The common range G/Su ratio has been published by geotechnical publications, and can be compared with the values used in the FE analysis. The values of G/Su used in the NC clay are estimated in Table 3.7.

Location	Depth (ft)	κ^*	Ko	σ'_{v0}	v	p (ksf)	G (ksf)	Su (ksf)	G/Su
Top of CL Clay	23	0.009	0.555	2.1	0.3	1.5	76.2	1	76.2
Mid. Embed. Depth in Clay	36.5	0.009	0.555	2.9	0.3	2.0	104.3	1	104.3
Pile Tip	50	0.009	0.555	3.7	0.3	2.6	172.0	1	172.0

Table 3.7 Estimations of Shear Modulus to Undrained Shear Strength

Using NC Boston Blue Clay as the reference CL clay, the range of G/Su (Ladd et. al, 1977) is between 150 to 300 for the factor of safety between 1.5 to 3. This shows that κ^*

underestimates the stiffness of the clay when the actual factor of safety is above 1.5, (say Q<250 /1.5 = 166kips). Therefore, several more models for the cased drilled pile were analyzed with κ^* reduced or the shear modulus increased to understand the effect on the initial pile head stiffness. Results, shown in Figure 3.23, clearly shows that the initial pile head stiffness converges with the measured stiffness as κ^* is reduced. Furthermore, even though the pile head stiffness is increased by increasing κ^*, the capacities of the pile remain constant throughout. In the MCC model, the capacity is determined by the CSL, and not by κ^*. This shows that the critical state line of MCC does predict the capacity of the driven piles accurately and κ^* is a the parameter that causes the analyzed response to deviate from measured response. In analyzing long-term behavior of the driven piles, if κ^* is adjusted accordingly, FE analysis can actually predict both the settlement response and the ultimate capacity of the pile quite accurately. On the other hand, the behavior of the drilled shafts in this study are far more difficult to estimate, since the installation of the piles includes the injection of bentonite. Although bentonite is removed before the concrete is pumped, small percentage of bentonite remains at the interface between the pile and the clay. The chemical effects at the interface are not modeled in the FE analyses, but if the percent of strength gain due to bentonite injection is determined in laboratory testing, then interface elements can be added to the FE model to analyze drilled shafts more precisely.

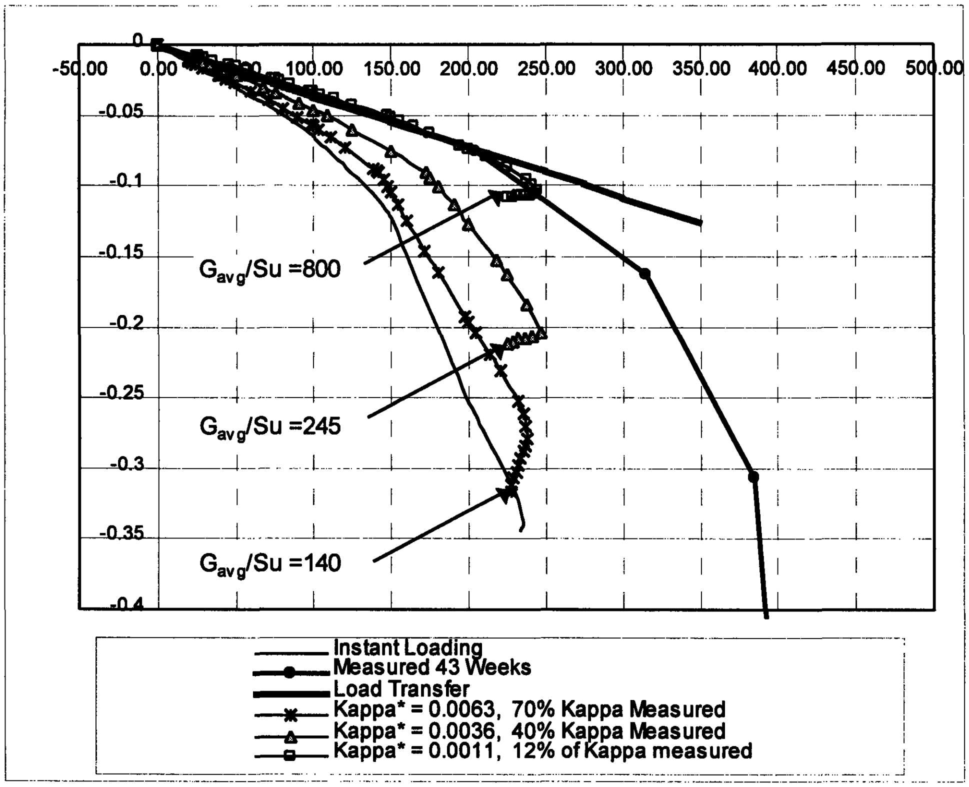

FIGURE 3.23 THE EFFECT OF κ^* IN PILE HEAD SETTLEMENT

3.4.3 Evaluating Skin Friction Distribution

Based on the measured axial load distributions along the length of the pile, the skin friction of the test piles can be back-calculated. These values are compared with the results from FE analysis, and the results are shown in Figure 3.24 to 3.26 for pipe, H, and drilled piles, respectively. Since the FE model setup for both drilled piles are identical (cased and slurried pile), all drilled piles data are presented in Figure3.26. Results from FE analysis shows that the predicted skin friction distributions for driven piles are lower than the measured values. Therefore, much of the load is transferred to the pile tip and supported by the end bearing, which compensates the reduced skin friction. Nevertheless, the general shape of skin distribution predicted by FE analysis matches with the measured shape for driven piles. Figures 3.27 and 3.28 show the predicted amount of loads that are support by skin friction and pile tip for pipe and H pile. Results clearly show that skin friction from sand and clay support a big portion of the total load except in the beginning of loading or when load reaches failure. The distributions of the loads carried by skin friction and end bearing for the drilled piles are shown in Figure 3.29. However, FE analysis does not predict closely the skin friction distribution for the drilled piles. Although the capacities for the drilled piles are much higher, the measured total skin friction (approximately 100kips) is slightly lower than the estimated skin friction (105 kips) from finite element analysis. This suggests that the measured skin friction maybe incorrect or much of the load may have been supported by the pile tip (very unlikely). The discrepancies in the skin friction distribution are probably caused by installation procedures that are not captured by the model.

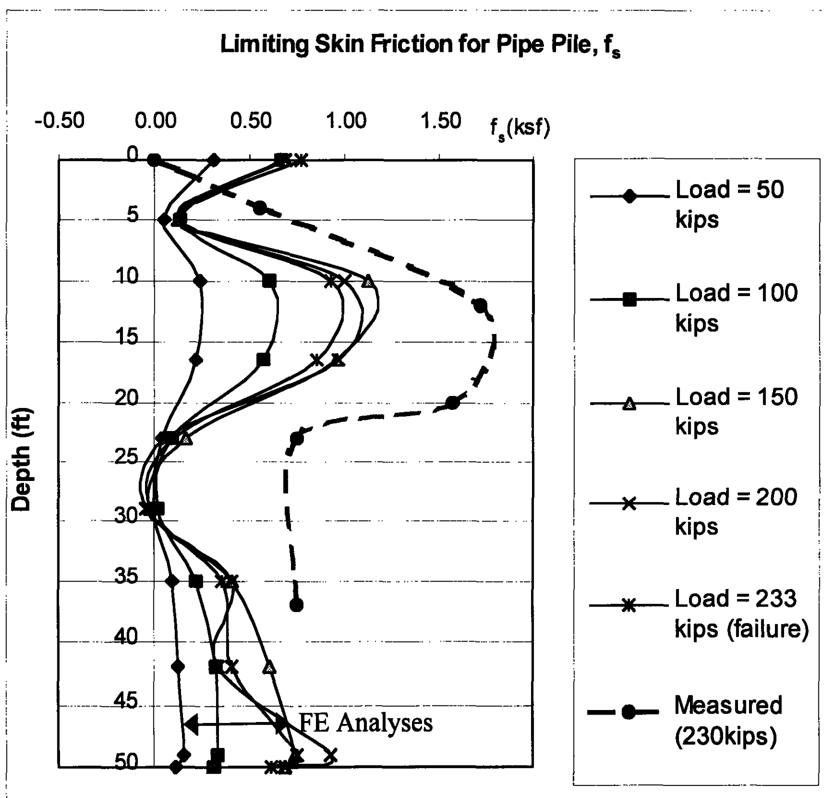

FIGURE 3.24 COMPARISON OF SKIN FRICTION DISTRIBUTION FOR PIPE PILE

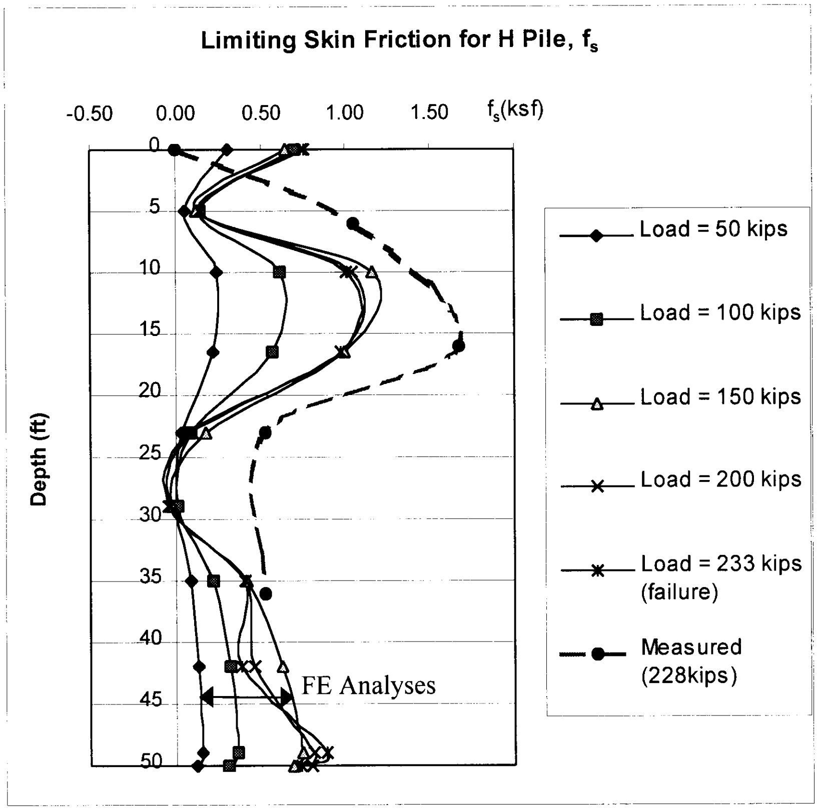

FIGURE 3.25 COMPARISON OF SKIN FRICTION DISTRIBUTION FOR H PILE

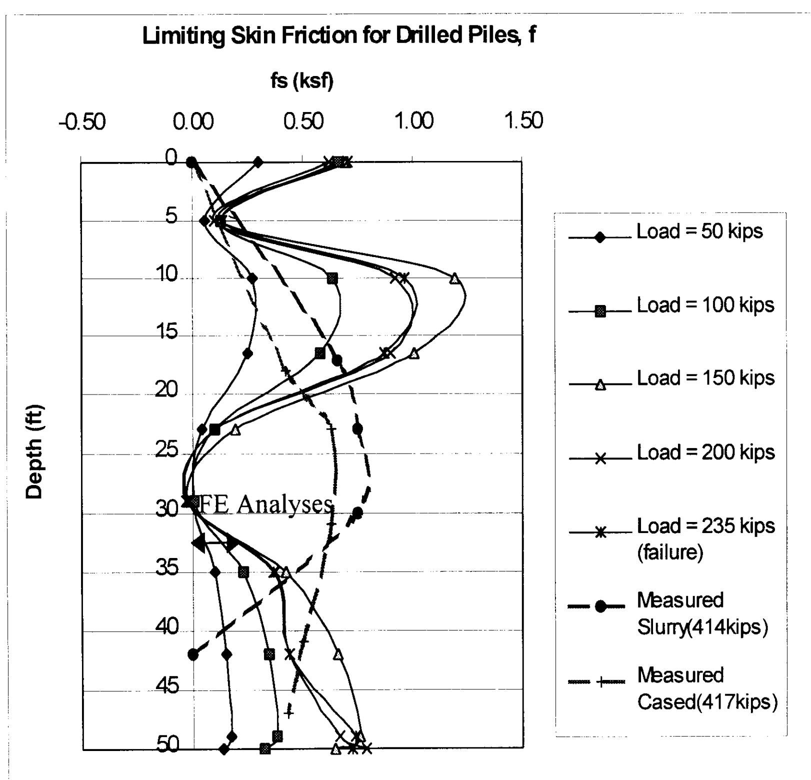

FIGURE 3.26 COMPARISON OF SKIN FRICTION DISTRIBUTION FOR DRILLED PILES

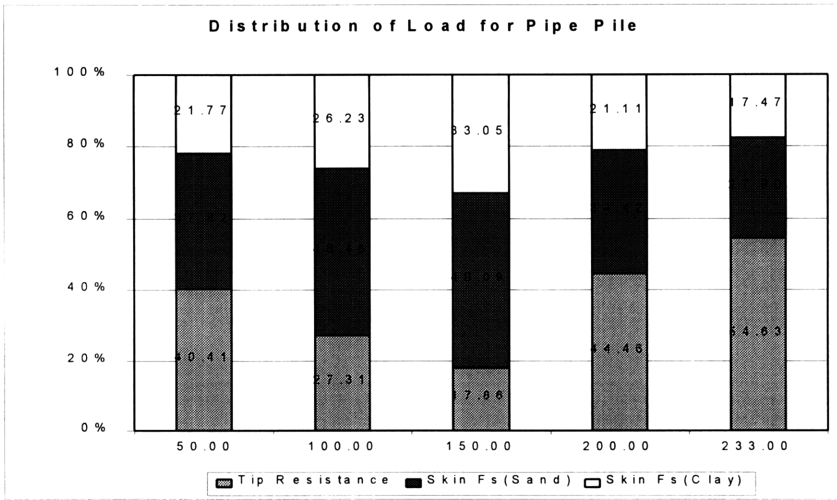

FIGURE 3.27DISTRIBUTION OF LOAD FOR PIPE PILE

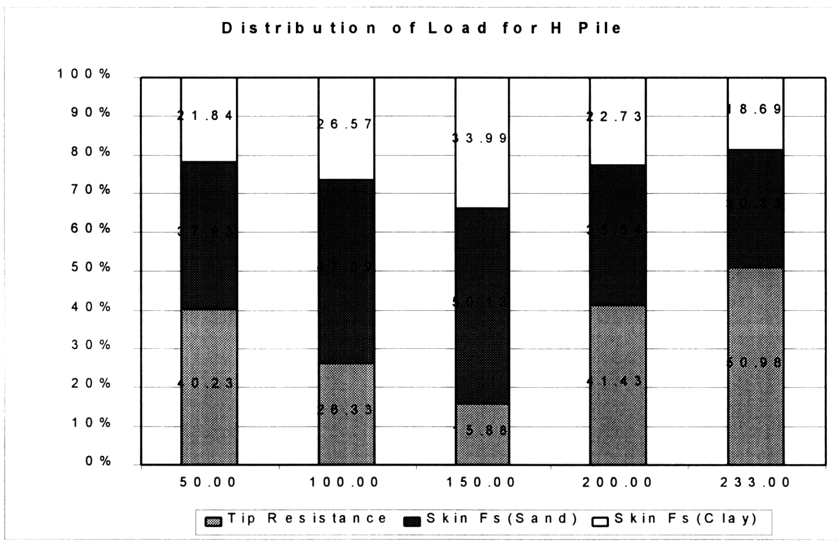

FIGURE 3.28 DISTRIBUTION OF LOAD FOR H PILE

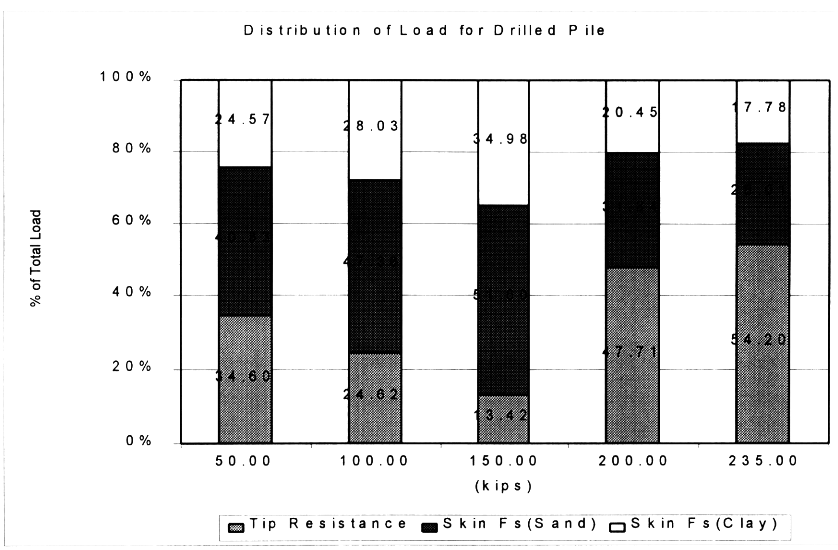

FIGURE 3.29 DISTRIBUTION OF LOAD FOR DRILLED PILES

3.5 Summary

Conventional design calculations and FE analyses have been compared with instrumented pile load test data from the NGES site at Northwester University. Although the design calculations underestimate the capacity of the drilled piles, the average design value is much closer than the values obtained from FE analysis. However, FE analysis seems to better predict the capacity and the skin friction distribution of the driven piles. The measured capacities for the driven piles are within one percent of estimated value with FE analysis. Nonetheless, capacity results from design analysis would improve and approach the measured capacities if end-bearing capacities in clay were also included. In settlement analyses, both design and FE analyses can not accurately predict the settlement of a single pile. The merits of load transfer method are its ability to predict the initial pile head. However, load transfer underestimates settlements at higher loads, and therefore, higher factor of safety is needed to lower the load within the predictable region of the curve. Nevertheless, predictable regions are different with different pile and installation procedure. For the pipe pile, measured settlements exceed the predicted values when the applied load is over 65% of the pile capacity. However, only 13% of the pile capacity are needed for the cased drilled, and load transfer will be unconservative for any load higher than that. For FE analysis, the settlement response predicted is conservative in all cases. The elastic parameter, κ^*, for the MCC model underestimates the stiffness of the clay and may not actually represent the actual response of the soil. However, less conservative may be obtained if κ^* is corrected according to the published G/Su data. On the other hand, FE analysis is able to capture the long-term pile capacity when installation effects are dissipated. This is shown by its 1% error in estimating the capacity of pipe and H-pile. The discrepancies between the estimated capacities and the measured capacities of drilled pile are related to the installation procedure and interface properties that are not modeled reliably in the analyses. In general, FE analysis with the MCC model will produce conservative settlement results due to the non-linear relationship between load and settlement, and the low initial pile head stiffness. However, the load-transfer method should only be used with high factor of safety in order to produce conservative result. In capacity analyses, both design and FE analyses predicted capacities that match closely with the long-term capacities of driven pile. For drilled pile, more understanding of the pile-soil interface is needed in order to create a more accurate FE model.

Chapter 4 Settlement Analysis of a Storage Building at Jernbanetollsted, Oslo

In addition to calculation for single pile analyses, this chapter describes the use of finite element analyses for predicting the settlement behavior of a piled raft foundation. The analyses are then compared with the measured settlement record for 50 year monitoring period (Anderson & Clausen, 1974). This problem is chosen for the analysis because it involves long term settlement of a heavily loaded building on a deep layer of compressible soft clay.

4.1 Background and Details of Site

This case study concerns the settlement of a six-story high storage building that was constructed in Oslo between 1919 to 1924 (Anderson & Clausen, 1974). The plan view of the building is shown in Figure 4.1. The structure is separated into two wings, A and B divided by a contraction joint.

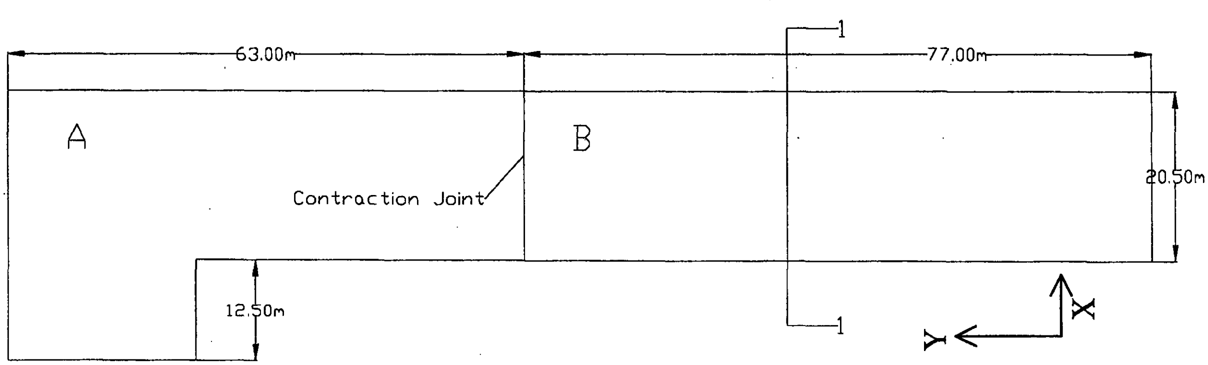

FIGURE 4.1 PLAN VIEW OF STORAGE BUILDING FOR FINITE ELEMENT ANALYSIS

Therefore, the whole structure can be treated as two separated buildings. The chapter presents FE calculation for the foundations of building B. The foundation comprises reinforced concrete slab supported by approximately 2500 wooden piles, with top diameter 0.15m and length of the piles 9m.

The soil profiles of the site is typical of conditions along the Drammen River in the Oslo area, comprising a silt crust overlying soft marine clay of moderate sensitivity. The top fill, placed during the construction period, consists of 3m of sand and gravel. The water Table also lies at the top of this layer. Beneath the fill, 7m of silty clay overlay 1.5 m of thin clay crust. The bottom layer is a 68.5m of fairly homogeneous of marine clay. The top 7.5m of the clay has relatively higher plasticity than the rest of the 61m of clay layer. The bedrock is at a depth of 80m. During the summer of 1968, the Norwegian Geotechnical Institute (NGI) performed a detailed investigation of the site including, 1) extensive fixed piston sampling (45mm ϕ) from within one borehole (extending to a depth of 30m); and 2) three vane borings to a similar depth. Six piezometers were also installed to monitor the presence of excess pore pressure. Thirty-two consolidation tests were run on the samples and the results of the geotechnical investigation are shown in Figure 4.2. From consolidation data and experiences of other sites, it is believed that the 61m of lean clay is NC and has an OCR close to 1.0. In addition, pore pressure and vertical stresses profiles after the placement of the 3m fill at different depths are given in Figure 4.3.

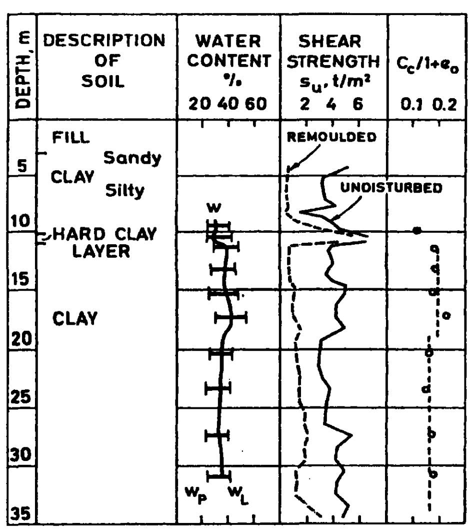

FIGURE 4.2 SUMMARY OF THE 1968 NGI GEOTECHNICAL INVESTIGATION IN OSLO

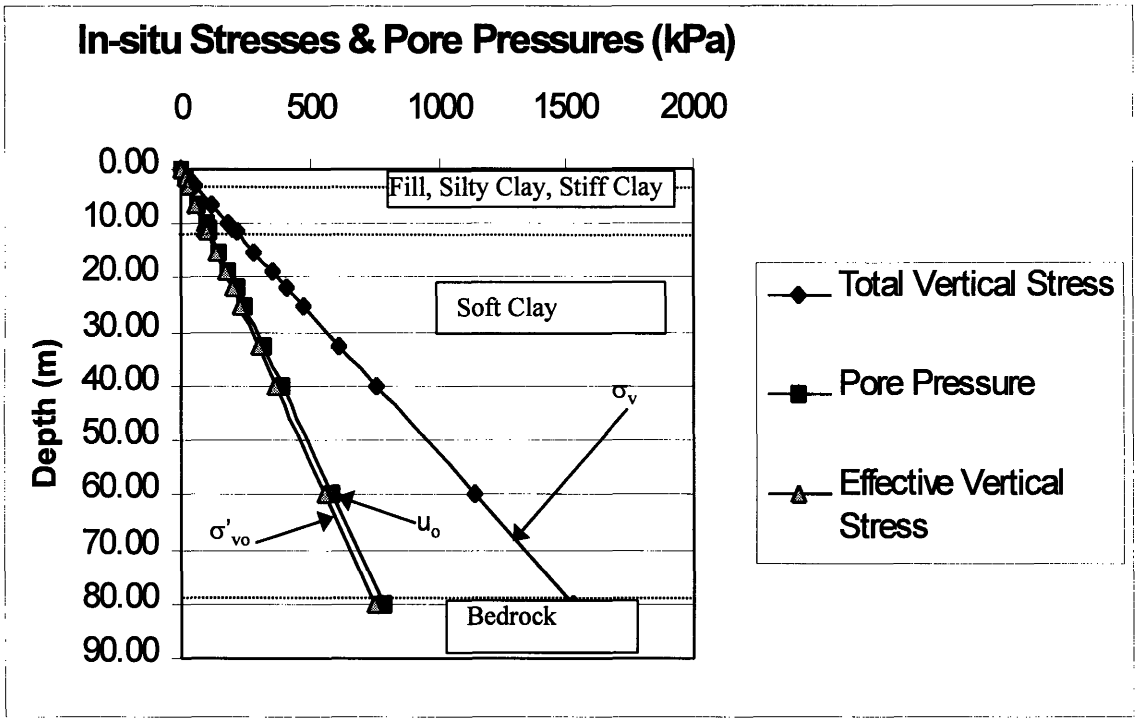

FIGURE 4.3 PORE PRESSURE AND STRESS PROFILE

4.3 Method of Analyzing Settlement

Finite element analysis will be used to analysis a cross-section of the site. The cross section located at the middle of building B is shown in Figure 4.1 section 1.1. Several assumptions are made before proceeding with FE analysis. Since the model is limited to two-dimensional loading condition while the actual geometry is 3-dimensional, the predicted settlements should be slightly larger than measured results. The load of the building is assumed to be similar to 2-D loading strip loading. This assumption is reasonable for section 1-1 due to the large aspect ratio (length/width) of the building. Therefore, plane strain instead of axisymmetric analysis are used in this problem. Due to the symmetry of the problem, only half of the section 1-1 will be analyzed. Figure 4.4 shows the boundary conditions, for deformation and flow, and the section of the foundation that are modeled in this analysis.

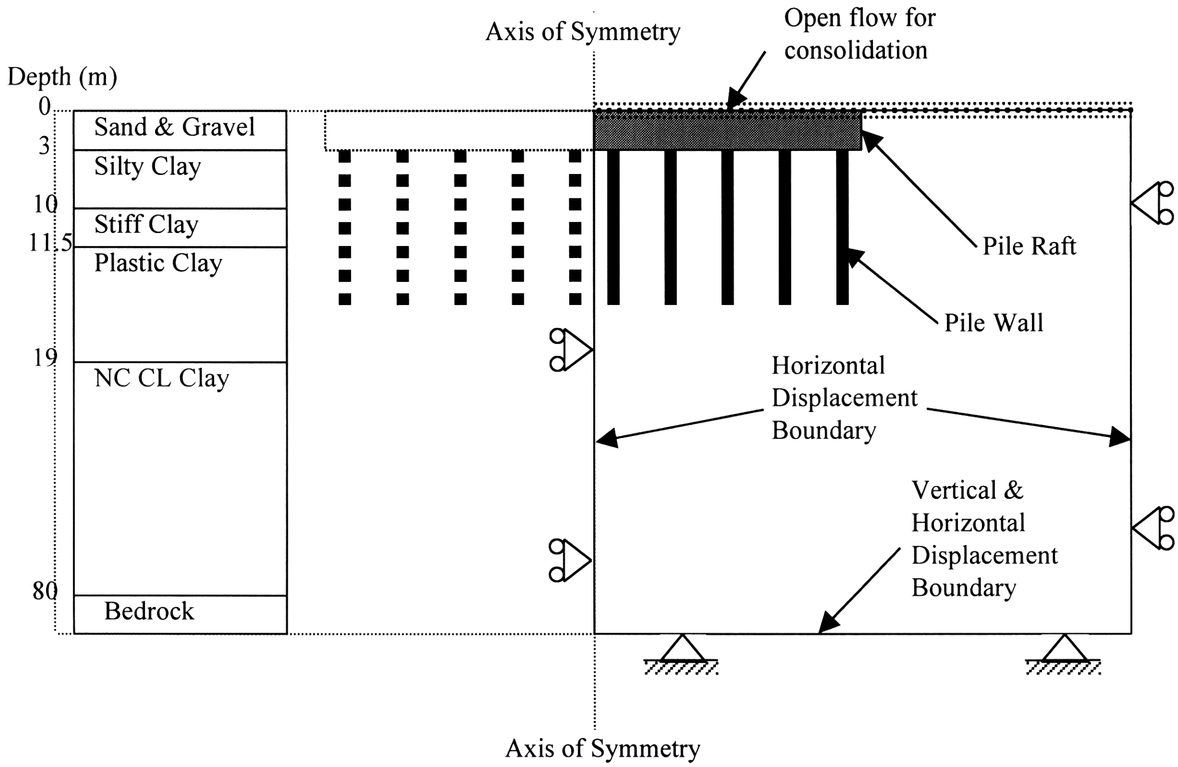

FIGURE 4.4 SECTION 1-1, DESIGNED SECTION

Figure 4.4 also shows the five different soil layers of soil that will be modeled in FE analysis. The properties of the soil layers will be discussed later. The bedrock is set at the base of the finite element model. The dotted section (half of the raft and piles) is not included in the FE modeling due to the symmetric properties of the problem. For the flow boundary, drainage is assumed to occur at the top only.

In modeling the piles, it is impossible to model 2500 piles individually. Instead rows of piles are modeled as equivalent pile wall. For this section, 5 pile walls are used to model approximately 1250 piles within half of the foundation (or 10 pile walls for the full foundation). In figure 4.5, an example of the pile wall is shown to illustrate how the pile wall represents the piles. The wall in the figure is similar to the one that is used in the model, except this wall only represents three piles.

The following equation shows the relationship between the modulus of the piles and the modulus of the 2 pile walls

$$E_{eq.\,wall\,1}A_{wall\,1} = \sum E_{pile\,1,n}A_{pile\,1,n} = EA_{1,1} + EA_{1,2} + EA_{1,3}$$
$$E_{eq.\,wall\,2}A_{wall\,2} = \sum E_{pile\,2,n}A_{pile\,2,n} = EA_{2,1} + EA_{2,2} + EA_{2,3}$$

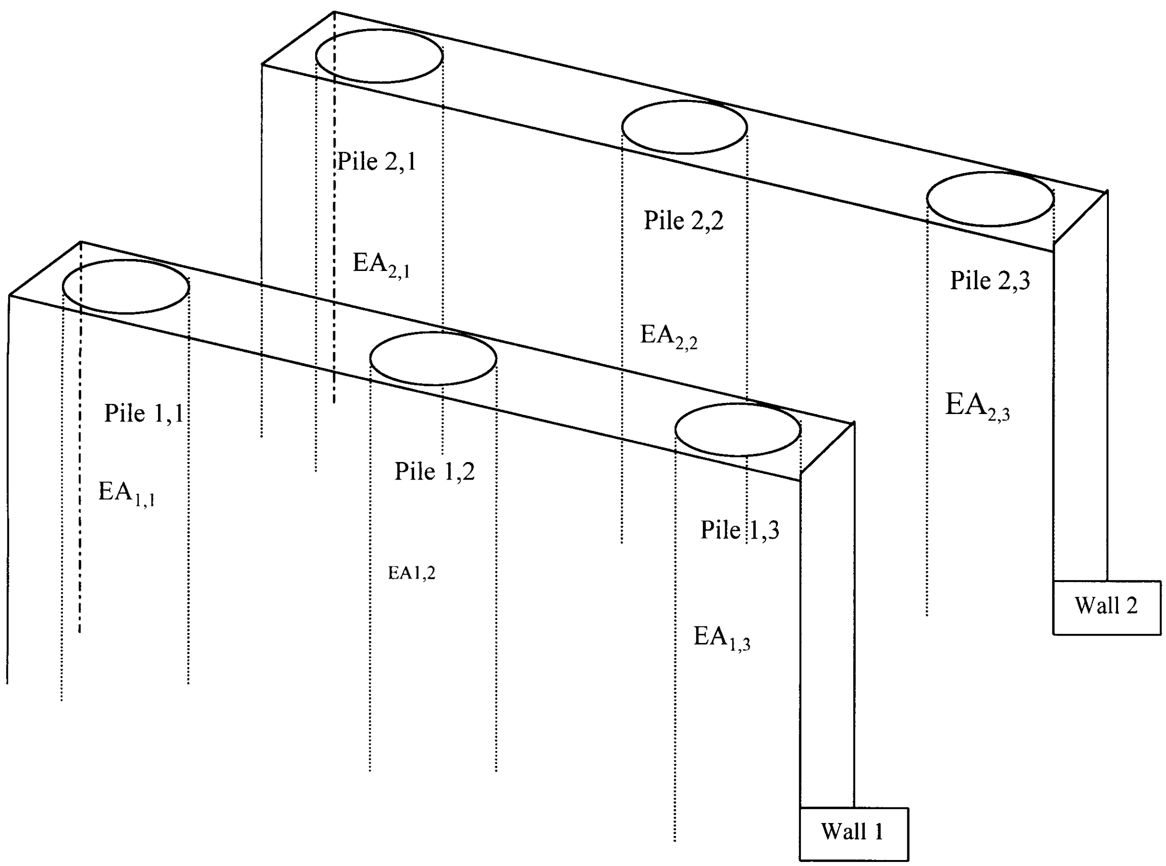

FIGURE 4.5 EQUIVALENT PILE WALL SETUP

For the FE model, each wall will represent 250 piles, and there are a total of 5 walls in the model (10 for the whole system).

4.4 Setting up Finite Element Analysis

After determining the methods in modeling the piles and the foundation, the Finite element model is set up accordingly. First, soil models are determined for the 5 different layer of soil. The following table shows the type of soil model that is used to represent each soil layer.

Depth (ft)	Soil Type	Soil Model
0-3	Sand & Gravel	Elastic Soil
3-10	Silty Clay	MCC
10-11.5	Stiff Clay	MCC
11.5-19	Plastic Clay	MCC
19-80	Lean NC Clay	MCC

Table 4.1 Soil Modeling for FE Analysis

With the soil model determined, the mesh is created. The dimension of the mesh is 70m by 80m (width by height). Then the width of the mesh was increased until the displacements of the concrete mat were not affected by the increased width. Finally, the width of the mesh is selected to be70m, about seven times the width of the section that is being modeled. The boundary conditions and the flow conditions are setup according to Figure 4.4.

In modeling the material properties for the pile, raft, and soil, two types of elements are used, wall and soil elements. Wall elements described in Chapter 2 are used to represent the pile walls. The typical modulus for timber is used to obtain equivalent parameters for the wall elements. Table 4.2 summarizes the parameters obtained for the wall elements. The entire cross section (instead of half) is used to calculate the pile wall properties; however, this would not influence the pile wall properties.

Entire Section Properties			
Total Area	Length	Width	Total # of Piles
(m2)	(m)	(m)	(#)
1579	77.0	20.5	2548
Pile Properties			
E_{pile}	$radius_{pile}$	A_{pile}	EA_{pile}
(kpa)	(m)	(m2)	(kN)
8.27E+06	0.075	0.018	1.46E+05
Pile Wall Properties			
Total # of Pile Walls	$Length_{wall}$	$width_{wall}$	A_{wall}
(#)	(m)	(m)	$(m^{2)}$
10.0	77	0.15	11.6
Total # of Piles per wall	Spacing btw. Pile Wall	$E_{wall\ eq.}$	Sum (EA_{pile})
(#)	(m)	(kpa)	(kN)
254.8	2.3	3.23E+06	3.73E+07

Table 4.2 Summary of Section, Pile, and Pile Wall Properties.

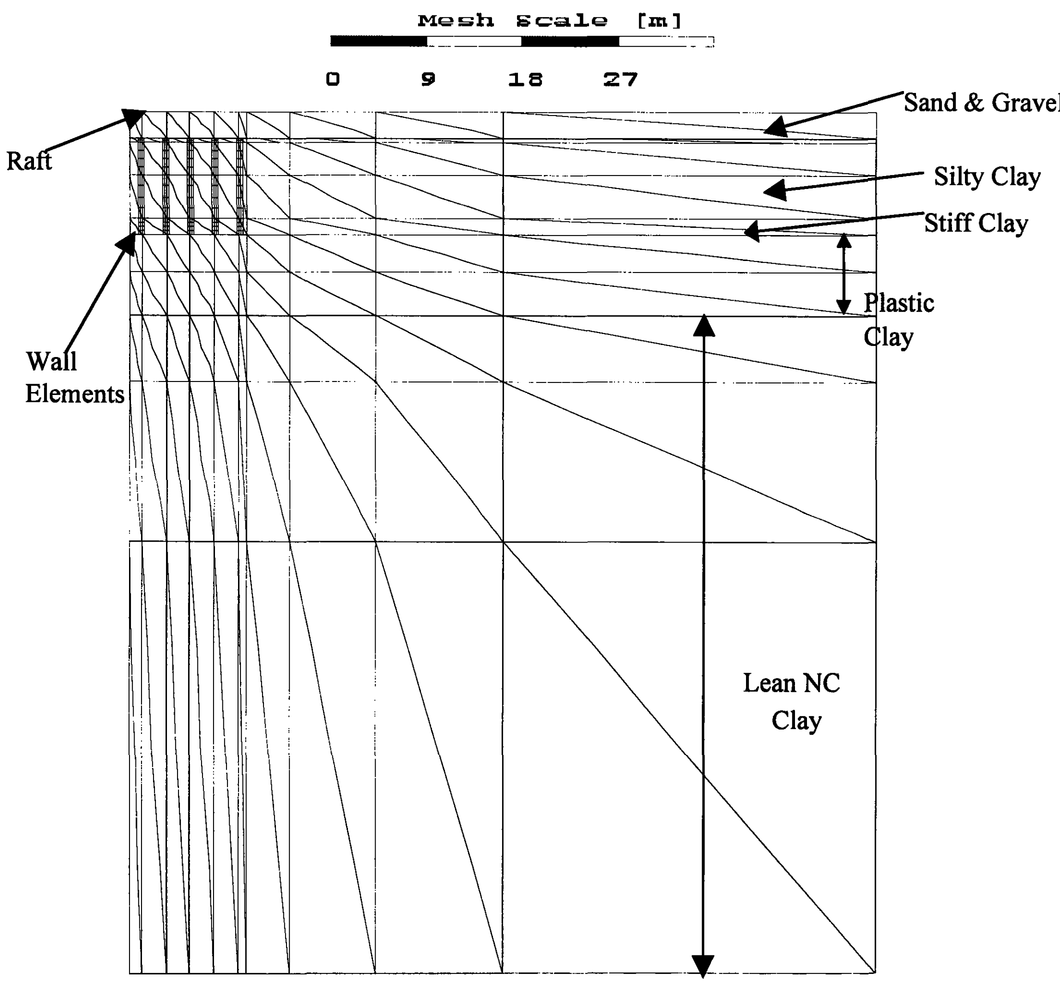

FIGURE 4.6 FE MESH FOR THE SETTLEMENT ANALYSIS OF THE STORAGE BUILDING IN OSLO

For setting up the soil models, more soil information is needed to define the parameters mainly for the MCC model. In order to obtain additional information regarding the OCR profile and compression index, soil properties proximate to Oslo are examined. Soil properties at Drammen (Bjerrum , 1967) are particularly useful because Drammen is located 40 kilometer from Oslo, and the soil profile of the two sites are very similar. One of the typical soil profiles in Drammen is given in Figure 4.7. This profile is used to estimate the OCR profile for the silty clay and plastic marine clay layers.

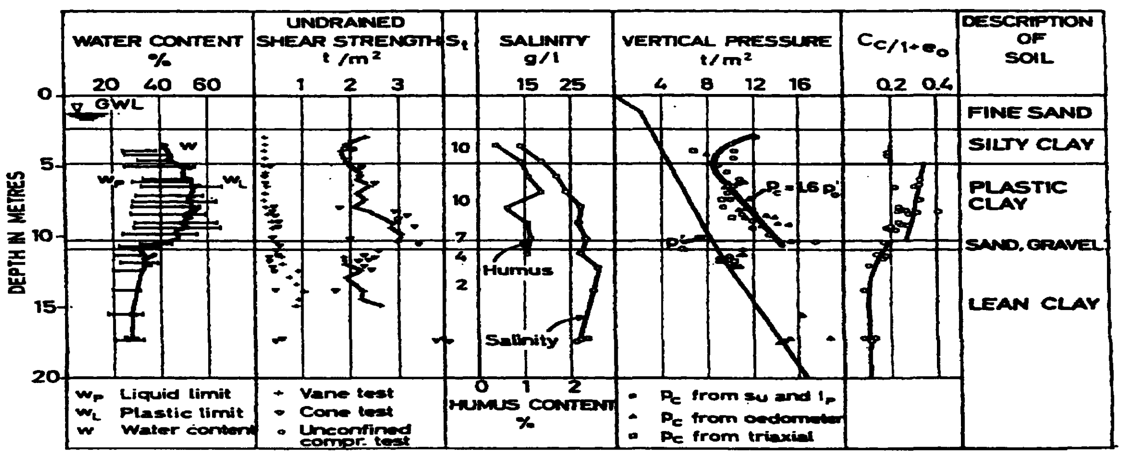

FIGURE 4.7 TYPICAL SOIL PROFILE IN DRAMMEN, (BJERRUM, 1967)

The OCR profile for the low plasticity marine clay is estimated to be NC from the consolidation tests performed by the NGI. For the stiff crust, all parameters are assumed to be equal to the plastic marine clay, and the OCR for this layer is approximately 3.0. The stiff crust should not influence the results from the FE analysis since it is relatively thin compared to all other soil strata and has little settlements during un-reloading. In addition to the OCR profile, it is also necessary to obtain the hydraulic conductivity of the soil. Hydraulic conductivity of the soil controls the rate of the dissipation of excess pore pressure. This in turn will control the rate of settlement. However, no information was found on this parameter. With no relevant information available, correlation (Lambe & Whitman, 1969) is used to obtain the range of permeability for naturally deposited clay. It is noted that naturally deposited clays have permeability ranging from 8.6e-5m/day to 8.6e-6m/day($1*10^{-7}$ to $1*10^{-8}$cm/sec). Therefore, the FE model will analyze settlement of the foundation with three different input values of permeability, $8.6x10^{-5}$, $4.3x10^{-5}$, and $8.6x10^{-6}$ m/yr. All other information used by the FE model is shown in Figure 4.8.

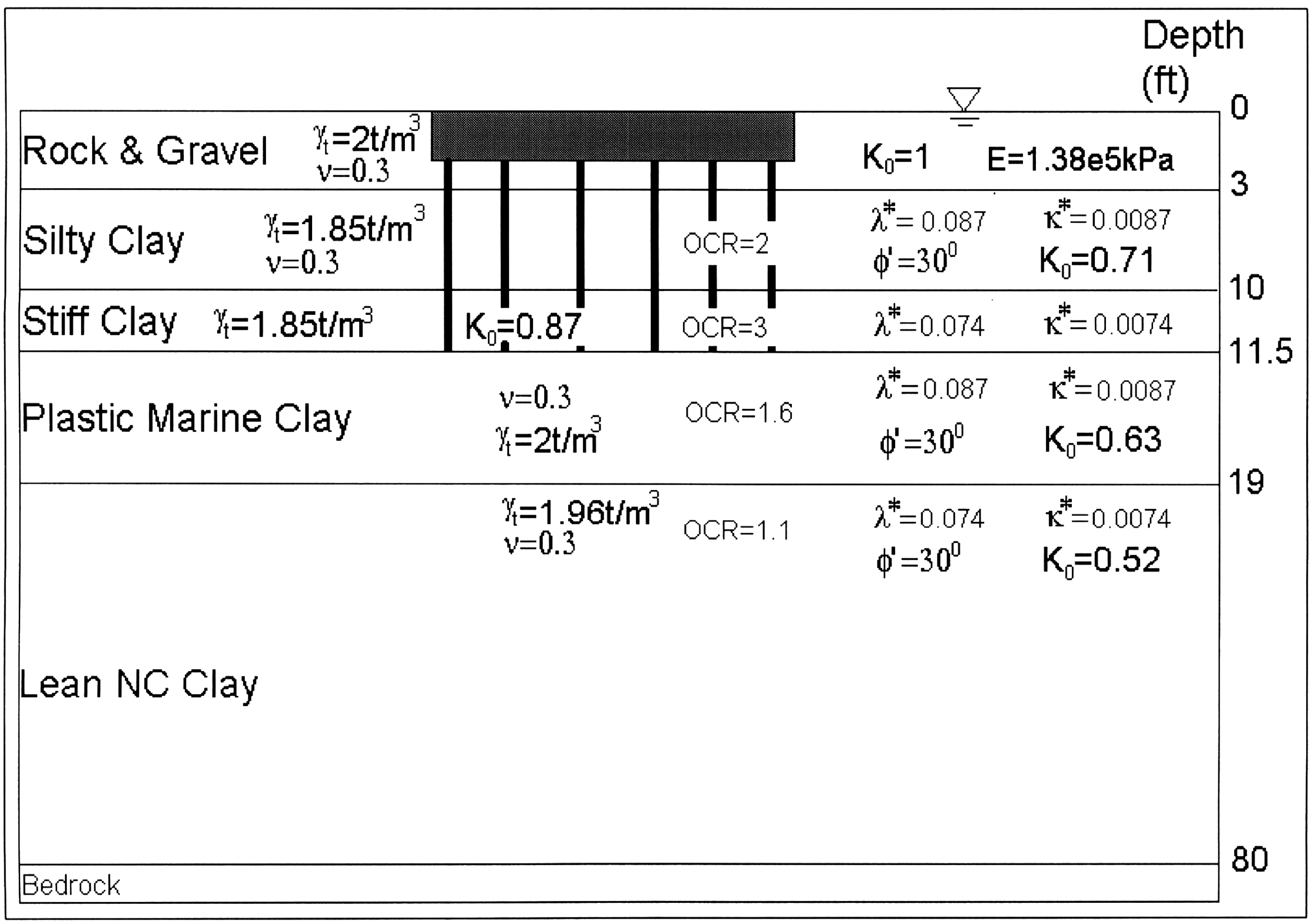

FIGURE 4.8 PARAMETERS FOR THE FE ANALYSIS

The initial loading/unloading of the site began at the end of 1919 (see figure 4.9) when construction began. Excavation of the top fill caused an unloading condition, and the unloading condition reached a maximum of $-5t/m^2$ by the end of 1920. Then the construction of the foundation and the structure causes a steady increase of load from $-2t/m^2$ (1921) to $3.2t/m^2$ (1924). After construction, the load remained constant (1924 to early 1925) until the storage building starts service. With a constant increase of storage, the live load increases the loading steadily from $3t/m^2$ to $9t/m^2$. Once the storage building reached the capacity, the dead load remains constant afterwards. Originally, the FE model is setup to replicate the actual loading condition; however, the length of the smallest possible time interval is controlled by the hydraulic conductivity of the soil. With smaller hydraulic conductivity, a larger time interval is necessary for accurate results. Therefore, the loading condition is simplified as linearly increasing from $0t/m^2$ (1922, beginning of recording settlement measurement) to $9t/m^2$ (1926).

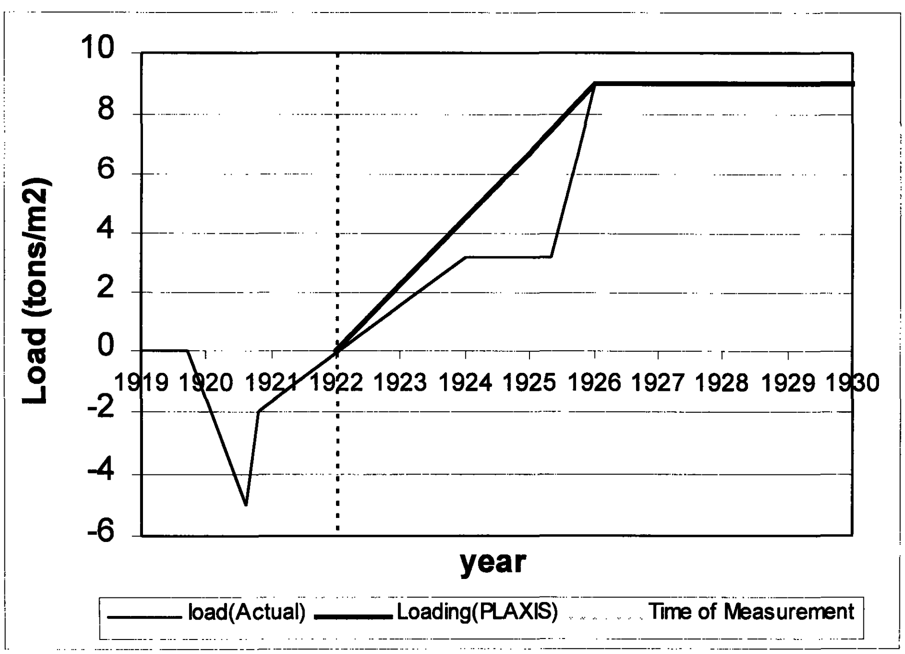

FIGURE 4.9 ACTUAL AND MODELED LOADING CONDITION

4.5 Comparing FE Settlement Results with Measured Settlements

First the results from the FE analysis will be compared with design calculations to check if FE results are reasonable. The average degree of consolidation calculated by FE analysis is plotted with the 2-D consolidation for a strip loading (Poulos & Davis, 1972) The H/B ratio (height of clay/loading width) used for the design calculation is 10 (the actual H/B = 8, but solutions are approximately the same). The range of coefficients for the design analysis are obtained from empirical correlations (DM7, 1982), using the liquidity index obtained from the boring sample. With liquid index falling between 40% to 50%, the estimated C_v is between 3.2m^2/year to 9.5m^2/year (1^{-3} to 3^{-3} cm^2/s). In figure 4.10, results show that FE results (with k_v = 4.3e-5m/day) falls close to the estimated design regions.

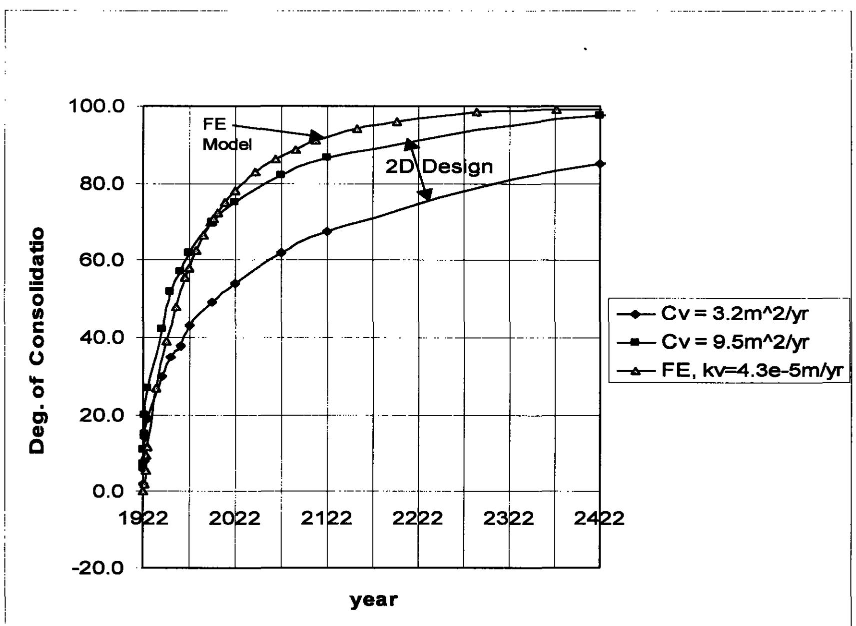

FIGURE 4.10 COMPARISON OF AVERAGE DEGREE OF CONSOLIDATION FROM FE ANALYSIS AND PUBLISHED RESULTS (ANDERSON & CLAUSEN, 1974)

With results from FE analysis obtaining reasonable results, further analyses are performed to obtain:

1) Load Supported by the Piles

2) Estimated Pore Water Pressure at Different Time

3) Settlements Comparison with Measured Data

4) Differential Settlement across the Concrete Mat

4.4.1 Load Supported by the Piles

Since the piles are represented by thin walls in the FE analysis. The total load of the piles will be estimated by the shear stress on the pile wall multiplied by the area of the wall. It is not meaningful to present the actual load supported by each pile wall since they do not represent the load that will be distributed to individual piles. However, it is interesting to estimate the fractions of load that are supported by the pile foundation, and by the concrete mat. From the results, summarized in Table 4.3, the piles support approximately 1/4 of the total deadload at full consolidation.

Total Stress applied (ton/m^2)	Load Supported by Piles (ton)	Load Support by Raft (ton)
9.0	3330.6	10875.9
Total Load (ton)	% of Total Load (%)	% of Total Load (%)
14206.5	23.4	76.6

Table 4.3 Estimated Load Supported by the Piles.

4.4.2 Estimated Excess Pore Pressure

In order to further verify the results from FE analysis, excess pore water pressure below the center of the mat (Figure 4.11) and the edge of the mat (Figure 4.12) are checked at selected time periods. Pore pressure estimated for the year of 1947 (25 yr. after loading start), 1972 (50yrs after loading start), 1999 (estimation for today), and 2423 (500 yr.

after loading start) are plotted in the figures. The hydraulic conductivity used in the analysis is the average of the range given in 4.3 (kv = 4.3e-5m/day). The results show that the distribution of excess pore pressure decreases along depth. This is reasonable, because the distribution of load applied by the building decreases as depth increases. In addition, the excess pore pressure at the edge is also checked how excess pore pressure varies across the width of the building. As expected, Figure 4.12 shows the excess pore pressure at a given time at the edge of the building is less than the excess pore pressure at the center of the building. This is caused by decrease of load distributed at the edge of the building causing a smaller amount of excess pore pressure.

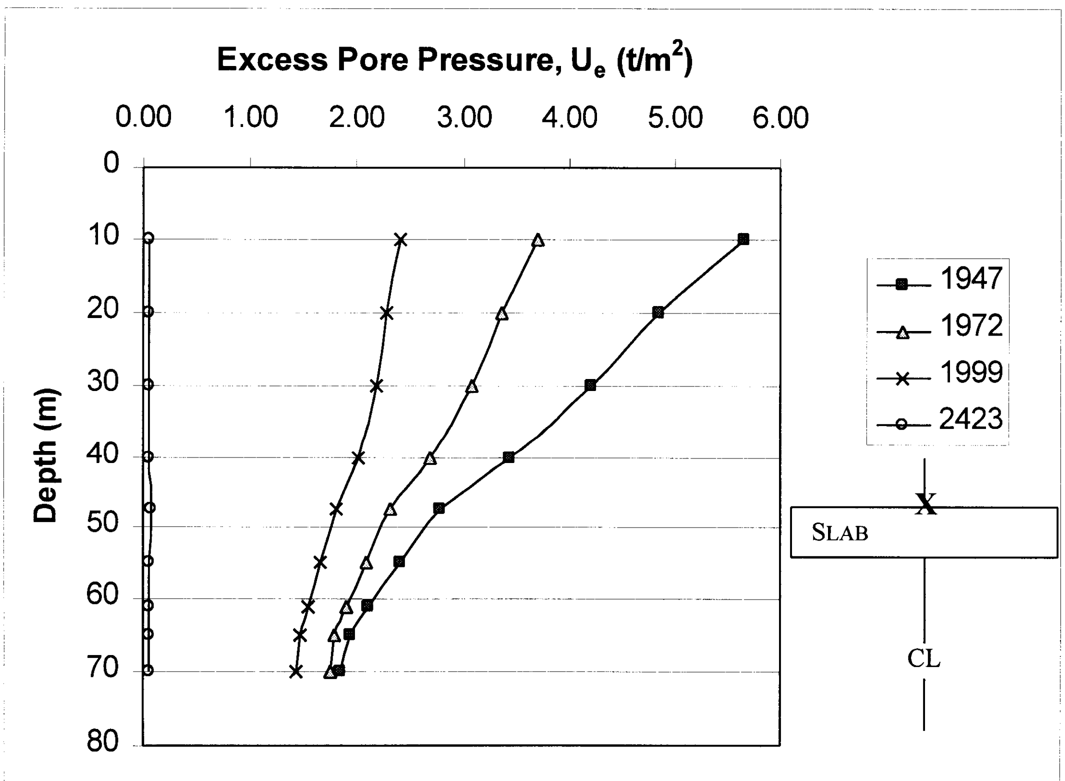

FIGURE 4.11 EXCESS PORE PRESSURE AT THE CENTER OF THE BUILDING

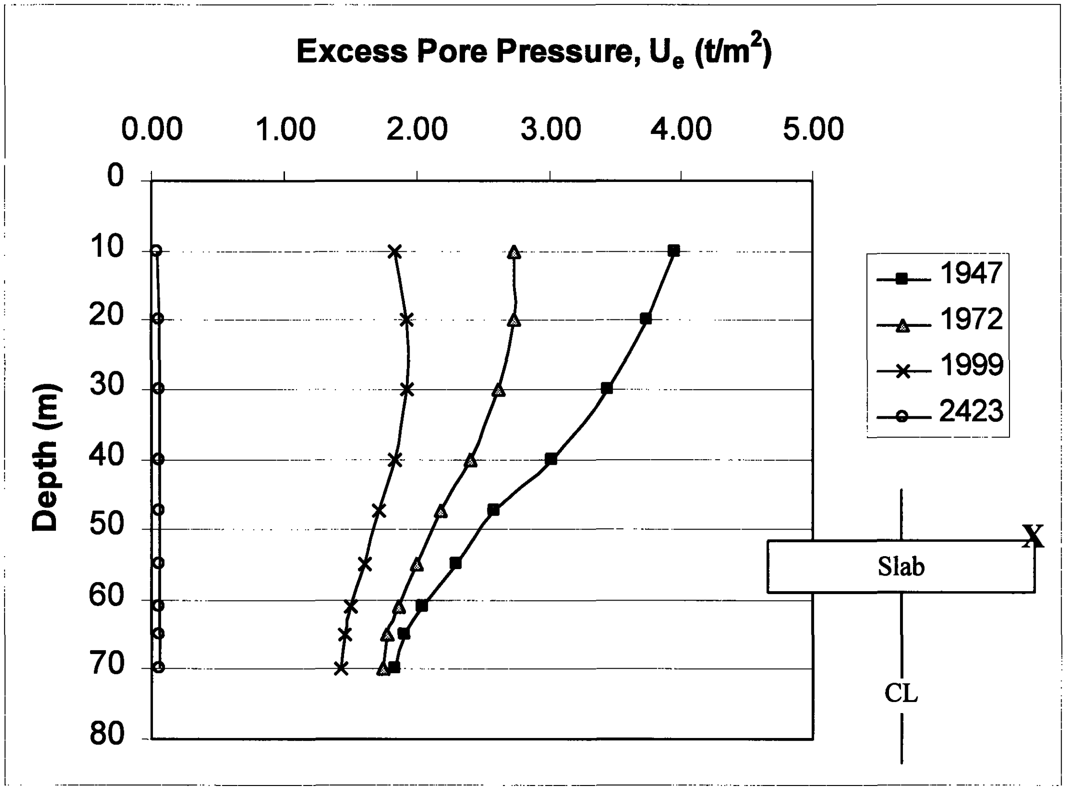

FIGURE 4.12 EXCESS PORE PRESSURE AT THE EDGE OF THE BUILDING

4.4.3 Settlements Comparison with Measured Settlements

After verifying the results from PLAXIS, settlement analysis is performed with the model and compared with the measured data. Measured settlement data were obtained at various points on the raft for a total of 50 years. There were no measurements on the piles, and therefore, only the raft settlement results will be compared in this section. The comparison of the measured data and results obtained from FE analyses with an estimated range of hydraulic conductivity are shown in Figure 4.13.

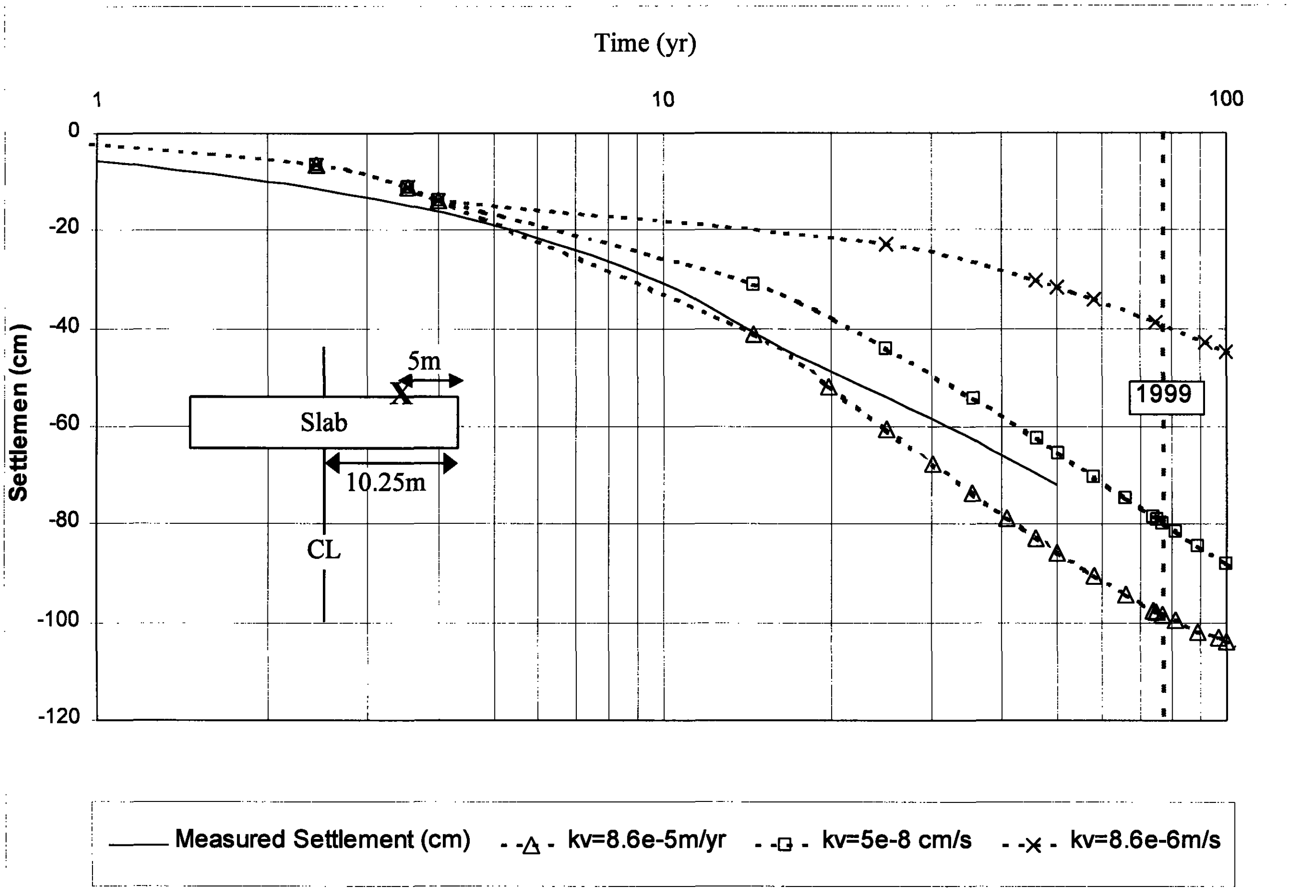

FIGURE 4.13 COMPARISON OF FE RESULTS AT PT. X WITH MEASURED SETTLEMENTS

From the results presented in Figure 4.13. It is apparent that the selection of clay permeability has a great effect on the settlements at 1973 (at the end of the 50 years of measurement). It is also clear from the measured settlements that the actual consolidation settlement on site has not reached the end of consolidation. The measured settlements match very closely with the calculated results for an assumed k_v = 4.3-5m/day to 8.5e-5m/day. The initial settlement response before 1932 (or 10 yr. after the initial loading) of

Time (year)

the measured results is generally underestimated by the FE model. This may be related to the assumed load history (Figure 4.9). For long term settlement behavior, results show PLAXIS can predict the degree and also the rate of the settlement quite well. The author has not managed to find any more recent settlement data for the Jernbanetollsted building (post 1973) and so it is not possible to evaluate predictions of the final consolidation settlement. Nevertheless, the final consolidation settlement at point X is estimated with the analyses from PLAXIS, and the results are shown in Figure 4.14. The final consolidation settlement predicted with different permeability has the same value and is approximately 1.14 m.

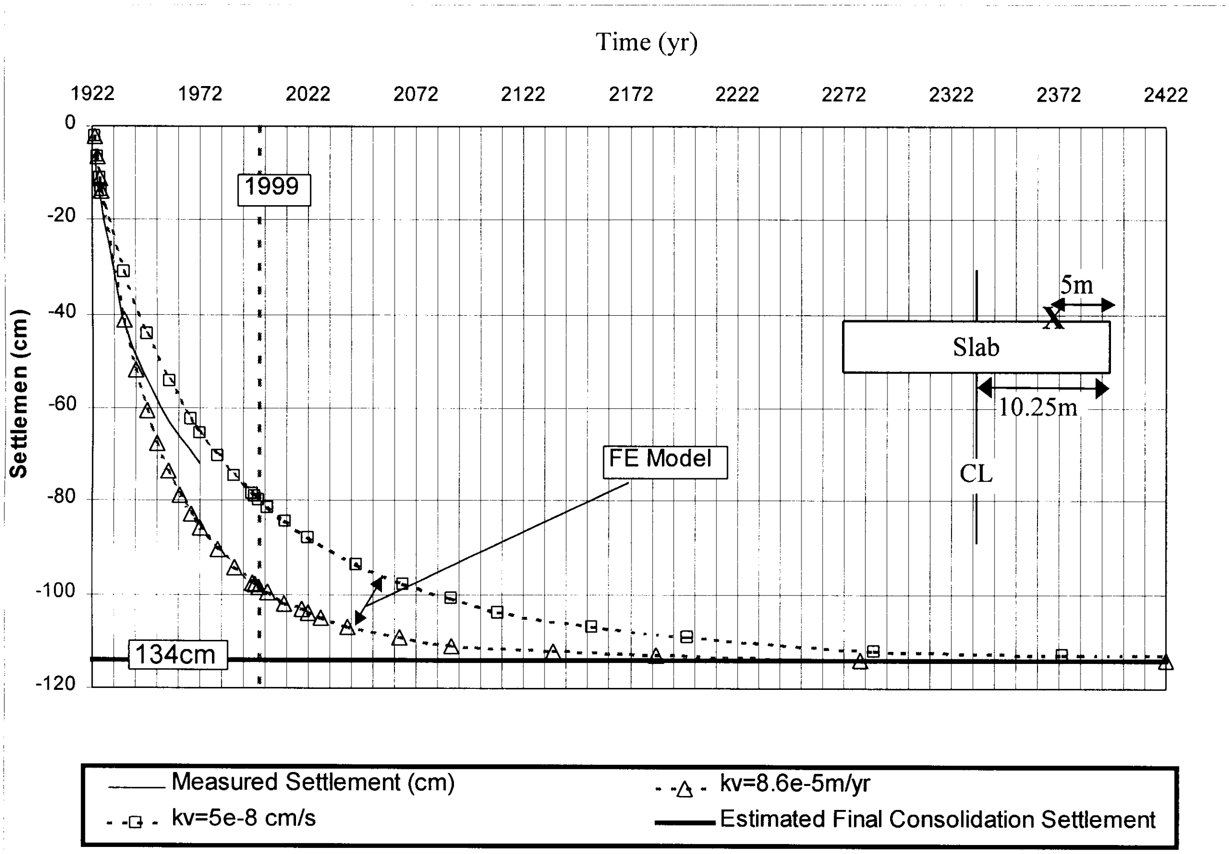

FIGURE 4.14 ESTIMATION OF FINAL SETTLEMENT AT PT X WITH FE ANALYSIS

An additional settlement analysis has been performed for a raft foundation without the timber piles. The purpose of this analysis is to illustrate the effect of the piles on the predicted consolidation settlement. Figure 4.15 compares the FE prediction for the case of 1) raft supported with piles 2) raft only. The results show that the final consolidation settlement (1.34m) for the raft with no piles is about 18% higher than the raft supported by piles. The larger settlement is caused by an increased of load causing an increase of dissipated pore pressure. Although more load causes the raft only foundation to settle more, the time it takes for the raft only foundation to reach final consolidation is approximately 500 years (year of 2422). This matches with theoretical results and shows that even when more load is applied to the soil, it takes the same amount of time to consolidate.

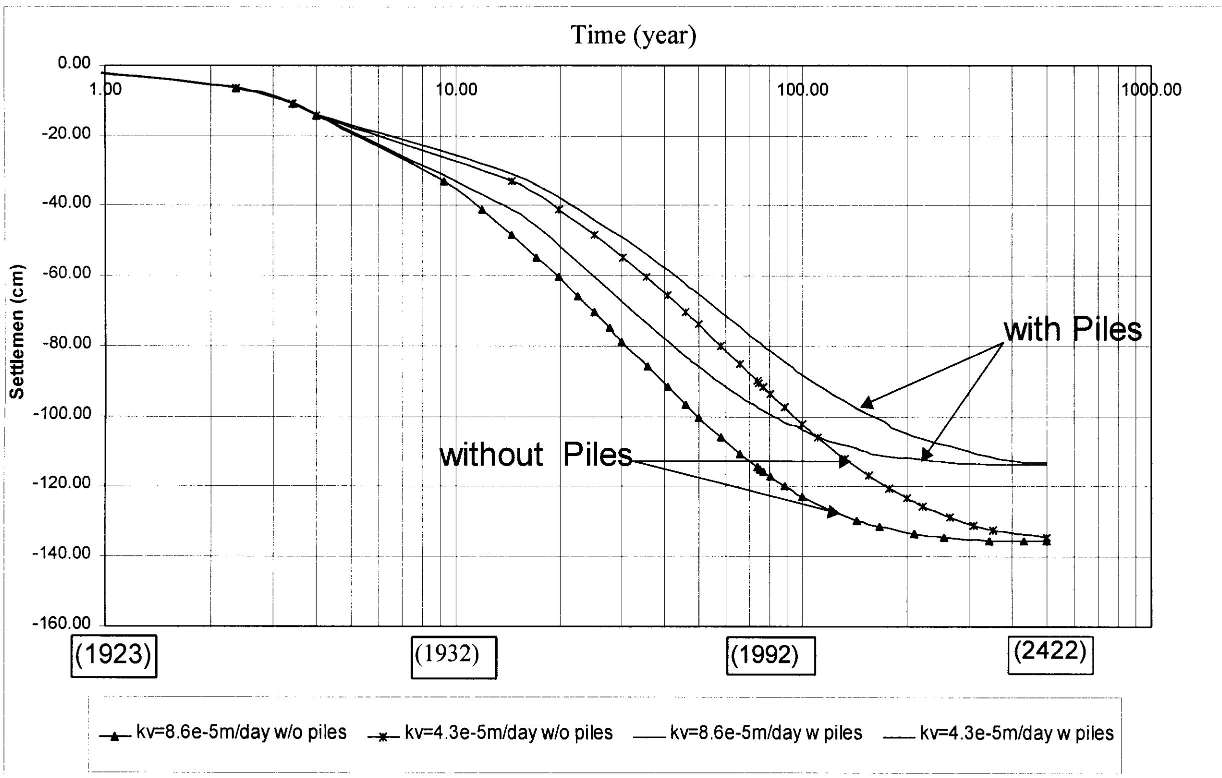

FIGURE 4.15 PREDICTED SETTLEMENT OF POINT X WITHOUT INSTALLATION OF PILES

4.4.4 Estimating Differential Settlement Center

With FE analysis, differential settlement across the cross-section can also be estimated. Figures 4.16 to 4.18 show the estimated settlements for different k_v from FE analysis. Once again, the results show the settlement at the center of the building is larger than the edge, as the excess pore pressure suggested in section 4.4.2. Results also show that as consolidation settlement increases, differential settlement also increases.

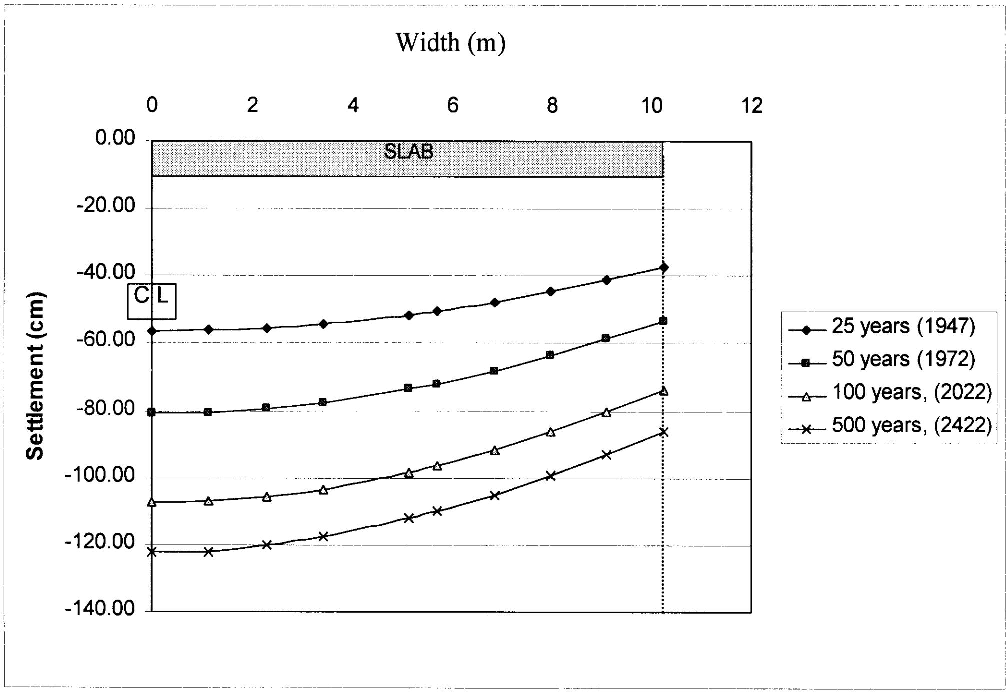

FIGURE 4.16 DIFFERENTIAL SETTLEMENT OF CROSS SECTION WITH KV = 8.6E-5M/DAY

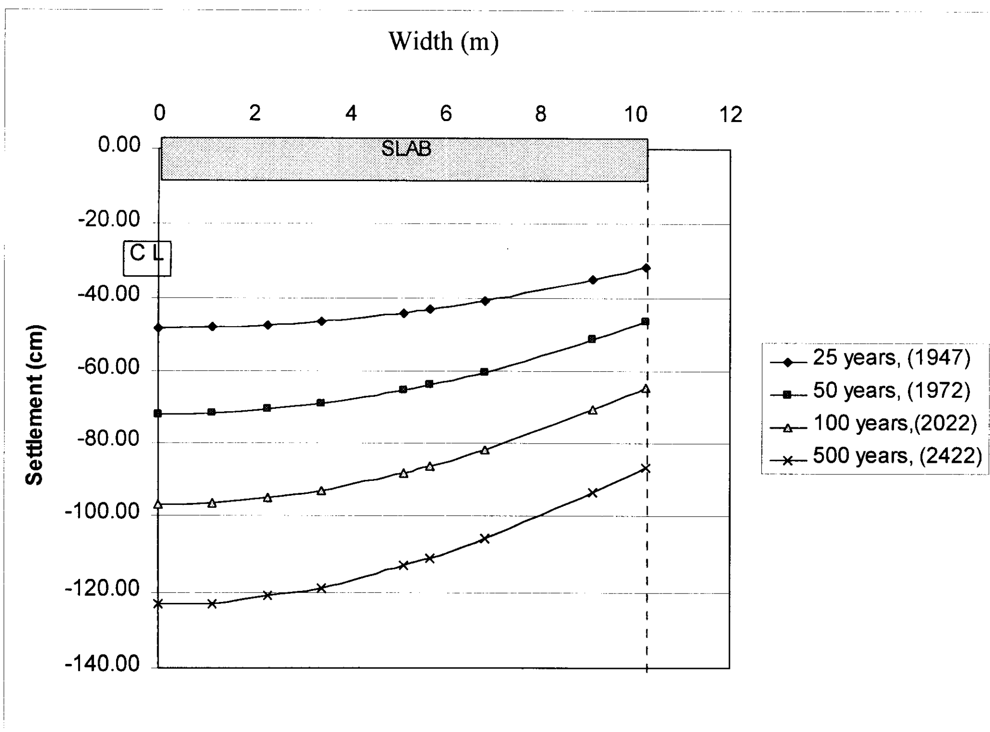

FIGURE 4.17 DIFFERENTIAL SETTLEMENT OF CROSS SECTION WITH KV = 4.3E-5M/DAY

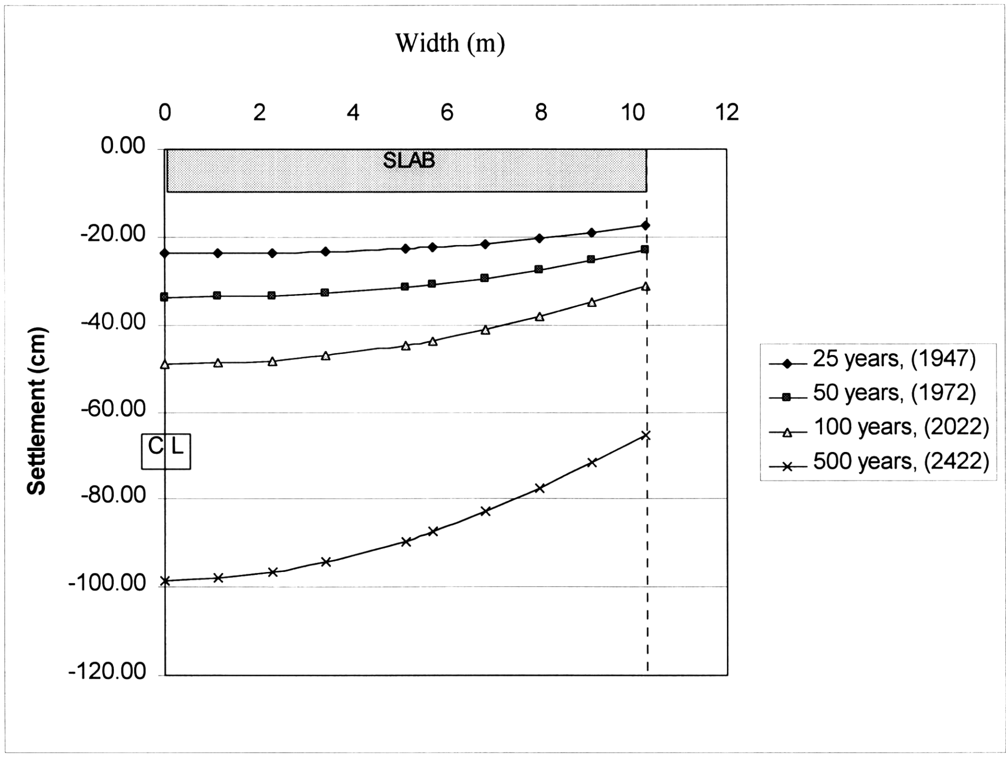

FIGURE 4.18 DIFFERENTIAL SETTLEMENT OF CROSS SECTION WITH KV = 8.6E-6M/DAY

4.5 Summary of Consolidation Settlement Analysis

Although only limited information on the soil parameters are available, the consolidation settlement analysis using MCC model produce reasonable results that match very well with the measured consolidation settlements fifty years after construction of Jernbanetollsted building in Oslo. Although this does not replicate the actual foundation geometry, it is a consistent approximation for a planar analysis. A full analysis of the foundation is beyond the capabilities of PLAXIS and requires a great increase in computational time. Nevertheless, the predicted range of settlement and degree of consolidation agree well with measured behavior. In addition, the final consolidation settlement predicted by Anderson & Clausen (1974), ρ_{final} = 1.1m, matches extremely well with the estimated value from PLAXIS.

Chapter 5 Summary, Conclusion and Recommendation

This thesis describes the application of finite element analyses for computing the load settlement response of piled foundations. Finite element models are compared with measured data for two 'case studies', 1) instrumented load tests on 4 individual piles (2 driven, 2 drilled shafts); and 2) long term response of piled-raft foundation over a deep layer of soft clay in Oslo. In general, the results from the FE analyses and design calculations provide reasonable estimates of the measured results. However, FE analysis in all cases provides more comprehensive information than the conventional design methods.

For the pile capacity analyses, FE analysis predicts capacity of the driven piles extremely close to the long-term measured values (within 1%). However, the FE analysis does not predict the capacity of the drilled pile within reasonable limits (underestimates by 50%). This is mainly caused by the installation procedure of the drilled pile. With bentonite slurry injected to the bored hole, chemical reaction may have increased the capacity. With more data on the effect of how bentonite influence the interface, better FE model can be used to obtain more accurate result. In analyzing the settlement response of the piles, FE modeling with MCC model shows that obtain results that match well with measured short-term settlement response. For driven piles, the predicted results are extremely close with the measured results at 5 weeks. However, FE analyses are not able to predict the long-term response for both drilled and driven piles. Results show that the MCC model does not accurately predict the stiffness of the soil. By modifying the stiffness of the model, FE can accurately predict both the capacities and the settlement responses of the driven piles.

For the long-term settlement analyses, FE analysis predicts both the final consolidation settlement and the rate of settlement very well. With no measured hydraulic conductivity data, calculations were performed using the common range of k_v for clay, matches the measured settlement 50yrs after loading. The rate of loading also agrees with the measured response. Even though, no measured result of the final consolidation settlement is available, the predicted final settlement from FE matches with results made by engineers.

The results from the two case studies show that FE modeling require good soil parameters and good soil models. The MCC model using κ^* as the elastic parameter for stress-strain relationship clearly does not represent the actual behavior. For accurate results, the parameters can be corrected using reliable sources (for correcting κ^*, G from measured can be used). However, this may change the other type of response (e.g. consolidation) of the soil model. This leads to the importance of development of better soil model for finite element analysis. More advanced soil models have been introduced in recent years. For example, the MIT-E3 soil model (Whittle & Kavvadas, 1994) uses 15 soil parameters to describe the behavior of soil under many different conditions (anisotropy effect, hysteretic response in unloading and loading, ...etc.). With better soil models and better parameters, more reliable FE predictions can be achieved.

One may question the need of finite element modeling when design analyses predict results matches with measured data in many cases. Design analyses are mainly based on simplified theory and empirical data. However, theoretical results often over-simplified the behavior of soil and interactions between soil and structures. For example, the load transfer method models both the pile and the soil as elastic material (highly unrealistic). Empirical design methods are mainly based on the correlation on observed results with measured parameters. This type of design analyses rarely captures the actual response of soils and structures. Furthermore, every site and project has different conditions, and only with FE analysis, one can examine how the results may differ. Differences in some conditions may not matter, but some may drastically influence the results. As construction and development becoming more advanced and fast paced, more in-depth and comprehensive geotechnical design tool is needed. With finite element modeling, engineer can fully understand and analyze the interactions between soil and structure that simple empirical and theoretical design solutions do not provide.

References

Lambe, W.T., & Whitman, R.V. 1969. *Soil Mechanics*. New York: John Wiley & Sons.

Brinkgreve, R.B.J., & Vermeer, P.A. 1995. *PLAXIS, Finite Element Code for Soil Analysis Version 6*. Brookfield: A.A. Baklema.

Anderson, K.H., & Frimann, C.J. 1974. "A Fifty-year Settlement Record of a Heavy Building on Compressible Clay." British Geotechnical Society Conference., Cambridge.

Bjerrum, L. 1967. "Engineering Geology of Norwegian Normally Consolidated Marine Clays as Related to Settlements of Buildings." 7th Rankine Lecture. Geotechnique, vol. 17, no. 2: 81-118.

Wood, D.M. 1990. *Soil Behavior & Critical State Soil Mechanics*. Cambridge: Cambridge University Press.

Randolph, M.F. 1994. "Design Methods for Pile Groups and Piled Rafts." XIII ICSMFE, New Delhi, India.

Ladd, C.C. 1997. "Advanced Soil Mechanics." MIT School of Engineering, 1.361 Class Notes.

Ladd, C.C. 1998. "Soil Behavior." MIT School of Engineering, 1.322 Class Notes.

Whittle, A.J. 1997. "Advanced Geotechnical Engineering." MIT School of Engineering, 1.364 Class Notes.

Finno, R.J. 1989. *Predicted and Observed Axial Behavior of Piles.* New York: ASCE.

Davis, E.H., & Davis, H.G. 1980. *Pile Foundation Analysis and Design*. New York: John Wiley and Sons.

ASTM Standards in Building Codes, Vol 3 (969-D2940). Philadelphia: ASTM

Appendix A

Results of Field and Laboratory Tests

Field Test Result

Laboratory Test Result

OWNER: Northwestern University
LOG OF BORING NUMBER: B-1
PROJECT NAME: ASCE Pile Load Test
ARCHITECT-ENGINEER: P A G Associates
SITE LOCATION: orthwestern University Lakefill, Evanston, IL

STS Consultants Ltd.

DEPTH (FT) | ELEVATION (FT) | SAMPLE NO | SAMPLE TYPE | SAMPLE DISTANCE | RECOVERY

DESCRIPTION OF MATERIAL

SURFACE ELEVATION

Clayey silt, trace gravel - brown - medium dense - moist (ML-Fill)

Fine to medium sand, trace gravel - light brown - very dense - moist (SP - Fill)

Medium sand, trace gravel - light brown - dense to medium dense - moist (SP - Fill)

Note: 3" seam of gravel encountered at 8'6"

Fine to medium sand, trace gravel - light brown - very dense - moist (SP - Fill)

Fine sand, trace silt, organics - gray - very dense - saturated (SP)

Silty clay, little gravel - brown - medium stiff (CL)

Silty clay, little gravel, trace sand - dark brown - medium stiff (CL)

Silty clay, little gravel - brownish gray - medium stiff (CL)

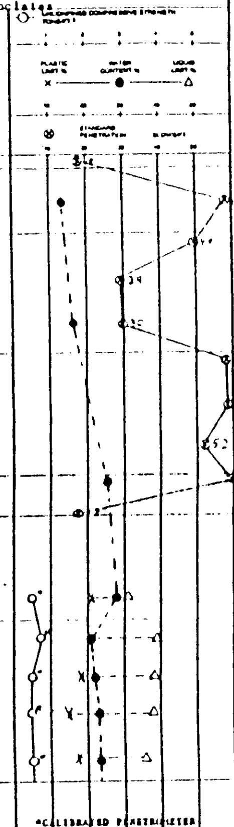

THE STRATIFICATION LINES REPRESENT THE APPROXIMATE BOUNDARY LINES BETWEEN SOIL TYPES. IN SITU THE TRANSITION MAY BE GRADUAL.

STS JOB NO | SHEET NO 1 OF 2

OWNER: Northwestern University
LOG OF BORING NUMBER: B 1
PROJECT NAME: ASCE Pile Load Test
ARCHITECT-ENGINEER: P A G Associates
SITE LOCATION: Northwestern University Lakefill, Evanston, IL

STS Consultants Ltd.

DESCRIPTION OF MATERIAL

SURFACE ELEVATION

Silty clay, little gravel - brownish gray - medium stiff (CL)

Silty clay, little gravel, trace sand - brown and gray - medium stiff (CL)

Silty clay, little gravel, trace sand - dark brown and gray - stiff (CL)

Fine sandy clay, little silt, trace gravel - dark brown - very stiff (CL)

END OF BORING

Borehole grouted upon completion

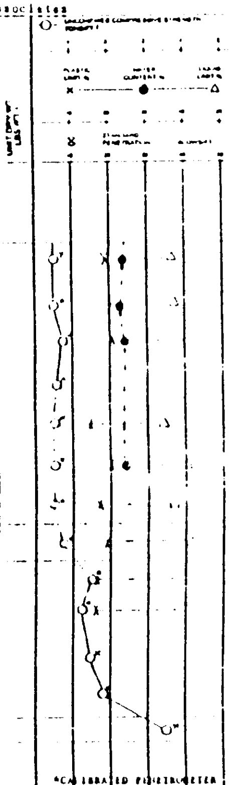

THE STRATIFICATION LINES REPRESENT THE APPROXIMATE BOUNDARY LINES BETWEEN SOIL TYPES. IN SITU THE TRANSITION MAY BE GRADUAL.

WL 9'	BORING STARTED 12/10/82	STS OFFICE Northbrook
WL BCR ACR	BORING COMPLETED 12/11/82	DRAWN BY BG / SHEET NO 2 OF 2
WL	RIG/FOREMAN Rotary-JFP	APP'D BY BG / STS JOB NO

Woodward-Clyde Consultants

LOG OF BORING PM-1 SHEET 1 OF 2

PROJECT: Foundation Engineering Congress	PROJECT NO.: 22128
LOCATION: Evanston, IL	ELEVATION AND DATUM:
DRILLING AGENCY: D&G Drilling New Lenox, IL	DATE STARTED: 4/30/88 / DATE FINISHED: 4/30/88
DRILLING EQUIPMENT: CME 75	COMPLETION DEPTH: 47.7 / ROCK DEPTH: —
DRILLING METHOD: 3 3/4 in roller bit, bentonite fluid; SIZE AND TYPE OF CASING: 4 in 0-5 ft	NO. SAMPLES: DIST. 6, UNDIST. — , CORE — ; WATER LEVEL: FIRST 10.5, COMPL. 15 , 24 HR. —
SAMPLER: SPT (S) 3 in Shelby Tube (ST)	FOREMAN: Barry, Dale Kadilek
SAMPLER HAMMER: Automatic; WEIGHT: 140 lb; DROP: 30 in.	INSPECTOR: Dick Davidson

DEPTH FT	SAMPLE DESCRIPTION	SAMPLES: NO.	RECOVERY	BLOWS	FIELD TESTS	REMARKS
	Brown Topsoil					Auger to 5 ft; Drove SPT; Drove 4 in casing; Rotary drilled with bentonite
5	Medium dense brown fine to medium SAND (SP)	S-1	1.5	8/11/14	N=25	
					PMT	Rotary drilled with 2 5/8 in roller bit from 6.5 to 10 ft; Center of probe 8.6 ft
10		S-2	1.5	4/5/5	N=10	
15		S-3	1.0	9/15/15	N=30	
					PMT	Rotary drilled with 2.5 in. roller bit from 16.5 to 20 ft; Center of probe 18.5 ft
20	Becoming gray	S-4	1.5	9/9/13	N=22	
25	Soft gray silty CLAY (CL)	S-5	1.5	WR	N=WR	
30					PMT	Pushed in PMT from 28 to 31 ft without drilling; Center of probe 30 ft

BORING NO. PM-1

Woodward-Clyde Consultants

LOG OF BORING PM-1 SHEET 2 OF 2

DEPTH FT	SAMPLE DESCRIPTION	SAMPLES: NO.	RECOVERY	BLOWS	FIELD TESTS	REMARKS
	Soft gray silty CLAY (CL)	S-6	1.5	1	N=1	
		ST-1	0			Pushed 3 in Shelby Tube, no recovery; Washed to 35.5 ft
35					PMT	Pushed in PMT from 35.5 to 38.5 ft without drilling; Probe 37.5 ft; Washed to 38.5 ft
40					PMT	Rotary drilled with 2 15/16 in roller bit from 38.5 to 42 ft; Center of probe 41 ft
45					DMT	Flat plate dilatometer advanced in 8 in. increments
50	BOTTOM OF BORING 47.7 ft					Borehole grouted with bentonite / sand back fill pumped from bottom

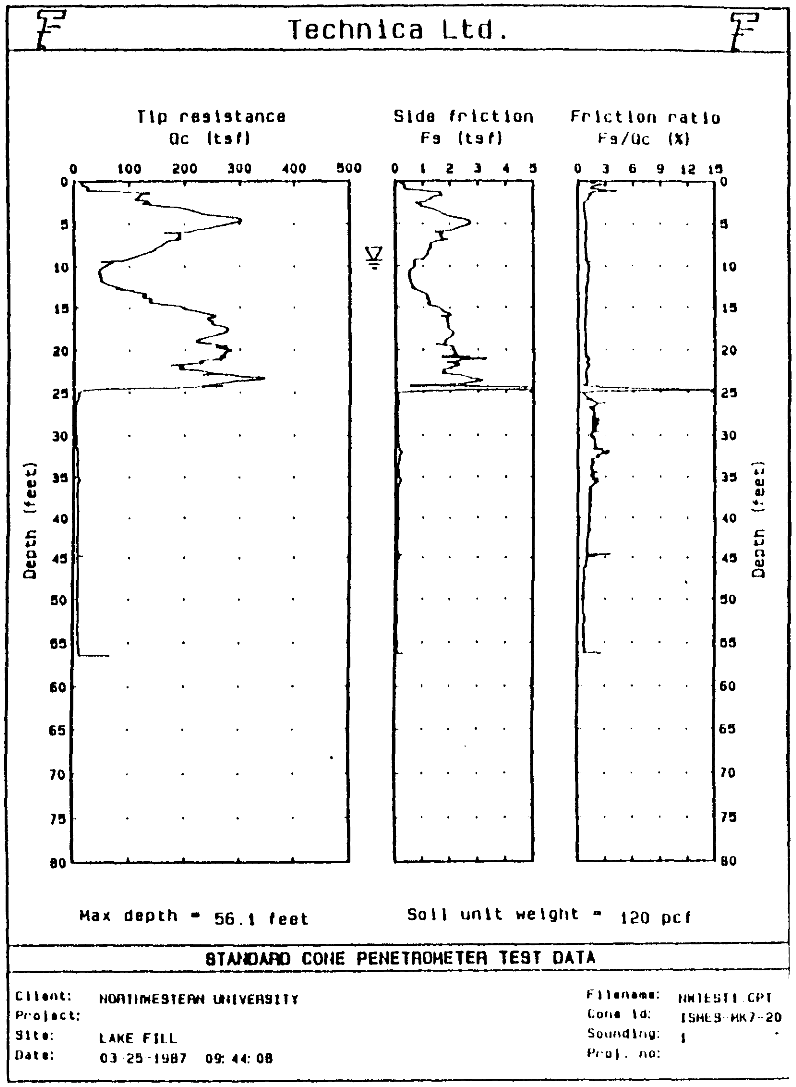
Technica Ltd.
Tip resistance
Qc (tsf)
Side friction
Fs (tsf)
Friction ratio
Fs/Qc (%)
Depth (feet)
Max depth = 56.1 feet
Soil unit weight = 120 pcf
STANDARD CONE PENETROMETER TEST DATA
Client: NORTHWESTERN UNIVERSITY
Project:
Site: LAKE FILL
Date: 03-25-1987 09:44:08
Filename: NWTEST1.CPT
Cone id: ISHES-HK7-20
Sounding: 1
Proj. no:

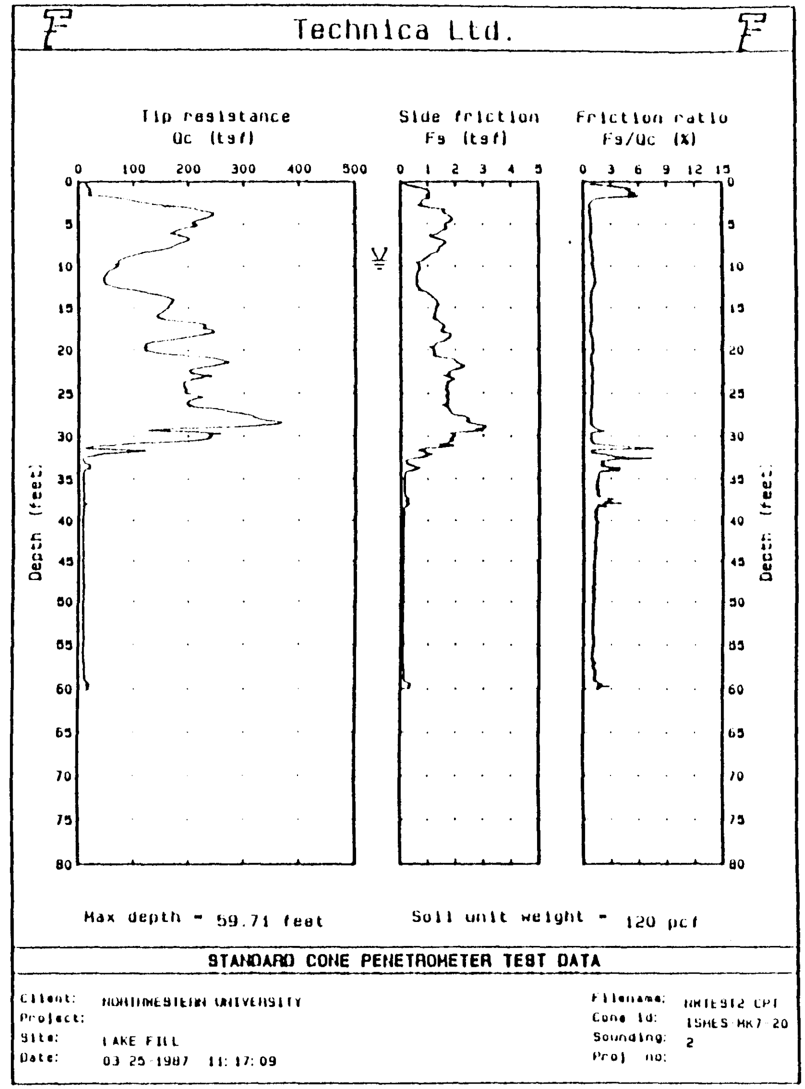
Technica Ltd.
Tip resistance
Qc (tsf)
Side friction
Fs (tsf)
Friction ratio
Fs/Qc (%)
Depth (feet)
Max depth = 59.71 feet
Soil unit weight = 120 pcf
STANDARD CONE PENETROMETER TEST DATA
Client: NORTHWESTERN UNIVERSITY
Project:
Site: LAKE FILL
Date: 03-25-1987 11:17:09
Filename: NWTEST2.CPT
Cone id: ISHES-HK7-20
Sounding: 2
Proj. no:

Technica Ltd.

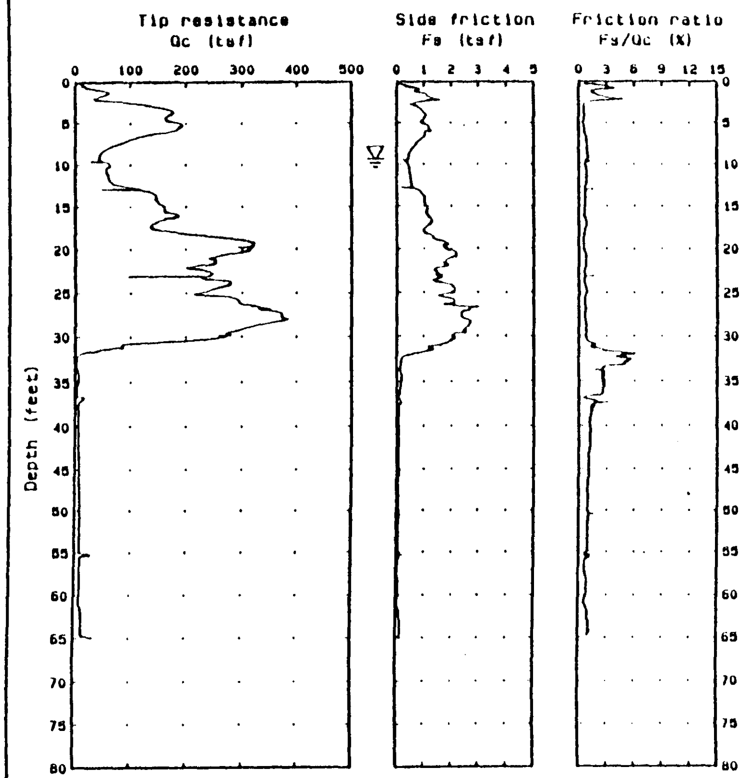

Max depth = 64.43999 feet   Soil unit weight = 120 pcf

STANDARD CONE PENETROMETER TEST DATA

Client: NORTHWESTERN UNIVERSITY
Project:
Site: LAKE FILL
Date: 03-25-1987 14:10:57

Filename: NWTEST3.CPT
Cone id: ISRES HK7 20
Sounding: 3
Proj. no:

Technica Ltd.

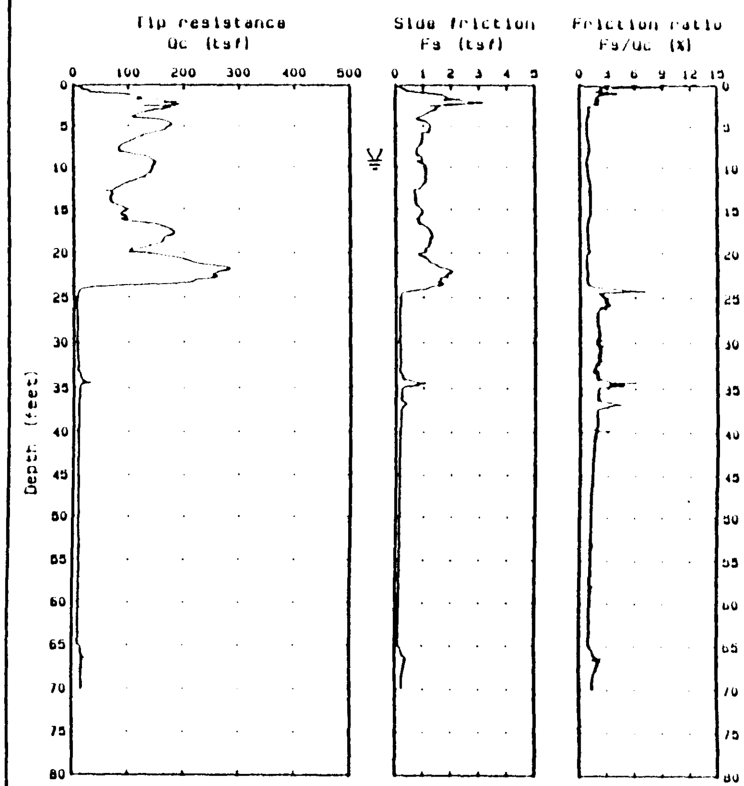

Max depth = 69.65 feet   Soil unit weight = 120 pcf

STANDARD CONE PENETROMETER TEST DATA

Client: NORTHWESTERN UNIVERSITY
Project:
Site: LAKE FILL
Date: 03-25-1987 15:27:53

Filename: NWTEST4.CPT
Cone id: ISRES HK7 20
Sounding: 4
Proj. no:

3.0 DATA REDUCTION

Measured data consist of depth, time, cone and sleeve resistance, total load on penetrometer, pore pressure and penetrometer inclination. Data are recorded and plotted at 0.8 inch intervals, and are presented in Figures 2 through 5. The following parameters were computed and are tabulated at 6 inch intervals in Tables 1 through 3 along with the measured data:

Friction ratio (%)

$$FR = fs/qc * 100; \qquad \text{(Eq. 1)}$$

Overburden normalized cone resistance

$$qc1 = qc(1.0-0.5*\log(Sv')); \qquad \text{(Eq. 2)}$$

Total cone resistance

$$qt = qc + m1(1-Ar)U; \qquad \text{(Eq. 3)}$$

Effective cone resistance

$$qe = qt - U; \text{ and} \qquad \text{(Eq. 4)}$$

Pore pressure ratio

$$Bq = (U-Uh)/(qt-Sv); \qquad \text{(Eq. 5)}$$

where:

fs is the measured sleeve resistance, in TSF;

qc is the measured cone resistance, in TSF;

Sv is the total vertical overburden pressure, in TSF;

m1 is a reduction factor to adjust pore pressures measured at the midheight of the cone tip, to those expected to act behind the cone tip; for soft to firm cohesive soils this factor is 0.75 for the STRATIGRAPHICS piezocone;

(1-Ar) is the portion of the cone tip area over which fluid pressures reduce cone resistance below full total stresses, equal to 0.40 for the STRATIGRAPHICS piezocone;

U is the measured pore pressure, in TSF; and

Uh is the calculated hydrostatic pressure, in TSF.

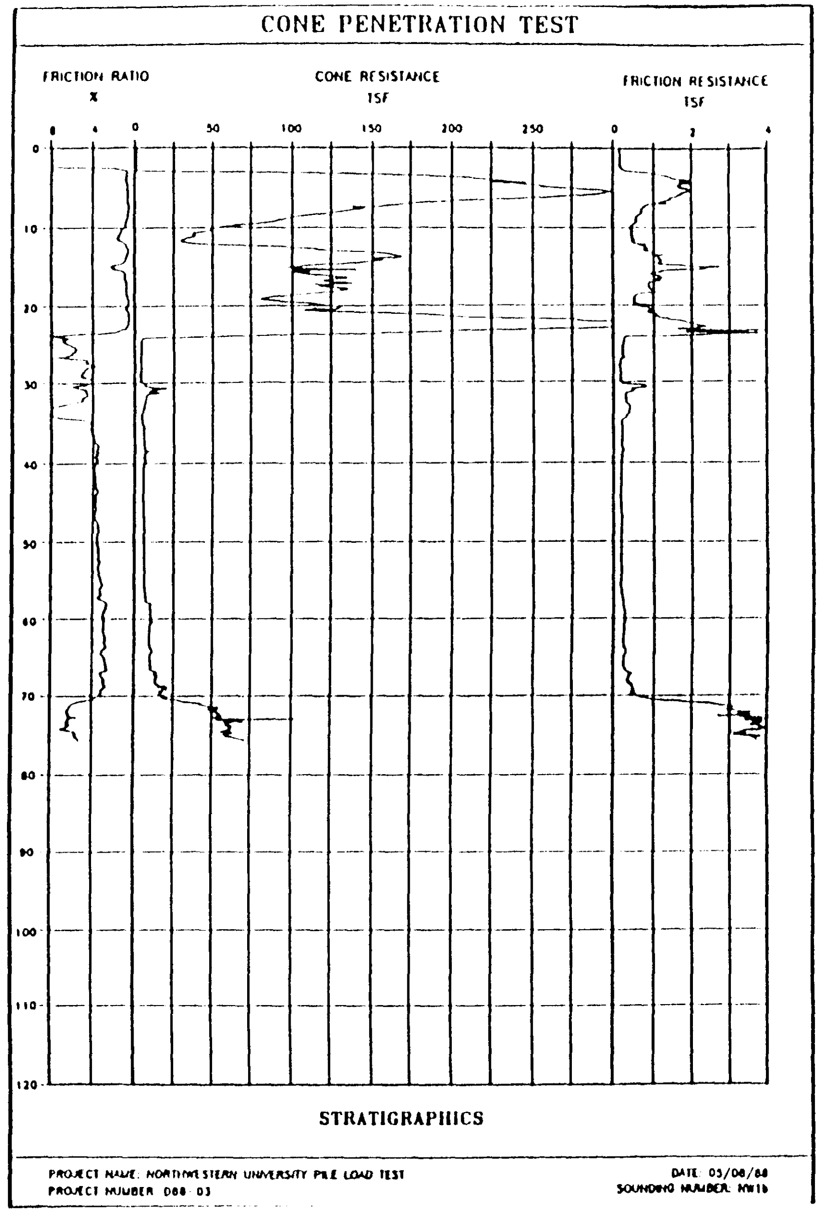

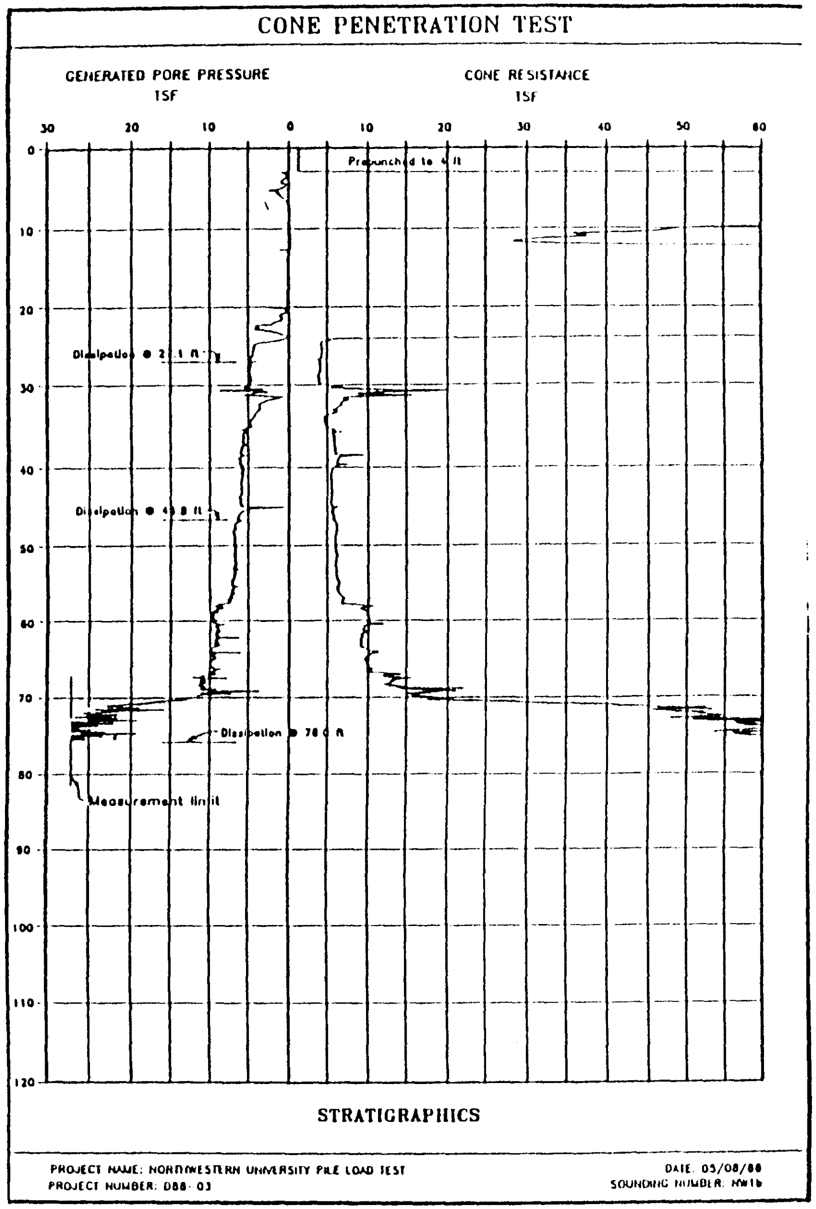
CONE PENETRATION TEST
GENERATED PORE PRESSURE
TSF
CONE RESISTANCE
TSF
Prepunched to 4 ft
Dissipation @ 27.1 ft
Dissipation @ 45.8 ft
Dissipation @ 76.0 ft
Measurement limit
STRATIGRAPHICS
PROJECT NAME: NORTHWESTERN UNIVERSITY PILE LOAD TEST
PROJECT NUMBER: D88-03
DATE: 05/08/88
SOUNDING NUMBER: NW1b

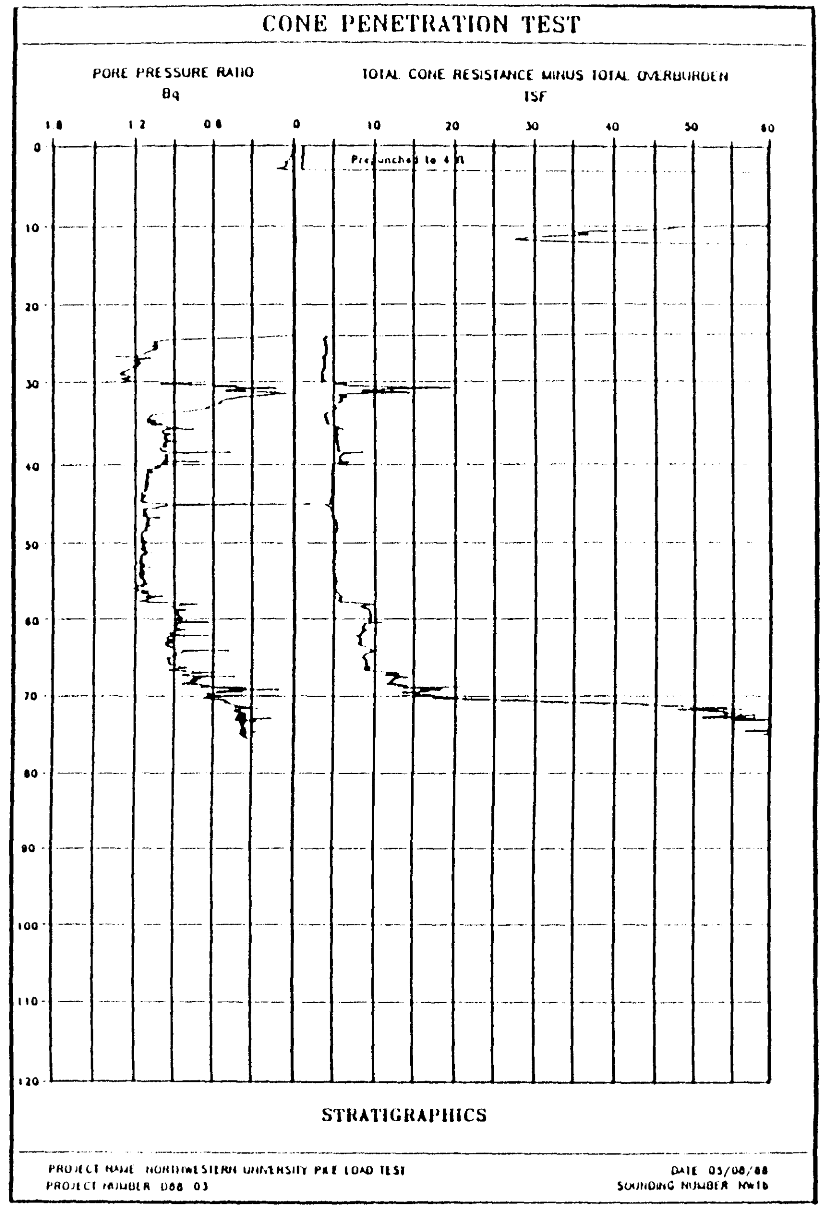
CONE PENETRATION TEST
PORE PRESSURE RATIO
Bq
TOTAL CONE RESISTANCE MINUS TOTAL OVERBURDEN
TSF
Prepunched to 4 ft
STRATIGRAPHICS
PROJECT NAME: NORTHWESTERN UNIVERSITY PILE LOAD TEST
PROJECT NUMBER: D88-03
DATE: 05/08/88
SOUNDING NUMBER: NW1b

STRATIGRAPHICS
THE GEOTECHNICAL DATA ACQUISITION CORP
430 TAYLOR AVENUE
GLEN ELLYN, IL 60137

PIEZOCONE PARAMETERS

JOB NO: C88-03
JOB NAME: NORTHWESTERN PILE LOAD TEST
SOUNDING NO: NW18

WATER TABLE : 15 FT
TOTAL UNIT WT : 0.058 TCF

d DEPTH* (FT)	Sv CALCULATED TOTAL OVERBURDEN PRESSURE (TSF)	Uh CALCULATED HYDROSTATIC PRESSURE (TSF)	qc MEASURED CONE RESISTANCE (TSF)	U MEASURED PIEZOCONE PORE PRESSURE (TSF)	qt CALCULATED TOTAL CONE RESISTANCE (TSF)	qe CALCULATED EFFECTIVE CONE RESISTANCE (TSF)	Bq CALCULATED PORE PRESSURE RATIO
0.5	0.03	0.00					
1.0	0.06	0.00					
1.5	0.09	0.00			PREPUNCHED TO 4 FT		
2.0	0.12	0.00					
2.5	0.14	0.00					
3.0	0.17	0.00					
3.5	0.20	0.00					
4.0	0.23	0.00	217.8	0.81	218.0	217.2	.00
4.5	0.26	0.00	240.5	0.21	240.5	240.3	.00
5.0	0.29	0.00	261.7	0.78	261.9	261.2	.00
5.5	0.32	0.00	300.7	1.27	301.0	299.8	.00
6.0	0.35	0.00	286.7	0.98	287.0	286.1	.00
6.5	0.38	0.00	232.8	0.50	233.0	232.5	.00
7.0	0.41	0.00	178.9	0.11	178.9	178.8	.00
7.5	0.44	0.00	153.4	0.01	153.4	153.4	.00
8.0	0.47	0.00	133.4	-0.11	133.4	133.5	.00
8.5	0.49	0.00	114.7	-0.08	114.7	114.8	.00
9.0	0.52	0.00	95.2	-0.08	95.2	95.3	.00
9.5	0.55	0.00	80.9	-0.12	80.9	81.0	.00
10.0	0.58	0.00	56.6	-0.17	56.6	56.7	.00
10.5	0.61	0.00	47.0	-0.12	46.9	47.1	.00
11.0	0.64	0.00	36.4	-0.25	36.4	36.6	-0.01
11.5	0.67	0.00	30.8	-0.25	30.7	31.0	-0.01
12.0	0.70	0.00	32.4	-0.26	32.4	32.6	-0.01
12.5	0.73	0.00	82.5	-0.19	82.4	82.6	.00
13.0	0.75	0.00	112.5	0.11	112.5	112.4	.00
13.5	0.78	0.00	158.0	0.12	158.0	157.9	.00
14.0	0.81	0.00	164.8	0.18	164.9	164.7	.00
14.5	0.84	0.00	150.4	0.15	150.4	150.3	.00

* NOTE: Data recorded and plotted at 0.06 ft intervals

SOUNDING NO: NW18

d DEPTH (FT)	Sv CALCULATED TOTAL OVERBURDEN PRESSURE (TSF)	Uh CALCULATED HYDROSTATIC PRESSURE (TSF)	qc MEASURED CONE RESISTANCE (TSF)	U MEASURED PIEZOCONE PORE PRESSURE (TSF)	qt CALCULATED TOTAL CONE RESISTANCE (TSF)	qe CALCULATED EFFECTIVE CONE RESISTANCE (TSF)	Bq CALCULATED PORE PRESSURE RATIO
15.0	0.87	0.00	103.5	0.14	103.6	103.4	.00
15.5	0.90	0.01	121.8	0.10	121.8	121.7	.00
16.0	0.93	0.03	102.8	0.17	102.8	102.7	.00
16.5	0.96	0.05	130.9	0.18	130.9	130.7	.00
17.0	0.98	0.06	118.8	0.19	118.9	118.7	.00
17.5	1.01	0.08	124.7	0.05	124.7	124.6	.00
18.0	1.04	0.09	133.9	0.19	134.0	133.8	.00
18.5	1.07	0.11	116.2	0.23	116.2	116.0	.00
19.0	1.10	0.12	84.9	0.21	84.9	84.7	.00
19.5	1.13	0.14	92.1	0.25	92.2	91.9	.00
20.0	1.16	0.16	121.6	0.27	121.7	121.4	.00
20.5	1.19	0.17	127.6	0.55	127.7	127.2	.00
21.0	1.22	0.19	148.2	1.01	146.5	147.5	0.01
21.5	1.25	0.20	196.6	0.84	196.8	196.0	.00
22.0	1.28	0.22	277.8	1.75	278.4	276.6	0.01
22.5	1.30	0.23	332.7	4.17	334.0	329.8	0.01
23.0	1.34	0.25	297.4	4.02	296.6	294.6	0.01
23.5	1.36	0.26	190.4	1.15	190.7	189.6	.00
24.0	1.39	0.28	53.6	0.31	53.7	53.4	.00
24.5	1.42	0.30	4.1	2.80	4.9	2.1	0.72
25.0	1.45	0.31	4.0	4.24	5.3	1.1	1.02
25.5	1.48	0.33	4.0	4.47	5.4	0.9	1.06
26.0	1.51	0.34	4.1	4.59	5.5	0.9	1.06
26.5	1.54	0.36	4.2	4.99	5.7	0.7	1.12
27.0	1.57	0.37	3.9	4.82	5.3	0.5	1.18
27.5	1.60	0.39	3.9	4.80	5.3	0.5	1.18
28.0	1.62	0.41	3.9	4.80	5.3	0.6	1.18
28.5	1.65	0.42	3.8	4.94	5.3	0.4	1.24
29.0	1.68	0.44	3.6	4.74	5.0	0.2	1.30
29.5	1.71	0.45	3.7	4.64	5.1	0.4	1.26
30.0	1.74	0.47	4.2	5.25	5.8	0.5	1.19
30.5	1.77	0.48	6.9	4.61	8.3	3.7	0.64
31.0	1.80	0.50	11.1	4.00	12.3	8.3	0.33
31.5	1.83	0.51	10.1	0.62	10.3	9.7	0.01
32.0	1.86	0.53	7.1	3.01	8.0	5.0	0.41
32.5	1.89	0.55	6.6	3.72	7.7	4.0	0.54
33.0	1.91	0.56	5.5	3.55	6.6	3.0	0.64
33.5	1.94	0.58	5.6	4.20	6.9	2.7	0.73
34.0	1.97	0.59	4.4	4.48	5.8	1.3	1.03
34.5	2.00	0.61	4.5	4.90	5.9	1.0	1.09

SOUNDING NO: NW18

d DEPTH (FT)	Sv CALCULATED TOTAL OVERBURDEN PRESSURE (TSF)	Uh CALCULATED HYDROSTATIC PRESSURE (TSF)	qc MEASURED CONE RESISTANCE (TSF)	U MEASURED PIEZOCONE PORE PRESSURE (TSF)	qt CALCULATED TOTAL CONE RESISTANCE (TSF)	qe CALCULATED EFFECTIVE CONE RESISTANCE (TSF)	Bq CALCULATED PORE PRESSURE RATIO
35.0	2.03	0.63	4.6	5.09	6.1	1.0	1.09
35.5	2.06	0.64	5.9	5.98	7.7	1.7	0.95
36.0	2.09	0.66	5.6	5.78	7.3	1.5	0.98
36.5	2.12	0.67	5.7	5.56	7.4	1.8	0.93
37.0	2.14	0.69	5.7	5.78	7.4	1.6	0.96
37.5	2.17	0.70	5.8	5.87	7.6	1.7	0.96
38.0	2.20	0.72	5.9	6.01	7.7	1.7	0.96
38.5	2.23	0.73	5.8	6.18	7.7	1.5	1.00
39.0	2.26	0.75	6.3	6.54	8.3	1.7	0.96
39.5	2.29	0.76	6.1	6.11	7.9	1.8	0.95
40.0	2.32	0.78	5.9	6.11	7.7	1.6	0.99
40.5	2.35	0.79	5.6	6.00	7.4	1.4	1.04
41.0	2.38	0.81	5.3	6.09	7.2	1.1	1.10
41.5	2.41	0.83	5.3	5.95	7.1	1.1	1.09
42.0	2.43	0.84	5.4	6.00	7.2	1.2	1.08
42.5	2.46	0.86	5.3	6.10	7.2	1.1	1.11
43.0	2.49	0.87	5.4	6.13	7.3	1.2	1.10
43.5	2.52	0.89	5.3	5.89	7.0	1.2	1.10
44.0	2.55	0.91	5.4	6.33	7.3	1.0	1.13
44.5	2.58	0.92	5.3	5.99	7.1	1.1	1.12
45.0	2.61	0.94	5.3	6.07	7.2	1.1	1.13
45.5	2.64	0.95	5.4	5.18	6.9	1.8	0.98
46.0	2.67	0.97	5.5	6.13	7.3	1.2	1.10
46.5	2.70	0.98	5.7	6.31	7.6	1.3	1.09
47.0	2.73	1.00	5.8	6.52	7.8	1.3	1.09
47.5	2.76	1.01	6.1	6.93	8.2	1.2	1.09
48.0	2.78	1.03	6.1	6.89	8.2	1.3	1.09
48.5	2.81	1.05	6.1	6.99	8.2	1.2	1.11
49.0	2.84	1.06	5.9	6.90	8.0	1.1	1.13
49.5	2.87	1.08	6.0	6.79	8.0	1.2	1.11
50.0	2.90	1.09	5.9	6.58	7.9	1.3	1.09
50.5	2.93	1.11	5.9	6.75	7.9	1.2	1.13
51.0	2.96	1.12	5.8	6.85	7.9	1.1	1.16
51.5	2.99	1.14	6.2	6.67	8.2	1.5	1.06
52.0	3.02	1.16	5.9	6.81	8.0	1.2	1.14
52.5	3.05	1.17	5.9	6.60	7.9	1.3	1.13
53.0	3.07	1.19	6.1	6.70	8.1	1.4	1.10
53.5	3.10	1.20	6.0	6.97	8.1	1.2	1.15
54.0	3.13	1.22	6.0	6.69	8.0	1.4	1.11
54.5	3.16	1.23	6.0	6.97	8.1	1.1	1.17

SOUNDING NO: NW18

d DEPTH (FT)	Sv CALCULATED TOTAL OVERBURDEN PRESSURE (TSF)	Uh CALCULATEL HYDROSTATIC PRESSURE (TSF)	qc MEASURED CONE RESISTANCE (TSF)	U MEASURED PIEZOCONE PORE PRESSURE (TSF)	qt CALCULATED TOTAL CONE RESISTANCE (TSF)	qe CALCULATED EFFECTIVE CONE RESISTANCE (TSF)	Bq CALCULATED PORE PRESSURE RATIO
55.0	3.19	1.25	6.3	7.17	8.5	1.3	1.12
55.5	3.22	1.26	6.3	7.11	8.5	1.4	1.11
56.0	3.25	1.28	6.1	7.16	8.2	1.1	1.19
56.5	3.28	1.30	6.2	7.35	8.4	1.1	1.18
57.0	3.30	1.31	6.7	7.34	8.9	1.5	1.08
57.5	3.34	1.33	6.8	7.47	9.1	1.6	1.07
58.0	3.36	1.34	6.8	8.17	9.3	1.1	1.16
58.5	3.39	1.36	9.0	8.42	11.6	3.1	0.86
59.0	3.42	1.37	10.1	8.94	12.8	3.8	0.81
59.5	3.45	1.39	9.9	9.70	12.8	3.1	0.89
60.0	3.48	1.40	10.1	9.73	13.0	3.3	0.87
60.5	3.51	1.42	11.3	9.13	14.0	4.9	0.73
61.0	3.54	1.43	9.6	9.07	12.3	3.3	0.87
61.5	3.57	1.45	9.9	8.80	12.6	3.8	0.82
62.0	3.60	1.47	9.3	9.03	12.1	3.0	0.89
62.5	3.63	1.48	9.0	9.25	11.8	2.6	0.95
63.0	3.65	1.50	9.2	9.22	11.9	2.7	0.93
63.5	3.68	1.51	9.1	9.31	11.9	2.6	0.95
64.0	3.71	1.53	10.1	9.93	13.0	3.1	0.90
64.5	3.74	1.55	10.5	9.63	13.4	3.8	0.84
65.0	3.77	1.56	9.7	9.12	12.5	3.3	0.87
65.5	3.80	1.57	9.8	10.00	12.8	2.8	0.94
66.0	3.83	1.59	9.9	10.05	12.9	2.8	0.93
66.5	3.86	1.61	10.0	8.50	12.5	4.1	0.79
67.0	3.89	1.62	12.8	9.76	15.8	6.0	0.68
67.5	3.91	1.64	12.0	11.21	15.4	4.2	0.84
68.0	3.94	1.65	13.4	10.43	16.5	6.1	0.70
68.5	3.97	1.67	12.4	11.48	15.9	4.4	0.83
69.0	4.00	1.68	13.7	10.61	16.9	6.3	0.69
69.5	4.03	1.70	17.3	8.43	19.8	11.4	0.43
70.0	4.06	1.72	15.6	11.59	19.0	7.5	0.66
70.5	4.09	1.73	17.9	12.81	21.8	8.9	0.63
71.0	4.12	1.75	30.1	17.43	35.3	17.9	0.50
71.5	4.15	1.76	44.5	20.44	50.6	30.2	0.40
72.0	4.17	1.78	53.5	23.24	60.5	37.3	0.38
72.5	4.21	1.79	52.3	21.29	58.7	37.4	0.36
73.0	4.23	1.81	51.4	21.90	57.9	36.0	0.37
73.5	4.27	1.83	56.9	26.90	64.9	38.0	0.41
74.0	4.29	1.84	59.1	25.55	66.8	41.2	0.38
74.5	4.32	1.86	60.7	24.56	68.1	43.5	0.36
75.0	4.35	1.87	61.7	18.93	67.4	48.5	0.27

PROJECT: NORTHWESTERN UNIV.
STS JOB NUMBER: P-4592
BORING NO. 2
OPERATOR: NHS
DATE: 12-14-87

VANE SHEAR RESULTS

DEPTH (meters)	DEPTH (feet)	Su (tsf)	Su (psf)	REMOLDED Su (tsf)	REMOLDED Su (psf)	SENSITIVITY
9.0	29.5	0.33	660	0.10	192	3.4
10.0	32.8	NO READING, POSSIBLE COBBLE OR GRAVEL				
10.5	34.4	0.41	820	0.21	420	2.0
11.5	37.7	0.33	660	0.15	300	2.2
12.5	41.0	0.37	740	0.19	380	1.9
13.5	44.3	0.40	800	0.21	420	1.9
14.5	47.6	0.41	820	0.21	420	2.0
15.5	50.8	0.38	760	0.16	320	2.4
16.5	54.1	0.43	860	0.19	380	2.3
17.5	57.4	0.34	680	0.21	420	1.6
18.5	60.7	0.78	1560	0.45	900	1.7
19.5	64.0	0.71	1420	0.44	880	1.6
20.2	66.3	1.79	3580	0.63	1260	2.8

POSSIBLE GRAVEL AT 66 FEET

NORTHWESTERN UNIVERSITY TEST NO. DMT-1
FILE NAME: LAKE FRONT SITE
FILE NUMBER: 1988-1

RECORD OF DILATOMETER TEST NO. DMT-1 (IN PMT BOREHOLE)
USING DATA REDUCTION PROCEDURES IN MARCHETTI (ASCE,J-GED,MARCH 80)
KO IN SANDS DETERMINED USING SCHMERTMANN METHOD (1983)
PHI ANGLE CALCULATION BASED ON DURGUNOGLU AND MITCHELL (ASCE,RALEIGH CONF,JUNE 75)
MODIFIED MAYNE AND KULHAWY FORMULA USED FOR OCR IN SANDS (ASCE,J-GED,JUNE 82)

LOCATION: PILE TEST LOCATION FOR ASCE CONGRESS
PERFORMED - DATE: APRIL 30, 1988
BY: MORAD MAHMOUD ,WOODWARD CLYDE
CONSULTUNTS AND D&G DRILLING

CALIBRATION INFORMATION:
DA= .13 BARS DB= .32 BARS ZM= .20 BARS ZW= 5.00 METERS VSO= 2.500 BARS
ROD DIA.= 3.70 CM FRICTION RED. DIA.= 4.80 CM ROD WEIGHT= 6.50 KG/M DELTA/PHI= .50

1 BAR = 1.019 KG/CM2 = 1.044 TSF = 14.51 PSI ANALYSIS USES H2O UNIT WEIGHT = 1.000 T/M3

Z (FT)	THRUST (KG)	A (BAR)	B (BAR)	ED (BAR)	ID	KD	UO (BAR)	GAMMA (T/M3)	SV (BAR)	PC (BAR)	OCR	KO	CU (BAR)	PHI (DEG)	M (BAR)	SOIL TYPE
45.67		5.10	6.20	24.	.16	2.50	.834	1.70	1.666	2.36	1.42	.67	.48		26.	CLAY
46.33		5.20	6.20	20.	.14	2.53	.854	1.70	1.680	2.42	1.44	.68	.50		22.	CLAY
47.00		5.20	6.40	27.	.19	2.49	.873	1.70	1.693	2.39	1.41	.67	.49		29.	CLAY
47.67		5.40	6.50	24.	.15	2.58	.893	1.70	1.707	2.54	1.49	.69	.52		26.	CLAY
48.33		5.40	6.50	24.	.16	2.55	.913	1.70	1.721	2.51	1.46	.68	.51		26.	CLAY

END OF SOUNDING

NORTHWESTERN UNIVERSITY TEST NO. DMT 2

FILE NAME: PILE CAPACITY PREDICTION EVENT

FILE NUMBER: 1988 2

RECORD OF DILATOMETER TEST NO. DMT 2 (IN DMT SOUNDING)
USING DATA REDUCTION PROCEDURES IN MARCHETTI (ASCE,J GED,MARCH 80)
KO IN SANDS DETERMINED USING SCHMERTMANN METHOD (1983)
PHI ANGLE CALCULATION BASED ON DURGUNOGLU AND MITCHELL (ASCE,RALEIGH CONF,JUNE 75)
MODIFIED MAYNE AND KULHAWY FORMULA USED FOR OCR IN SANDS (ASCE,J GED,JUNE 82)

LOCATION: ON CAMPUS LAKE FILL PILE TEST SITE FOR CONGRESS CONF.
PERFORMED - DATE: MAY 14, 1988
BY: MURAD MAHMUD AND PSI
(PROFESSIONAL SERVICE INDUSTRIES)

CALIBRATION INFORMATION:
DA= .12 BARS DB= .29 BARS ZM= .20 BARS ZW= 5.00 METERS VSO= 1.200 BARS
ROD DIA.= 3.70 CM FRICTION RED. DIA.= 4.80 CM ROD WEIGHT= 6.50 KG/M DELTA/PHI= .50

1 BAR = 1.019 KG/CM2 = 1.044 TSF = 14.51 PSI ANALYSIS USES H2O UNIT WEIGHT = 1.000 T/M3

Z (FT)	THRUST (KG)	A (BAR)	B (BAR)	ED (BAR)	ID	KD	UO (BAR)	GAMMA (T/M3)	SV (BAR)	PC (BAR)	OCR	KO	CU (BAR)	PHI (DEG)	M (BAR)	SOIL TYPE
18.00		3.60	40.00	1311.	23.29	1.47	.098	1.90	1.102						1115.	SAND
19.00		3.60	40.00	1311.	23.77	1.41	.131	1.90	1.131						1115.	SAND
20.00		1.80	9.00	247.	5.84	1.05	.164	1.80	1.159						210.	SAND
21.00		2.10	22.00	710.	24.10	.72	.196	1.80	1.185						604.	SAND
22.00		4.10	40.00	1293.	18.48	1.66	.229	1.90	1.213						1218.	SAND
23.00		5.20	40.00	1253.	11.51	2.52	.262	2.00	1.245						1633.	SAND
24.00		5.20	40.00	1253.	11.63	2.43	.294	2.00	1.277						1594.	SAND
25.00		4.00	5.10	25.	.20	2.73	.327	1.70	1.304	2.12	1.62	.72	.42		29.	CLAY
26.00		4.00	5.10	25.	.21	2.64	.360	1.70	1.328	2.07	1.56	.71	.42		29.	CLAY
27.00		4.00	5.00	21.	.18	2.59	.393	1.70	1.350	2.02	1.50	.69	.41		24.	CLAY
28.00		4.60	5.60	21.	.15	2.96	.425	1.70	1.373	2.53	1.84	.78	.49		27.	CLAY
29.00		4.40	5.80	36.	.27	2.73	.458	1.70	1.396	2.27	1.62	.73	.45		42.	CLAY
30.00		4.00	5.00	21.	.18	2.40	.491	1.70	1.419	1.88	1.33	.65	.39		22.	CLAY
33.00		4.40	5.80	36.	.28	2.47	.589	1.70	1.488	2.07	1.39	.67	.43		39.	CLAY
34.00		4.20	6.00	51.	.43	2.27	.621	1.70	1.511	1.84	1.22	.62	.39		50.	SILTY CLAY
35.00		4.70	5.40	11.	.08	2.58	.655	1.50	1.531	2.28	1.49	.69	.46		12	MUD
36.00		4.40	5.40	21.	.17	2.32	.687	1.70	1.550	1.96	1.26	.63	.41		22.	CLAY
37.00		4.80	5.90	25.	.18	2.52	.719	1.70	1.573	2.26	1.44	.68	.46		27.	CLAY
38.00		4.90	5.90	21.	.15	2.53	.753	1.70	1.596	2.30	1.44	.68	.47		23.	CLAY
39.00		4.90	6.00	25.	.18	2.47	.785	1.70	1.619	2.25	1.39	.66	.46		27.	CLAY
40.00		4.90	6.00	25.	.18	2.42	.817	1.70	1.641	2.21	1.34	.65	.46		26.	CLAY
41.00		4.90	5.80	18.	.13	2.37	.851	1.70	1.665	2.17	1.30	.64	.45		18.	CLAY
42.00		4.90	5.40	3.	.02	2.33	.883	1.50	1.684	2.14	1.27	.63	.45		3	MUD
43.00		5.20	6.20	21.	.15	2.45	.916	1.70	1.704	2.34	1.37	.66	.48		23.	CLAY
44.00		5.40	6.20	14.	.09	2.52	.949	1.70	1.727	2.48	1.43	.68	.51		15.	CLAY
45.00		5.40	6.20	14.	.09	2.47	.981	1.70	1.750	2.43	1.39	.66	.50		15.	CLAY
46.00		5.40	6.20	14.	.10	2.42	1.014	1.70	1.772	2.38	1.35	.65	.49		15.	CLAY
47.00		5.40	6.40	21.	.15	2.36	1.047	1.70	1.796	2.33	1.30	.64	.49		22.	CLAY
48.00		5.40	6.40	21.	.15	2.32	1.079	1.70	1.818	2.29	1.26	.63	.48		22.	CLAY
49.00		5.40	6.40	21.	.15	2.27	1.112	1.70	1.841	2.26	1.22	.61	.47		21.	CLAY

END OF SOUNDING

Symbols:

DA	Free air correction to the "A" reading in bars.
DB	Free air correction to the "B" reading in bars.
ZM	Control unit reading when system is vented (gage zero) in bars.
ZW	Depth to ground water table in meters.
VSO	Total vertical overburden stress at depth of first test reading.
Z(I)	Test reading depth in ft.
A	Control unit "A" reading in bars.
B	Control unit "B" reading in bars.
Thrust(I)	Thrust force required to advance dilatometer from previous to current test reading.
UO	Pore water pressure in bars .
ED	Dilatometers modulus.
ID	Dilatometer material index.
KD	Dilatometer horizontal stress index
GAMMA	Total unit weight of soil.
SV	Effective vertical stress.
PC	Preconsolidation pressure.
OCR	Overconsolidation ratio .
KO	In situ coefficient of lateral earth pressure.
CU	Undrained shear strength.
Phi	The soil's drained friction angle.
M	Tangent drained constrained modulus.

CONSOLIDATION TEST DATA

Load	SAMPLE 15		SAMPLE 16		SAMPLE 17		SAMPLE 18	
(t/ft^2)	$\epsilon_{vert.}$ (%)	C_v $x10^{-4}cm^2/sec$	$\epsilon_{vert.}$ (%)	C_v $x10^{-4}cm^2/sec$	$\epsilon_{vert.}$ (%)	C_v $x10^{-4}cm^2/sec$	$\epsilon_{vert.}$ (%)	C_v $x10^{-4}cm^2/sec$
1/16	0.8	4.35	0.5	5.69	0.8	7.54	1.0	2.38
1/8	1.3	1.47	0.9	-	1.1	1.40	1.3	1.49
1/4	1.9	0.96	1.5	4.47	1.8	1.85	1.9	1.70
1/2	3.2	3.60	2.5	2.96	2.8	1.45	2.9	1.55
1	4.7	4.36	3.8	4.34	3.8	1.94	4.5	2.10
2	6.6	8.04	5.9	0.78	6.0	5.21	6.6	5.06
4	8.7	28.9	9.0	5.07	8.7	10.7	8.7	4.81
8	11.4	16.5	12.3	7.15	11.2	7.3	11.2	8.30
16			15.7	11.8			14.0	14.3
4			14.6	16.7			13.1	31.5
1	10.0	26.5	12.9	5.79	10.1	23.2	12.6	6.26
1/2	8.3	3.70			9.8	3.52		
1	9.2	25.3			9.9	31.1		
2	10.0	37.3	13.3	15.0	10.2	23.2	12.8	13.5
4	10.9	45.7	14.0	21.3	10.7	36.7	13.3	18.2
8	11.9	58.9	15.0	24.5	11.6	45.1	14.1	26.1
16	13.7	69.4	16.4	36.0	14.1	23.5	15.5	30.1
32	16.1	220.0	19.4	17.8	17.2	30.7	18.3	21.1

CONSOLIDATION TEST DATA

Load	SAMPLE 19		SAMPLE 20		SAMPLE 21		SAMPLE 22	
(t/ft^2)	$\epsilon_{vert.}$ (%)	C_v $x10^{-4}cm^2/sec$	$\epsilon_{vert.}$ (%)	C_v $x10^{-4}cm^2/sec$	$\epsilon_{vert.}$ (%)	C_v $x10^{-4}cm^2/sec$	$\epsilon_{vert.}$ (%)	C_v $x10^{-4}cm^2/sec$
1/16	0.5	0.31	0.7	1.51	0.9	3.73	0.3	5.72
1/8	0.8	0.87	1.0	0.75	1.3	5.85	0.3	1.14
1/4	1.4	0.80	1.8	1.48	2.4	4.26	1.2	0.98
1/2	2.3	3.43	3.0	2.31	3.4	5.33	2.6	2.73
1	3.9	8.22	4.6	2.62	5.0	8.61	4.8	4.11
2	6.0	7.31	6.9	5.59	6.0	14.4	6.9	5.57
4	8.8	8.38	9.8	8.59	*10.0	10.9	11.2	17.3
8	11.9	10.0	13.1	13.5	12.7	6.72	13.5	10.2
16	15.1	16.8	16.7	14.0	16.0	8.11	16.0	10.9
4	14.2	33.8	15.8	23.2	15.4	26.2	15.4	26.4
1	12.8	4.71	14.2	7.67	11.3	2.55	14.2	5.65
1/2								
1								
2	13.0	21.7	14.5	14.0	12.8	5.79	14.3	13.0
4	13.6	26.4	15.1	18.4	14.2	15.3	14.9	19.6
8	14.4	33.8	16.0	40.6	15.4	29.8	15.5	14.6
16	15.6	35.1	17.3	24.7	16.9	26.5	16.7	8.01
32	18.2	15.5	20.2	20.6	19.6	18.7	19.1	16.6

* 5 tsf

CONSOLIDATION TEST DATA

Load	SAMPLE 23		SAMPLE 24		SAMPLE 25		SAMPLE 26	
	$\epsilon_{vert.}$	C_v	$\epsilon_{vert.}$	C_v	$\epsilon_{vert.}$	C_v	$\epsilon_{vert.}$	C_v
(t/ft^2)	(%)	x10^{-4}cm^2/sec	(%)	x10^{-4}cm^2/sec	(%)	x10^{-4}cm^2/sec	(%)	x10^{-4}cm^2/sec
1/16	1.6	1.71	1.3	2.12	0.5	0.30	0.7	3.00
1/8	2.5	1.56	1.8	0.37	0.8	1.12	1.2	6.96
1/4	3.4	2.34	2.8	2.37	1.2	2.53	1.7	3.68
1/2	4.9	2.32	4.0	2.19	2.0	4.07	2.9	1.30
1	6.5	3.60	5.7	5.10	3.3	2.67	4.5	4.45
2	8.4	4.84	7.9	2.55	5.3	5.71	6.8	4.34
4	10.7	5.43	10.5	6.82	8.3	5.23	9.9	5.65
8	13.1	7.44	13.4	12.3	11.7	7.19	13.2	7.20
16	15.7	11.0	16.4	16.8	15.4	6.60	16.5	12.9
4	15.1	28.6	15.5	25.0	14.3	20.4	15.7	24.9
1	14.0	5.15	14.1	5.25	12.9	6.90	14.5	5.86
1/2								
1								
2	14.1	9.68	14.4	23.2	13.1	24.6	14.6	15.1
4	14.6	28.0	14.9	27.5	13.7	18.5	15.2	25.3
8	15.2	33.1	15.8	32.5	14.6	20.8	15.9	23.1
16	16.2	37.8	16.9	39.6	16.0	43.8	17.1	33.6
32	18.5	19.3	19.9	20.0	19.6	20.2	20.3	16.3

CONSOLIDATION TEST DATA

Load	SAMPLE 27		SAMPLE 28		SAMPLE 29		SAMPLE 30	
	$\epsilon_{vert.}$	C_v	$\epsilon_{vert.}$	C_v	$\epsilon_{vert.}$	C_v	$\epsilon_{vert.}$	C_v
(t/ft^2)	(%)	x10^{-4}cm^2/sec	(%)	x10^{-4}cm^2/sec	(%)	x10^{-4}cm^2/sec	(%)	x10^{-4}cm^2/sec
1/16								
1/8	0.7	3.04	0.7	10.2	0.7	3.75	1.6	2.19
1/4	1.2	2.38	1.2	-	1.3	1.48	2.2	1.82
1/2	2.1	5.35	2.2	6.63	2.3	3.12	3.1	2.7
1	3.4	5.34	3.7	17.7	3.7	4.83	4.1	6.38
2	5.1	5.42	5.9	5.97	5.5	4.88	5.6	5.82
4	7.5	4.91	9.0	6.57	8.0	5.54	7.4	6.54
8	10.5	7.10	12.6	8.01	10.9	7.04	9.4	11.1
16	13.8	8.59	16.0	12.5	14.1	10.0	11.8	26.4
32	17.2	10.2	20.0	13.8	17.6	13.6	14.3	20.2
8	16.1	17.8	18.1	24.9	16.3	24.2	13.6	24.3
2	14.2	5.07	17.1	5.58	14.4	5.95	12.4	6.47
4	14.6	15.9	17.4	15.6	14.8	23.7	12.6	19.4
8	15.4	14.9	18.2	19.6	15.6	14.2	13.1	25.3
16	16.0	23.5	19.2	24.9	16.7	26.5	13.8	42.5
32	18.0	23.8	20.7	28.9	18.3	31.4	14.8	39.6
64	21.1	16.7	24.0	17.6	21.3	19.1	17.3	17.6

* Note New Loads

CONSOLIDATION TEST DATA

	SAMPLE 31		SAMPLE		SAMPLE		SAMPLE	
Load (t/ft^2)	$\epsilon_{vert.}$ (%)	C_v $x10^{-4}cm^2/sec$	$\epsilon_{vert.}$ (%)	C_v $x10^{-4}cm^2/sec$	$\epsilon_{vert.}$ (%)	C_v $x10^{-4}cm^2/sec$	$\epsilon_{vert.}$ (%)	C_v $x10^{-4}cm^2/sec$
1/16								
1/8	0.9	8.65						
1/4	1.6	2.50						
1/2	2.7	8.14						
1	4.0	7.13						
2	5.8	10.3						
4	7.9	6.58						
8	10.0	9.44						
16	12.2	14.4						
32	14.6	18.0						
8	13.9	38.1						
2	12.8	7.63						
4	13.1	34.3						
8	13.5	38.5						
16	14.1	45.1						
32	15.0	48.0						
64	17.2	21.7						

* Note New Loads

UNCONSOLIDATED - UNDRAINED TRIAXIAL
COMPRESSION TEST DATA

SAMPLE No.	DEPTH (ft)	$(\frac{\sigma_1 - \sigma_3}{2})$peak ($16/ft^2$)	ϵ_{peak} (1) (%)	$\epsilon_{50\%}$ (2) (%)	Comments
15	29.5	532	8.88	1.58	
16	32.0	840	6.83	1.74	
17	34.5	604	16.07	2.38	Bulge Failure
18	37.0	532	11.74	1.95	
19	39.5	625	8.77	1.69	
20	42.0	604	8.33	2.22	
21	44.5	502	8.33	1.48	
22	47.0	573	13.53	2.94	Bulge Failure
25	54.5	522	1.18		

(1) Axial Strain at $(\sigma_1 - \sigma_3)$peak

(2) Axial Strain at $1/2(\sigma_1 - \sigma_3)$peak

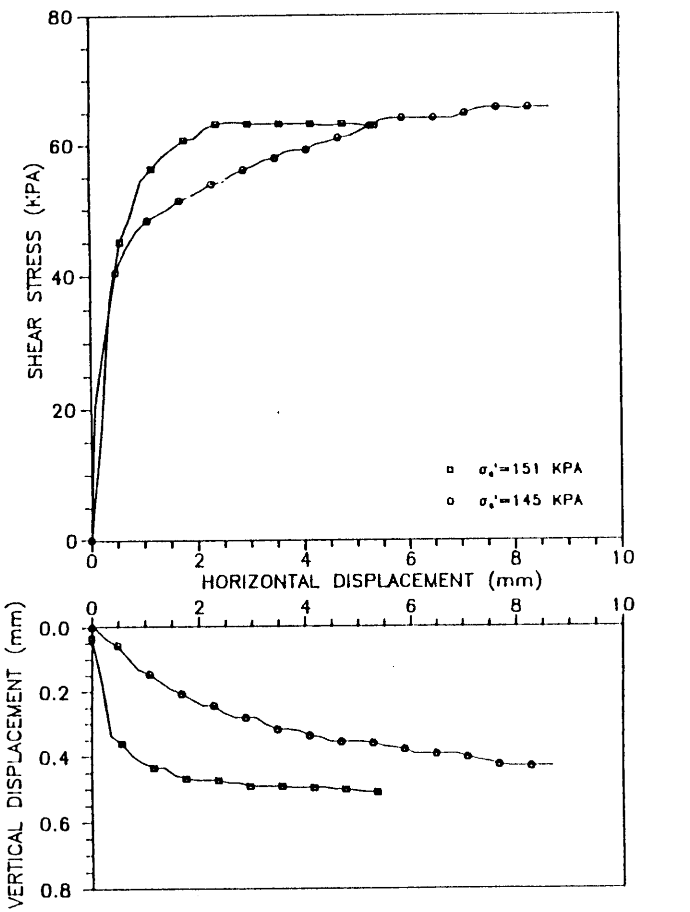

NOTES : 1. Last consolidation increment held for 24 hours.
2. Rate of horizontal displacement varied from 0.002 to 0.003 mm/min.
3. Specimens taken from tube 19.

RESULTS OF DIRECT SHEAR TESTS

<u>Summary of CK_oU Triaxial Data</u>

	Compression	Extension
σ'_{vc}	138 kPa	132 kPa
K_o	0.5	0.5
S_u	40.5 kPa	30.5 kPa
Su/σ'_{vc}	0.33	0.23
E_u(initial)	4200 kPa	21,900 kPa
$E_{(50)}$	1290 kPa	10,700 kPa
$E_{(peak)}$	410 kPa	750 kPa

<u>NOTE</u>: E_u(initial) was taken as secant modulus at 0.05% strain. $E_{(50)}$ and $E_{(peak)}$ are also secant moduli.

Appendix B

Soil Properties Calculation for NGES at Northwestern University

Sample 15 e_o: **0.6** **Depth: 29.5ft**

Load	Load	ε_{vert}	$\Delta\varepsilon_{vert}$	e	C_v	C_v	m_v	k_v
(t/ft^2)	(k/ft^2)	(%)	(%)		$*10^{-4}cm^2/s$	ft^2/day	(ft^2/k)	(ft/day)
0.0625	0.125	0.8	0.8	0.5872	4.35	0.014	0.064	5.46E-05
0.125	0.25	1.3	0.5	0.5792	1.47	0.014	0.040	3.41E-05
0.25	0.5	1.9	0.6	0.5696	0.96	0.009	0.024	1.34E-05
0.5	1	3.2	1.3	0.5488	3.6	0.033	0.026	5.43E-05
1	2	4.7	1.5	0.5248	4.36	0.041	0.015	3.80E-05
2	4	6.6	1.9	0.4944	8.04	0.075	0.010	4.43E-05
4	8	8.7	2.1	0.4608	28.9	0.269	0.005	8.80E-05
8	16	11.4	2.7	0.4176	16.5	0.153	0.003	3.23E-05
16	32	\	\	\	\	\	\	\
4	8	\	\	\	\	\	\	\
1	2	10	\	0.44	26.5	0.246	\	\
0.5	1	8.3	-1.7	0.4672	3.7	0.034	0.017	3.65E-05
1	2	9.2	0.9	0.4528	25.3	0.235	0.009	1.32E-04
2	4	10	0.8	0.44	37.3	0.347	0.004	8.66E-05
4	8	10.9	0.9	0.4256	45.7	0.425	0.002	5.97E-05
8	16	11.9	1	0.4096	58.9	0.548	0.001	4.27E-05
16	32	13.7	1.8	0.3808	69.4	0.645	0.001	4.53E-05
32	64	16.1	4.2	0.3424	220	2.046	0.001	1.12E-04

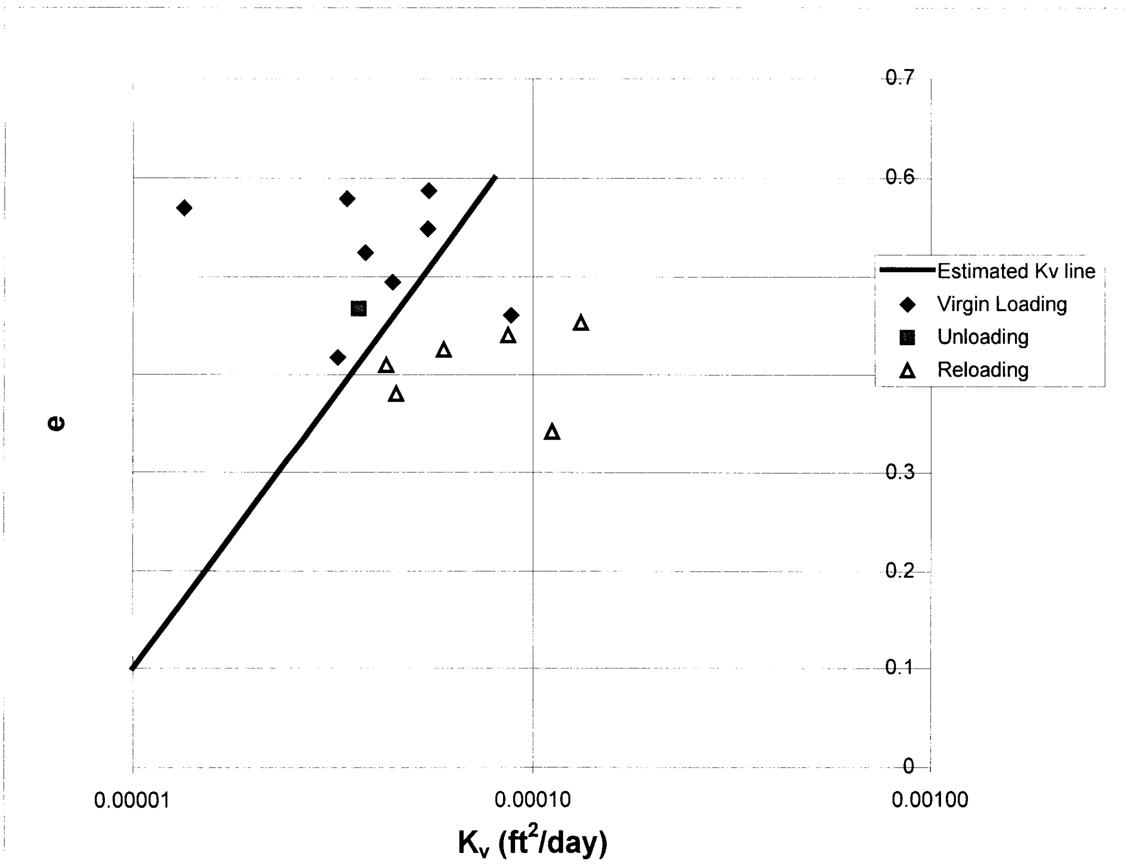

Sample 16 e_o: **0.65** **Depth: 32ft**

Load	Load	ε_{vert}	$\Delta\varepsilon_{vert}$	e	C_v	C_v	m_v	k_v
(t/ft^2)	(k/ft^2)	(%)	(%)		*10^{-4}cm^2/s	ft^2/day	(ft^2/k)	(ft/day)
0.0625	0.125	0.5	0.5	0.64175	5.69	0.080	0.040	2.00E-04
0.125	0.25	0.9	0.4	0.63515	\	\	0.032	\
0.25	0.5	1.5	0.6	0.62525	4.47	0.042	0.024	6.23E-05
0.5	1	2.5	1	0.60875	2.96	0.028	0.020	3.44E-05
1	2	3.8	1.3	0.5873	4.34	0.040	0.013	3.27E-05
2	4	5.9	2.1	0.55265	0.78	0.007	0.011	4.75E-06
4	8	9	3.1	0.5015	5.07	0.047	0.008	2.28E-05
8	16	12.3	3.3	0.44705	7.15	0.066	0.004	1.71E-05
16	32	15.7	3.4	0.39095	11.8	0.110	0.002	1.46E-05
4	8	14.6	-1.1	0.4091	16.9	0.157	0.000	4.50E-06
1	2	12.9	-1.7	0.43715	5.79	0.054	0.003	9.52E-06
0.5	1	\	\	\	\	\	\	\
1	2	\	\	\	\	\	\	\
2	4	13.3	\	0.43055	15	0.140	\	\
4	8	14	0.7	0.419	21.3	0.198	0.002	2.16E-05
8	16	15	1	0.4025	24.5	0.228	0.001	1.78E-05
16	32	16.4	1.4	0.3794	36	0.335	0.001	1.83E-05
32	64	19.4	4.4	0.3299	17.8	0.166	0.001	1.42E-05

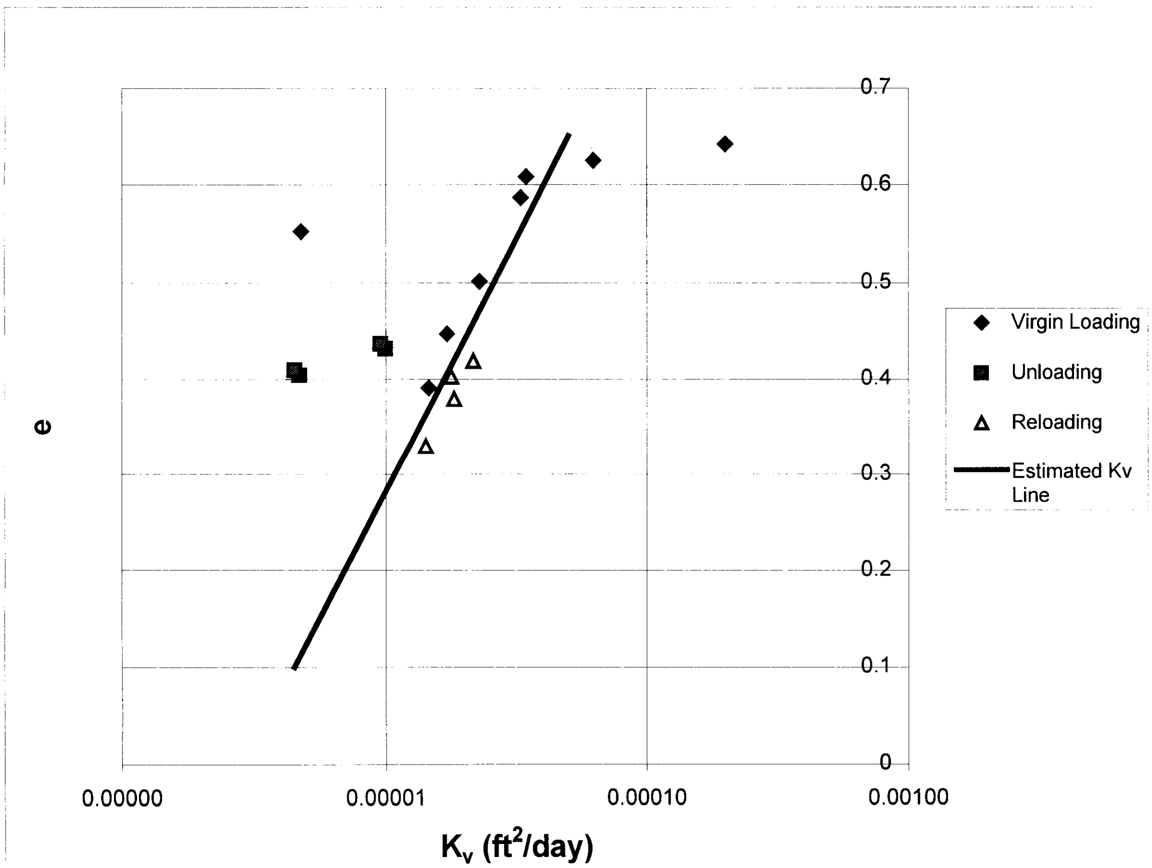

Sample 17 e_o: **0.63** **Depth: 34.5ft**

Load	Load	ε_{vert}	$\Delta\varepsilon_{vert}$	e	C_v	C_v	m_v	k_v
(t/ft^2)	(k/ft^2)	(%)	(%)		$*10^{-4}cm^2/s$	ft^2/day	(ft^2/k)	(ft/day)
0.0625	0.125	0.8	0.8	0.61696	7.54	0.014	0.064	0.000
0.125	0.25	1.1	0.3	0.61207	1.4	0.013	0.024	0.00002
0.25	0.5	1.8	0.7	0.60066	1.45	0.013	0.028	0.00002
0.5	1	2.8	1	0.58436	1.94	0.018	0.020	0.00002
1	2	3.8	1	0.56806	1.94	0.018	0.010	0.00001
2	4	6	2.2	0.5322	5.21	0.048	0.011	0.00003
4	8	8.7	2.7	0.48819	10.7	0.100	0.007	0.00004
8	16	11.2	2.5	0.44744	7.3	0.068	0.003	0.00001
16	32	\	\	\	\	\	\	\
4	8	\	\	\	\	\	\	\
1	2	10.1	\	0.46537	23.2	0.216	\	\
0.5	1	9.8	-0.3	0.47026	3.52	0.033	0.003	0.00001
1	2	9.9	0.1	0.46863	31.1	0.289	0.001	0.00002
2	4	10.2	0.3	0.46374	23.2	0.216	0.001	0.00002
4	8	10.7	0.5	0.45559	36.7	0.341	0.001	0.00003
8	16	11.6	0.9	0.44092	45.1	0.419	0.001	0.00003
16	32	14.1	2.5	0.40017	23.5	0.219	0.002	0.00002
32	64	17.2	5.6	0.34964	30.7	0.286	0.002	0.00003

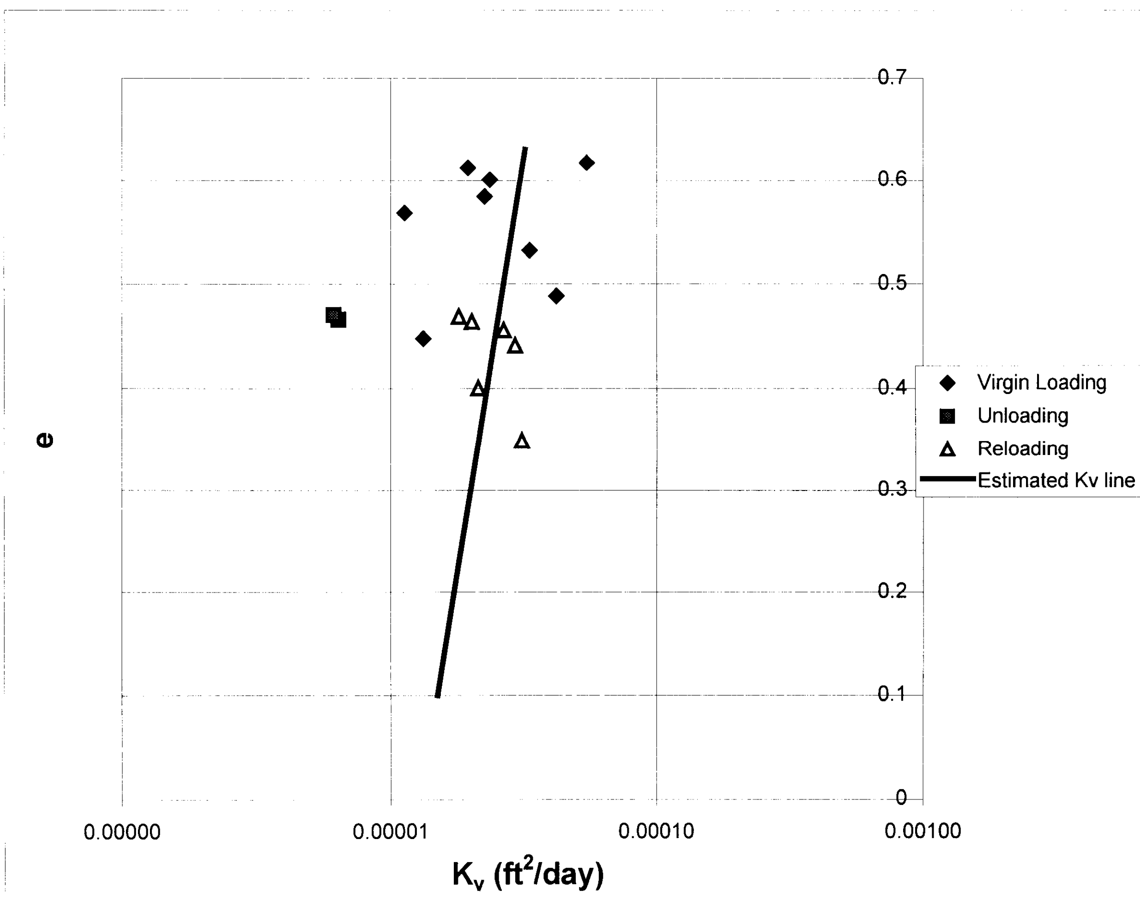

Sample 18 e_o: **0.62** **Depth: 37ft**

Load	Load	ε_{vert}	$\Delta\varepsilon_{vert}$	e	C_v	C_v	m_v	k_v
(t/ft^2)	(k/ft^2)	(%)	(%)		$*10^{-4}cm^2/s$	ft^2/day	(ft^2/k)	(ft/day)
0.0625	0.125	1	1	0.6038	2.38	0.022	0.080	1.10E-04
0.125	0.25	1.3	0.3	0.59894	1.49	0.014	0.024	2.08E-05
0.25	0.5	1.9	0.6	0.58922	1.7	0.016	0.024	2.37E-05
0.5	1	2.9	1	0.57302	1.55	0.014	0.020	1.80E-05
1	2	4.5	1.6	0.5471	2.1	0.020	0.016	1.95E-05
2	4	6.6	2.1	0.51308	5.06	0.047	0.011	3.08E-05
4	8	8.7	2.1	0.47906	4.81	0.045	0.005	1.47E-05
8	16	11.2	2.5	0.43856	8.3	0.077	0.003	1.51E-05
16	32	14	2.8	0.3932	14.3	0.133	0.002	1.45E-05
4	8	13.1	-0.9	0.40778	31.5	0.293	0.000	6.86E-06
1	2	12.6	-0.5	0.41588	6.26	0.058	0.001	3.03E-06
0.5	1	\	\	\	\	\	\	\
1	2	\	\	\	\	\	\	\
2	4	12.8	\	0.41264	13.5	0.126	\	\
4	8	13.3	0.5	0.40454	18.2	0.169	0.001	1.32E-05
8	16	14.1	0.8	0.39158	26.1	0.243	0.001	1.51E-05
16	32	15.5	1.4	0.3689	30.1	0.280	0.001	1.53E-05
32	64	18.3	4.2	0.32354	21.1	0.196	0.001	1.61E-05

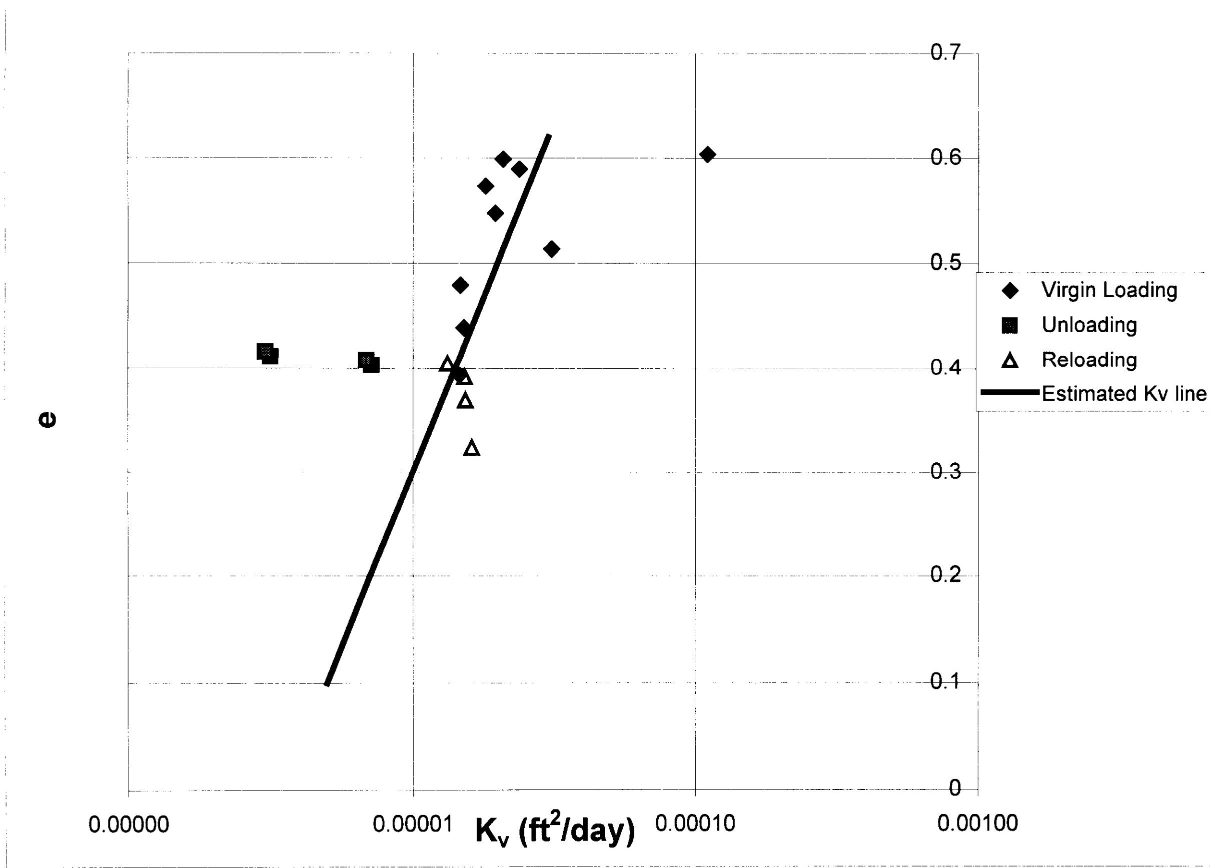

ample 19 **e_o: 0.6** **Depth: 39.5ft**

Load	Load	ε_{vert}	$\Delta\varepsilon_{vert}$	e	C_v	C_v	m_v	k_v
(t/ft^2)	(k/ft^2)	(%)	(%)		*10^{-4}cm^2/s	ft^2/day	(ft^2/k)	(ft/day)
0.0625	0.125	0.5	0.5	0.592	0.31	0.003	0.040	7.20E-0
0.125	0.25	0.8	0.3	0.5872	0.87	0.008	0.024	1.21E-0
0.25	0.5	1.4	0.6	0.5776	0.8	0.007	0.024	1.11E-0
0.5	1	2.3	0.9	0.5632	3.43	0.032	0.018	3.58E-0
1	2	3.9	1.6	0.5376	8.22	0.076	0.016	7.63E-0
2	4	6	2.1	0.504	7.31	0.068	0.011	4.45E-0
4	8	8.8	2.8	0.4592	8.38	0.078	0.007	3.40E-0
8	16	11.9	3.1	0.4096	10	0.093	0.004	2.25E-0
16	32	15.1	3.2	0.3584	16.8	0.156	0.002	1.95E-0
4	8	14.2	-0.9	0.3728	33.8	0.314	0.000	7.36E-0
1	2	12.8	-1.4	0.3952	4.71	0.044	0.002	6.38E-0
0.5	1	\	\	\	\	\	\	\
1	2	\	\	\	\	\	\	\
2	4	13	\	0.392	21.7	0.202	\	\
4	8	13.6	0.6	0.3824	26.4	0.246	0.002	2.30E-0
8	16	14.4	0.8	0.3696	33.8	0.314	0.001	1.96E-0
16	32	15.6	1.2	0.3504	35.1	0.326	0.001	1.53E-0
32	64	18.2	3.8	0.3088	15.5	0.144	0.001	1.07E-0

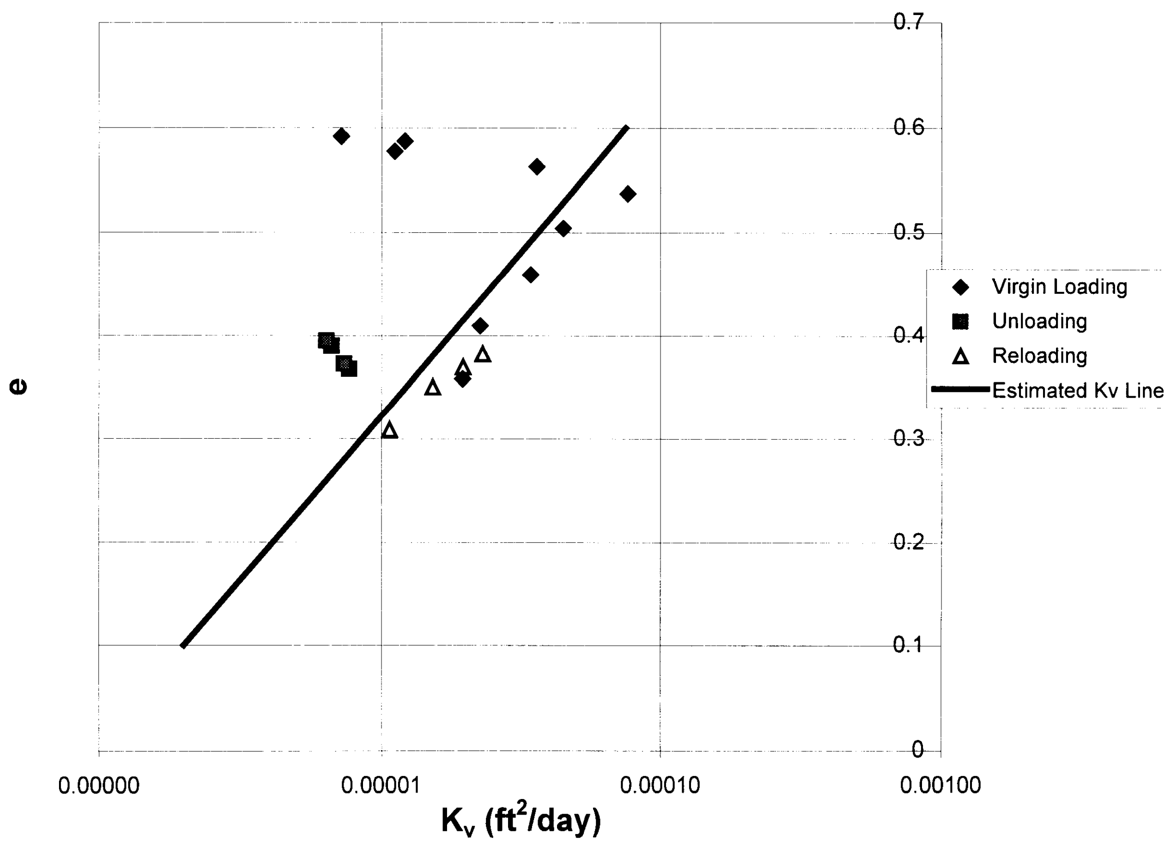

Sample 20 e_o: **0.54** **Depth: 42ft**

Load	Load	ε_{vert}	$\Delta\varepsilon_{vert}$	e	C_v	C_v	m_v	k_v
(t/ft^2)	(k/ft^2)	(%)	(%)		$*10^{-4}cm^2/s$	ft^2/day	(ft^2/k)	(ft/day)
0.0625	0.125	0.7	0.7	0.52922	1.51	0.014	0.056	4.91E-05
0.125	0.25	1	0.3	0.5246	0.75	0.007	0.024	1.04E-05
0.25	0.5	1.8	0.8	0.51228	1.48	0.014	0.032	2.75E-05
0.5	1	3	1.2	0.4938	2.31	0.021	0.024	3.22E-05
1	2	4.6	1.6	0.46916	2.62	0.024	0.016	2.43E-05
2	4	6.9	2.3	0.43374	5.59	0.052	0.012	3.73E-05
4	8	9.8	2.9	0.38908	8.59	0.080	0.007	3.61E-05
8	16	13.1	3.3	0.33826	13.5	0.126	0.004	3.23E-05
16	32	16.7	3.6	0.28282	14	0.130	0.002	1.83E-05
4	8	15.8	-0.9	0.29668	23.2	0.216	0.000	5.05E-06
1	2	14.2	-1.6	0.32132	7.67	0.071	0.003	1.19E-05
0.5	1	\	\	\	\	\	\	\
1	2	\	\	\	\	\	\	\
2	4	14.5	\	0.3167	14	0.130	\	\
4	8	15.1	0.6	0.30746	18.4	0.171	0.002	1.60E-05
8	16	16	0.9	0.2936	40.6	0.378	0.001	2.65E-05
16	32	17.3	1.3	0.27358	24.7	0.230	0.001	1.16E-05
32	64	20.2	4.2	0.22892	20.6	0.192	0.001	1.57E-05

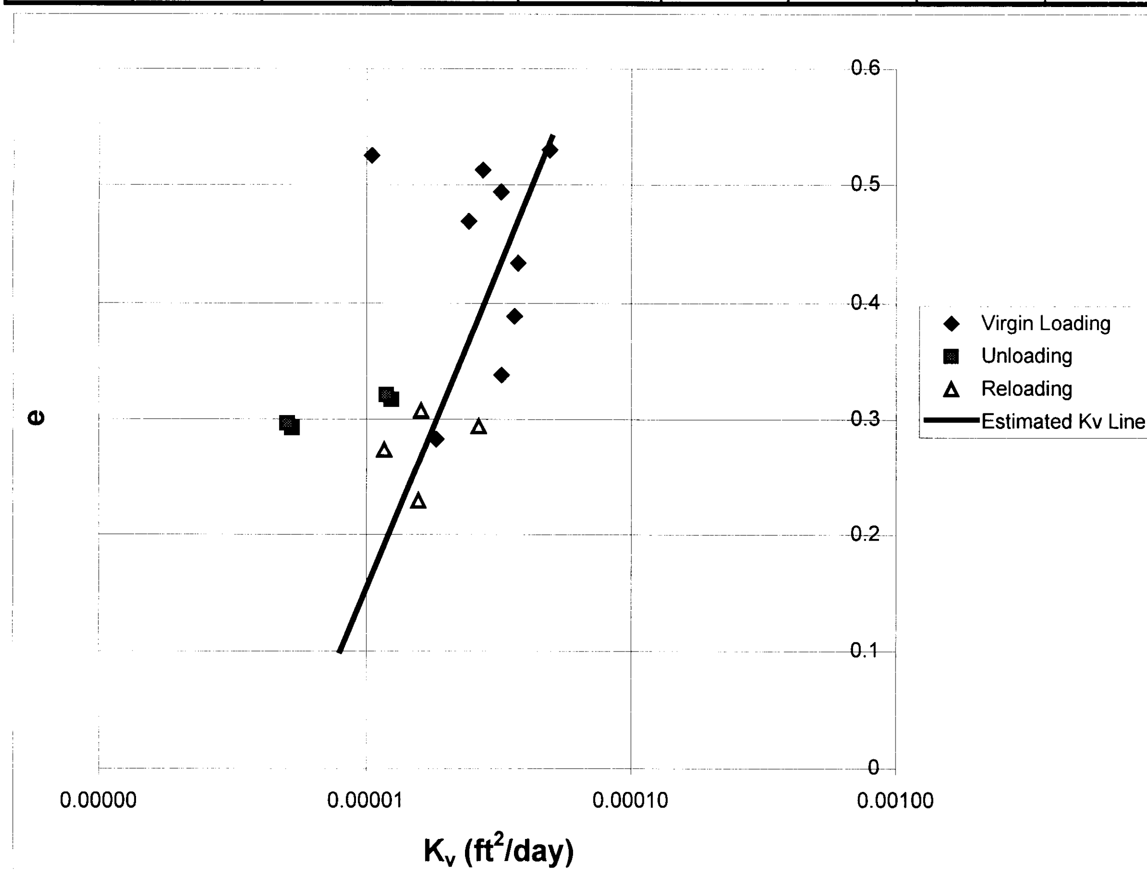

Sample 21 e_o: **0.62** **Depth: 44.5ft**

Load	Load	ε_{vert}	$\Delta\varepsilon_{vert}$	e	C_v	C_v	m_v	k_v
(t/ft^2)	(k/ft^2)	(%)	(%)		*10^{-4}cm^2/s	ft^2/day	(ft^2/k)	(ft/day)
0.0625	0.125	0.9	0.9	0.60542	3.73	0.035	0.072	1.56E-04
0.125	0.25	1.3	0.4	0.59894	5.85	0.054	0.032	1.09E-04
0.25	0.5	2.4	1.1	0.58112	4.26	0.040	0.044	1.09E-04
0.5	1	3.4	1	0.56492	5.33	0.050	0.020	6.19E-05
1	2	5	1.6	0.539	8.61	0.080	0.016	7.99E-05
2	4	6	1	0.5228	14.4	0.134	0.005	4.18E-05
4	8	10	4	0.458	10.9	0.101	0.010	6.33E-05
8	16	12.7	2.7	0.41426	6.72	0.062	0.003	1.32E-05
16	32	16	3.3	0.3608	8.11	0.075	0.002	9.71E-06
4	8	15.4	-0.6	0.37052	26.2	0.244	0.000	3.80E-06
1	2	11.3	-4.1	0.43694	2.55	0.024	0.007	1.01E-05
0.5	1	\	\	\	\	\	\	\
1	2	\	\	\	\	\	\	\
2	4	12.8	\	0.41264	5.79	0.054	\	\
4	8	14.2	1.4	0.38996	15.3	0.142	0.004	3.11E-05
8	16	15.4	1.2	0.37052	29.8	0.277	0.002	2.59E-05
16	32	16.9	1.5	0.34622	26.5	0.246	0.001	1.44E-05
32	64	19.6	4.2	0.30248	18.7	0.174	0.001	1.42E-05

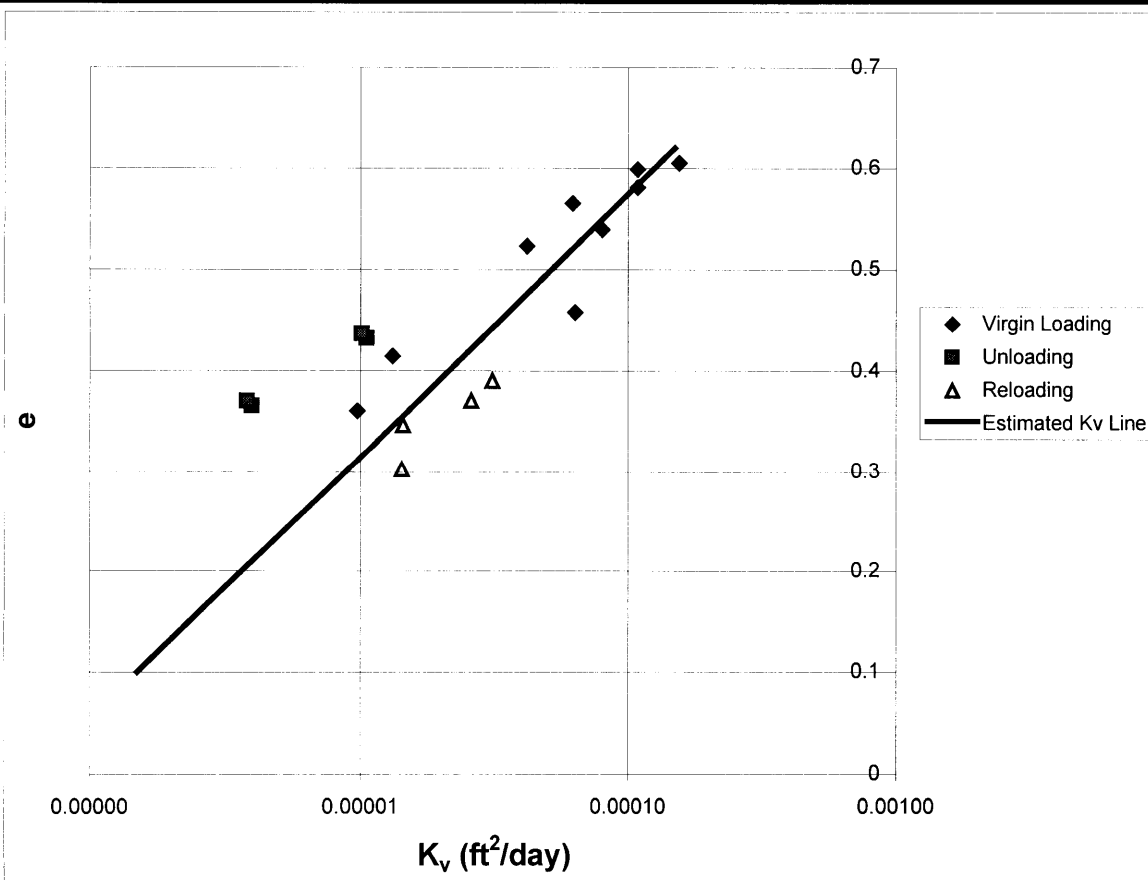

Sample 22 **e_o: 0.6** **Depth: 47ft**

Load	Load	ε_{vert}	$\Delta\varepsilon_{vert}$	e	C_v	C_v	m_v	k_v
(t/ft^2)	(k/ft^2)	(%)	(%)		*10^{-4}cm^2/s	ft^2/day	(ft^2/k)	(ft/day)
0.0625	0.125	0.3	0.3	0.5952	5.72	0.053	0.024	7.97E-05
0.125	0.25	0.3	0	0.5952	1.14	0.011	0.000	0.00E+00
0.25	0.5	1.2	0.9	0.5808	0.98	0.009	0.036	2.05E-05
0.5	1	2.6	1.4	0.5584	2.73	0.025	0.028	4.44E-05
1	2	4.8	2.2	0.5232	4.11	0.038	0.022	5.25E-05
2	4	6.9	2.1	0.4896	5.57	0.052	0.011	3.39E-05
4	8	11.2	4.3	0.4208	17.3	0.161	0.011	1.08E-04
8	16	13.5	2.3	0.384	10.2	0.095	0.003	1.70E-05
16	32	16.1	2.6	0.3424	10.9	0.101	0.002	1.03E-05
4	8	15.4	-0.7	0.3536	26.4	0.246	0.000	4.47E-06
1	2	14.2	-1.2	0.3728	5.65	0.053	0.002	6.56E-06
0.5	1	\	\	\	\	\	\	\
1	2	\	\	\	\	\	\	\
2	4	14.3	\	0.3712	13	0.121	\	\
4	8	14.9	0.6	0.3616	19.6	0.182	0.002	1.71E-05
8	16	15.5	0.6	0.352	14.6	0.136	0.001	6.35E-06
16	32	16.7	1.2	0.3328	8.01	0.074	0.001	3.49E-06
32	64	19.1	3.6	0.2944	16.6	0.154	0.001	1.08E-05

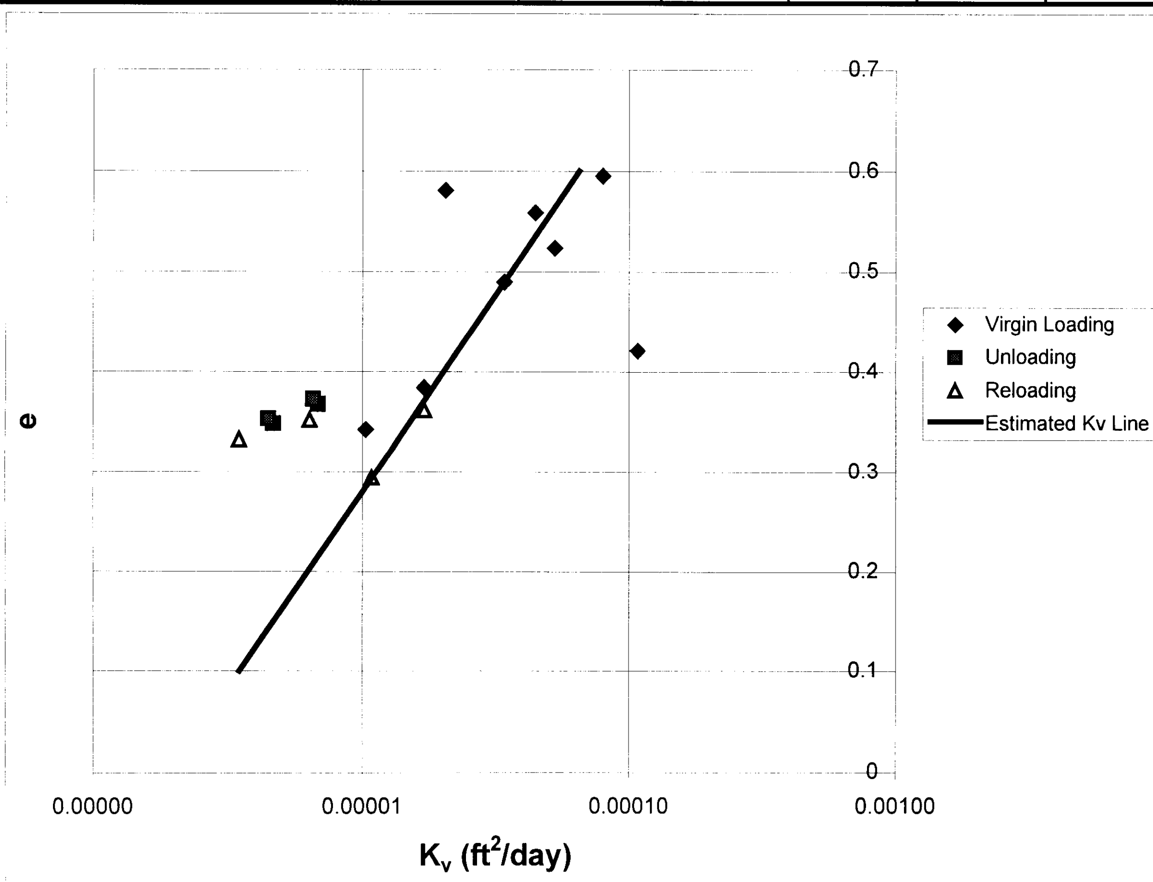

Sample 23 e_o: **0.6** **Depth: 49.5ft**

Load	Load	ε_{vert}	$\Delta\varepsilon_{vert}$	e	C_v	C_v	m_v	k_v
(t/ft^2)	(k/ft^2)	(%)	(%)		$*10^{-4}cm^2/s$	ft^2/day	(ft^2/k)	(ft/day)
0.0625	0.125	1.6	1.6	0.5744	1.71	0.016	0.128	1.27E-04
0.125	0.25	2.5	0.9	0.56	1.56	0.015	0.072	6.52E-05
0.25	0.5	3.4	0.9	0.5456	2.34	0.022	0.036	4.89E-05
0.5	1	4.9	1.5	0.5216	2.32	0.022	0.030	4.04E-05
1	2	6.5	1.6	0.496	3.6	0.033	0.016	3.34E-05
2	4	8.4	1.9	0.4656	4.84	0.045	0.010	2.67E-05
4	8	10.7	2.3	0.4288	5.43	0.050	0.006	1.81E-05
8	16	13.1	2.4	0.3904	7.44	0.069	0.003	1.30E-05
16	32	15.7	2.6	0.3488	11	0.102	0.002	1.04E-05
4	8	15.1	-0.6	0.3584	28.6	0.266	0.000	4.15E-06
1	2	14	-1.1	0.376	5.15	0.048	0.002	5.48E-06
0.5	1	\	\	\	\	\	\	\
1	2	\	\	\	\	\	\	\
2	4	14.1	\	0.3744	9.68	0.090	\	\
4	8	14.6	0.5	0.3664	28	0.260	0.001	2.03E-05
8	16	15.2	0.6	0.3568	33.1	0.308	0.001	1.44E-05
16	32	16.2	1	0.3408	37.8	0.352	0.001	1.37E-05
32	64	18.5	3.3	0.304	19.3	0.179	0.001	1.16E-05

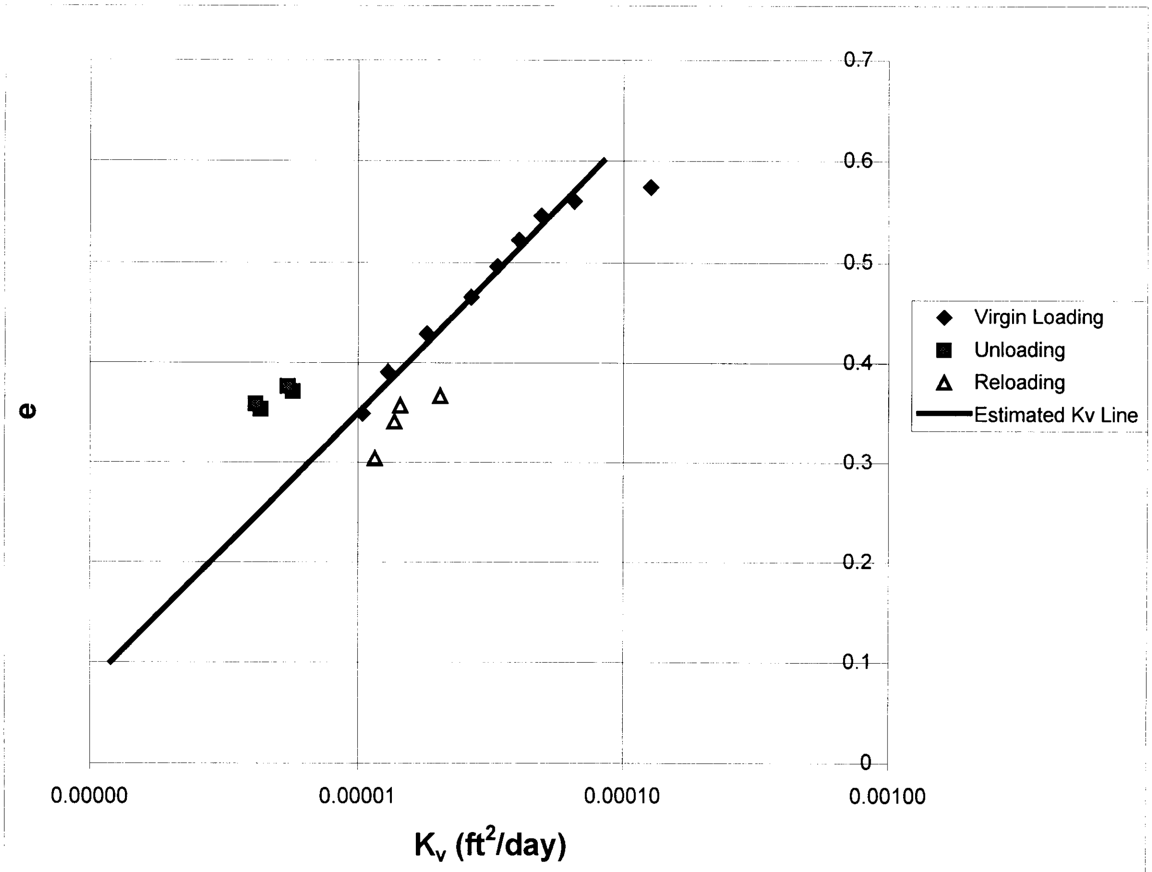

Sample 24 e_o: **0.61** **Depth: 52ft**

Load (t/ft^2)	Load (k/ft^2)	ε_{vert} (%)	$\Delta\varepsilon_{vert}$ (%)	e	C_v $*10^{-4} cm^2/s$	C_v ft^2/day	m_v (ft^2/k)	k_v (ft/day)
0.0625	0.125	1.3	1.3	0.58907	2.12	0.020	0.104	1.28E-04
0.125	0.25	1.8	0.5	0.58102	0.37	0.003	0.040	8.59E-06
0.25	0.5	2.8	1	0.56492	2.37	0.022	0.040	5.50E-05
0.5	1	4	1.2	0.5456	2.19	0.020	0.024	3.05E-05
1	2	5.7	1.7	0.51823	5.1	0.047	0.017	5.03E-05
2	4	7.9	2.2	0.48281	2.55	0.024	0.011	1.63E-05
4	8	10.5	2.6	0.44095	6.82	0.063	0.007	2.57E-05
8	16	13.4	2.9	0.39426	12.3	0.114	0.004	2.59E-05
16	32	16.4	3	0.34596	16.8	0.156	0.002	1.83E-05
4	8	15.5	-0.9	0.36045	25	0.233	0.000	5.44E-06
1	2	14.1	-1.4	0.38299	5.25	0.049	0.002	7.11E-06
0.5	1	\	\	\	\	\	\	\
1	2	\	\	\	\	\	\	\
2	4	14.4	\	0.37816	23.2	0.216	\	\
4	8	14.9	0.5	0.37011	27.5	0.256	0.001	1.99E-05
8	16	15.8	0.9	0.35562	32.5	0.302	0.001	2.12E-05
16	32	16.9	1.1	0.33791	39.6	0.368	0.001	1.58E-05
32	64	19.9	4.1	0.28961	20	0.186	0.001	1.49E-05

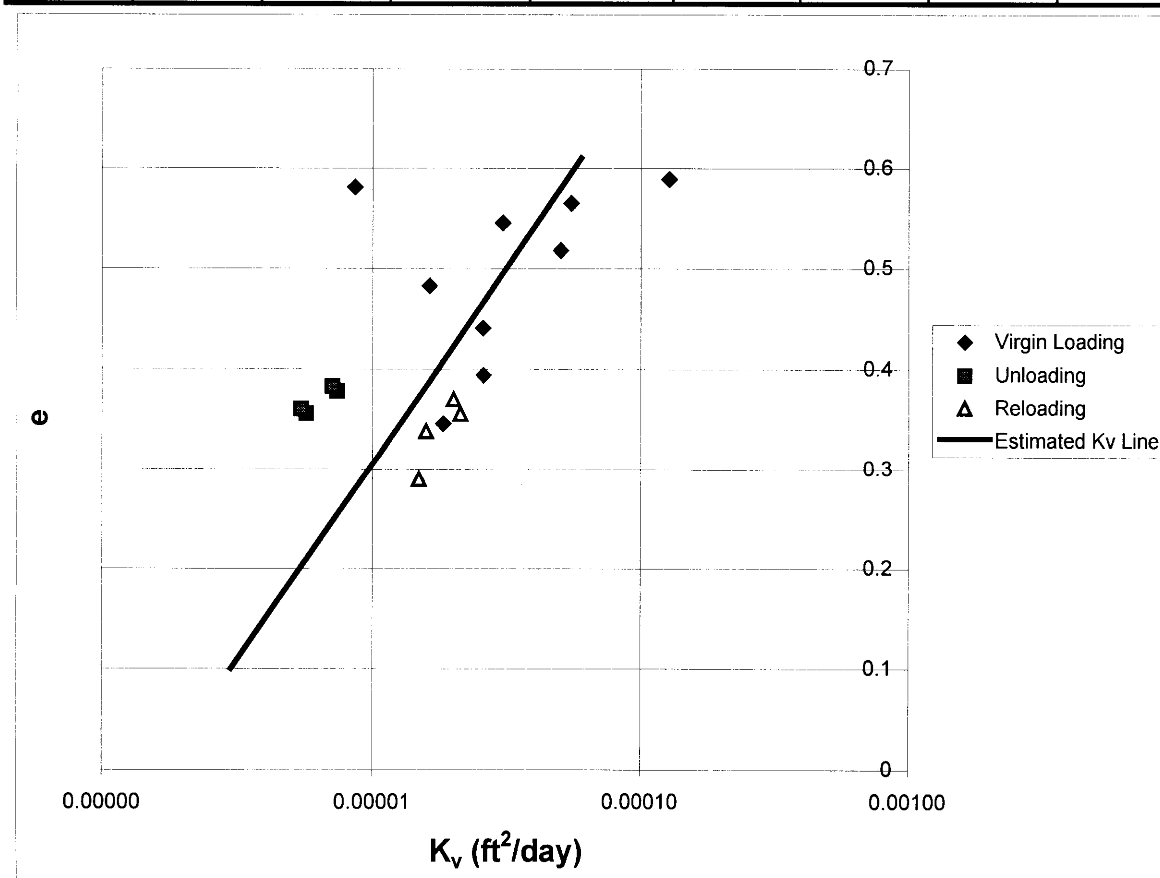

Sample 25 e_o: **0.62** **Depth: 54.5ft**

Load	Load	ε_{vert}	$\Delta\varepsilon_{vert}$	e	C_v	C_v	m_v	k_v
(t/ft^2)	(k/ft^2)	(%)	(%)		*10^{-4}cm^2/s	ft^2/day	(ft^2/k)	(ft/day)
0.0625	0.125	0.5	0.5	0.6119	0.3	0.003	0.040	6.96E-06
0.125	0.25	0.8	0.3	0.60704	1.12	0.010	0.024	1.56E-05
0.25	0.5	1.2	0.4	0.60056	2.53	0.024	0.016	2.35E-05
0.5	1	2	0.8	0.5876	4.07	0.038	0.016	3.78E-05
1	2	3.3	1.3	0.56654	2.67	0.025	0.013	2.01E-05
2	4	5.3	2	0.53414	5.71	0.053	0.010	3.31E-05
4	8	8.3	3	0.48554	5.23	0.049	0.008	2.28E-05
8	16	11.7	3.4	0.43046	7.19	0.067	0.004	1.77E-05
16	32	15.4	3.7	0.37052	6.6	0.061	0.002	8.86E-06
4	8	14.3	-1.1	0.38834	20.4	0.190	0.000	5.43E-06
1	2	12.9	-1.4	0.41102	6.9	0.064	0.002	9.34E-06
0.5	1	\	\	\	\	\	\	\
1	2	\	\	\	\	\	\	\
2	4	13.1	\	0.40778	24.6	0.229	\	\
4	8	13.7	0.6	0.39806	18.5	0.172	0.002	1.61E-05
8	16	14.6	0.9	0.38348	20.8	0.193	0.001	1.36E-05
16	32	16	1.4	0.3608	43.8	0.407	0.001	2.22E-05
32	64	19.6	5	0.30248	20.2	0.188	0.002	1.83E-05

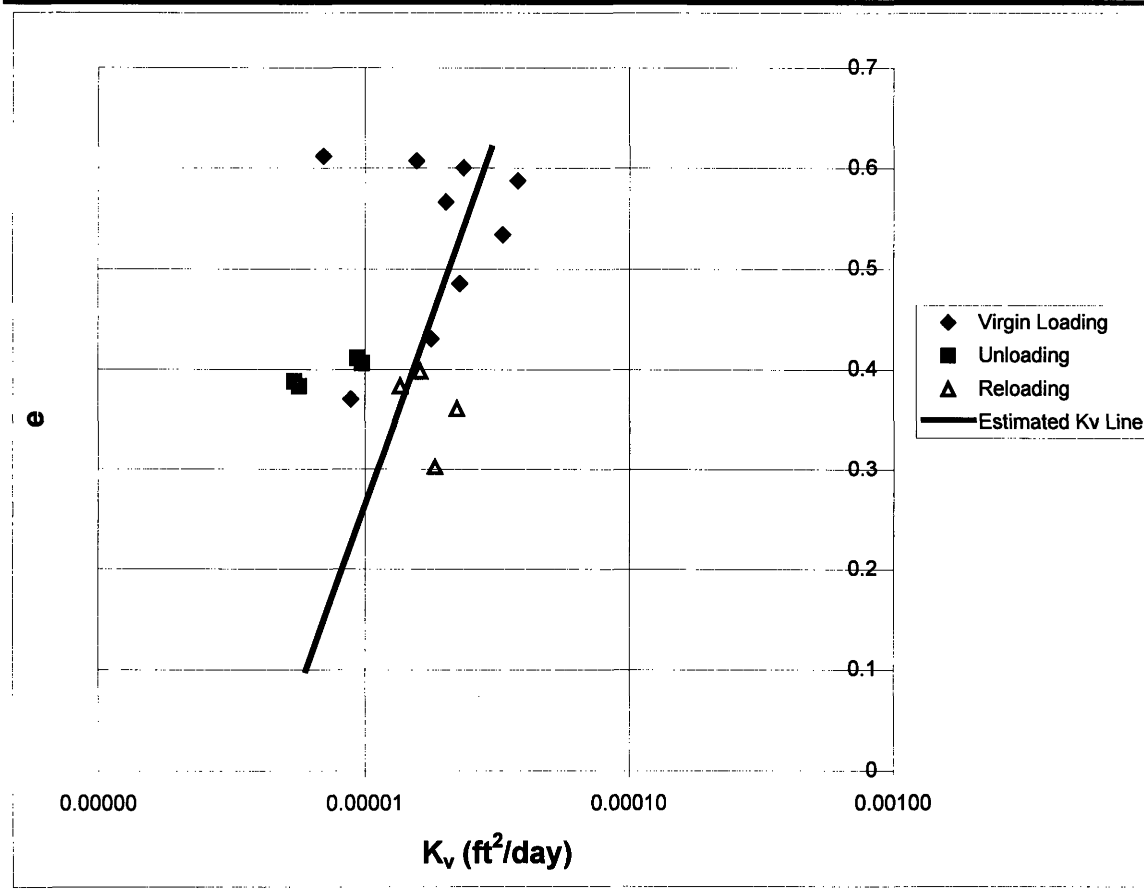

Sample 26 e_o: **0.65** **Depth: 57ft**

Load	Load	ε_{vert}	$\Delta\varepsilon_{vert}$	e	C_v	C_v	m_v	k_v
(t/ft^2)	(k/ft^2)	(%)	(%)		$*10^{-4}cm^2/s$	ft^2/day	(ft^2/k)	(ft/day)
0.0625	0.125	0.7	0.7	0.63845	3	0.028	0.056	9.75E-05
0.125	0.25	1.2	0.5	0.6302	6.96	0.065	0.040	1.62E-04
0.25	0.5	1.7	0.5	0.62195	3.68	0.034	0.020	4.27E-05
0.5	1	2.9	1.2	0.60215	1.3	0.012	0.024	1.81E-05
1	2	4.5	1.6	0.57575	4.45	0.041	0.016	4.13E-05
2	4	6.8	2.3	0.5378	4.34	0.040	0.012	2.90E-05
4	8	9.9	3.1	0.48665	5.65	0.053	0.008	2.54E-05
8	16	13.2	3.3	0.4322	7.2	0.067	0.004	1.72E-05
16	32	16.5	3.3	0.37775	12.9	0.120	0.002	1.54E-05
4	8	15.7	-0.8	0.39095	24.9	0.232	0.000	4.82E-06
1	2	14.3	-1.4	0.41405	5.86	0.054	0.002	7.93E-06
0.5	1	\	\	\	\	\	\	\
1	2	\	\	\	\	\	\	\
2	4	14.6	\	0.4091	15.1	0.140	\	\
4	8	15.2	0.6	0.3992	25.3	0.235	0.002	2.20E-05
8	16	15.9	0.7	0.38765	23.1	0.215	0.001	1.17E-05
16	32	17.1	1.2	0.36785	33.6	0.312	0.001	1.46E-05
32	64	20.3	4.4	0.31505	16.3	0.152	0.001	1.30E-05

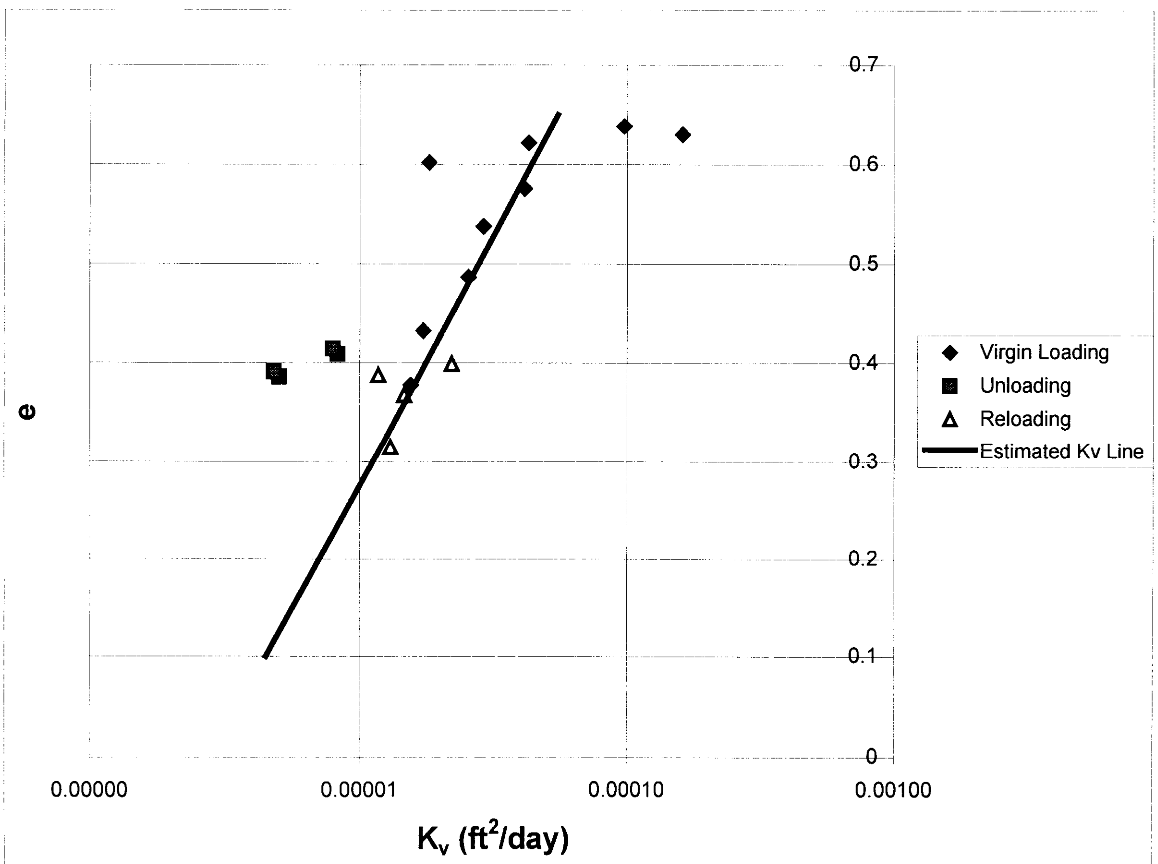

Sample 27 e_o: **0.61** **Depth: 59.5ft**

Load (t/ft^2)	Load (k/ft^2)	ε_{vert} (%)	$\Delta\varepsilon_{vert}$ (%)	e	C_v $*10^{-4}cm^2/s$	C_v ft^2/day	m_v (ft^2/k)	k_v (ft/day)
0.0625	0.125							
0.125	0.25	0.7	0.7	0.59873	3.04	0.028	0.056	9.88E-05
0.25	0.5	1.2	0.5	0.59068	2.38	0.022	0.020	2.76E-05
0.5	1	2.1	0.9	0.57619	5.35	0.050	0.018	5.59E-05
1	2	3.4	1.3	0.55526	5.34	0.050	0.013	4.03E-05
2	4	5.1	1.7	0.52789	5.42	0.050	0.009	2.67E-05
4	8	7.5	2.4	0.48925	4.91	0.046	0.006	1.71E-05
8	16	10.5	3	0.44095	7.1	0.066	0.004	1.55E-05
16	32	13.8	3.3	0.38782	8.59	0.080	0.002	1.03E-05
32	64	17.2	3.4	0.33308	10.2	0.095	0.001	6.29E-06
8	16	16.1	-1.1	0.35079	17.8	0.166	0.000	2.37E-06
2	4	14.2	-1.9	0.38138	5.07	0.047	0.002	4.66E-06
4	8	14.6	0.4	0.37494	15.9	0.148	0.001	9.23E-06
8	16	15.4	0.8	0.36206	14.9	0.139	0.001	8.65E-06
16	32	16	0.6	0.3524	23.5	0.219	0.000	5.11E-06
32	64	18	2	0.3202	23.8	0.221	0.001	8.63E-06
64	128	21.1	3.1	0.27029	16.7	0.155	0.000	4.69E-06

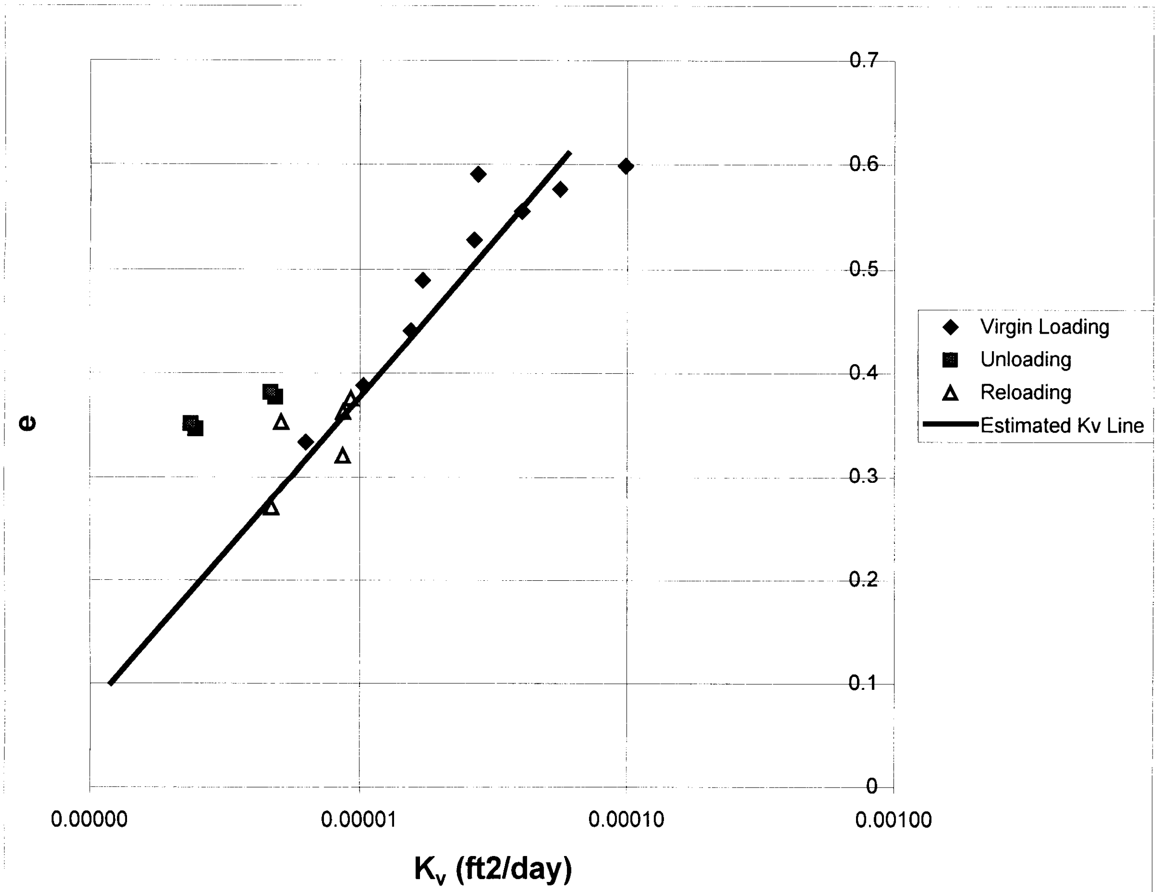

Sample 28 e_o: **0.64** **Depth: 62ft**

Load	Load	ε_{vert}	$\Delta\varepsilon_{vert}$	e	C_v	C_v	m_v	k_v
(t/ft^2)	(k/ft^2)	(%)	(%)		$*10^{-4}cm^2/s$	ft^2/day	(ft^2/k)	(ft/day)
0.0625	0.125	0						
0.125	0.25	0.7	0.7	0.62852	10.2	0.095	0.056	3.31E-04
0.25	0.5	1.2	0.5	0.62032	\	\	0.020	\
0.5	1	2.2	1	0.60392	6.63	0.062	0.020	7.70E-05
1	2	3.7	1.5	0.57932	17.7	0.165	0.015	1.54E-04
2	4	5.9	2.2	0.54324	5.97	0.056	0.011	3.81E-05
4	8	9	3.1	0.4924	6.57	0.061	0.008	2.95E-05
8	16	12.6	3.6	0.43336	8.01	0.074	0.005	2.09E-05
16	32	16	3.4	0.3776	12.5	0.116	0.002	1.54E-05
32	64	20	4	0.312	13.8	0.128	0.001	1.00E-05
8	16	18.1	-1.9	0.34316	24.9	0.232	0.000	5.72E-06
2	4	17.1	-1	0.35956	5.58	0.052	0.001	2.70E-06
4	8	17.4	0.3	0.35464	15.6	0.145	0.001	6.79E-06
8	16	18.2	0.8	0.34152	19.6	0.182	0.001	1.14E-05
16	32	19.2	1	0.32512	24.9	0.232	0.001	9.03E-06
32	64	20.7	1.5	0.30052	28.9	0.269	0.000	7.86E-06
64	128	24	3.3	0.2464	17.6	0.164	0.001	5.27E-06

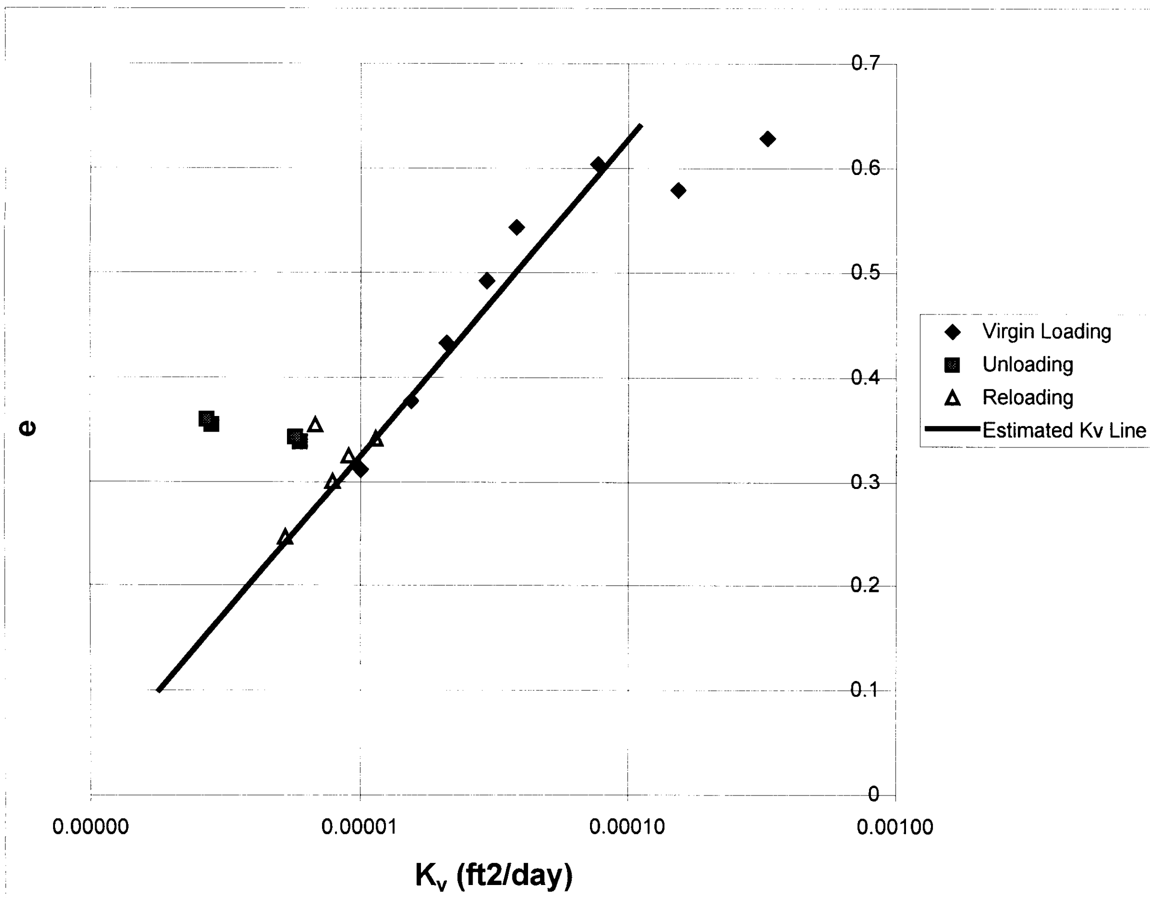

Sample 29 e_o: **0.63** **Depth: 64.5ft**

Load	Load	ε_{vert}	$\Delta\varepsilon_{vert}$	e	C_v	C_v	m_v	k_v
(t/ft^2)	(k/ft^2)	(%)	(%)		$*10^{-4}cm^2/s$	ft^2/day	(ft^2/k)	(ft/day)
0.0625	0.125	0						
0.125	0.25	0.7	0.7	0.61859	3.75	0.035	0.056	1.22E-04
0.25	0.5	1.3	0.6	0.60881	1.48	0.014	0.024	2.06E-05
0.5	1	2.3	1	0.59251	3.12	0.029	0.020	3.62E-05
1	2	3.7	1.4	0.56969	4.83	0.045	0.014	3.92E-05
2	4	5.5	1.8	0.54035	4.88	0.045	0.009	2.55E-05
4	8	8	2.5	0.4996	5.54	0.052	0.006	2.01E-05
8	16	10.9	2.9	0.45233	7.04	0.065	0.004	1.48E-05
16	32	14.1	3.2	0.40017	10	0.093	0.002	1.16E-05
32	64	17.6	3.5	0.34312	13.6	0.126	0.001	8.63E-06
8	16	16.3	-1.3	0.36431	24.2	0.225	0.000	3.80E-06
2	4	14.4	-1.9	0.39528	5.95	0.055	0.002	5.47E-06
4	8	14.8	0.4	0.38876	23.7	0.220	0.001	1.38E-05
8	16	15.6	0.8	0.37572	14.2	0.132	0.001	8.24E-06
16	32	16.7	1.1	0.35779	26.5	0.246	0.001	1.06E-05
32	64	18.3	1.6	0.33171	31.4	0.292	0.001	9.11E-06
64	128	21.3	3	0.28281	19.1	0.178	0.000	5.20E-06

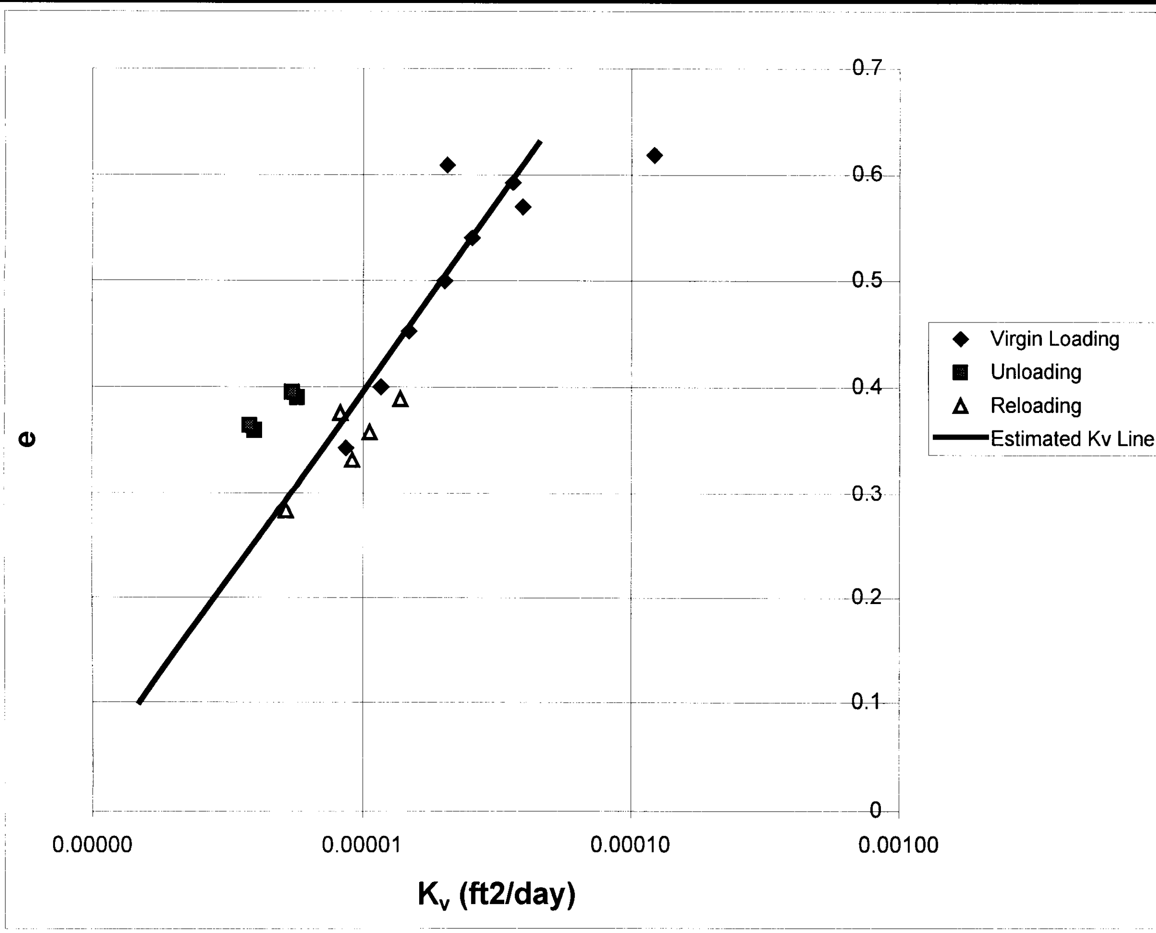

Sample 30 **e_o: 0.42** **Depth: 67ft**

Load	Load	ε_{vert}	$\Delta\varepsilon_{vert}$	e	C_v	C_v	m_v	k_v
(t/ft^2)	(k/ft^2)	(%)	(%)		$*10^{-4}cm^2/s$	ft^2/day	(ft^2/k)	(ft/day)
0.0625	0.125	0						
0.125	0.25	1.6	1.6	0.39728	2.19	0.020	0.128	1.63E-04
0.25	0.5	2.2	0.6	0.38876	1.82	0.017	0.024	2.53E-05
0.5	1	3.1	0.9	0.37598	2.7	0.025	0.018	2.82E-05
1	2	4.1	1	0.36178	6.38	0.059	0.010	3.70E-05
2	4	5.6	1.5	0.34048	5.82	0.054	0.008	2.53E-05
4	8	7.4	1.8	0.31492	6.54	0.061	0.005	1.71E-05
8	16	9.4	2	0.28652	11.1	0.103	0.003	1.61E-05
16	32	11.8	2.4	0.25244	26.4	0.246	0.002	2.30E-05
32	64	14.3	2.5	0.21694	20.2	0.188	0.001	9.16E-06
8	16	13.6	-0.7	0.22688	24.3	0.226	0.000	2.06E-06
2	4	12.4	-1.2	0.24392	6.47	0.060	0.001	3.75E-06
4	8	12.6	0.2	0.24108	19.4	0.180	0.000	5.63E-06
8	16	13.1	0.5	0.23398	25.3	0.235	0.001	9.18E-06
16	32	13.8	0.7	0.22404	42.5	0.395	0.000	1.08E-05
32	64	14.8	1	0.20984	39.6	0.368	0.000	7.18E-06
64	128	17.3	2.5	0.17434	17.6	0.164	0.000	3.99E-06

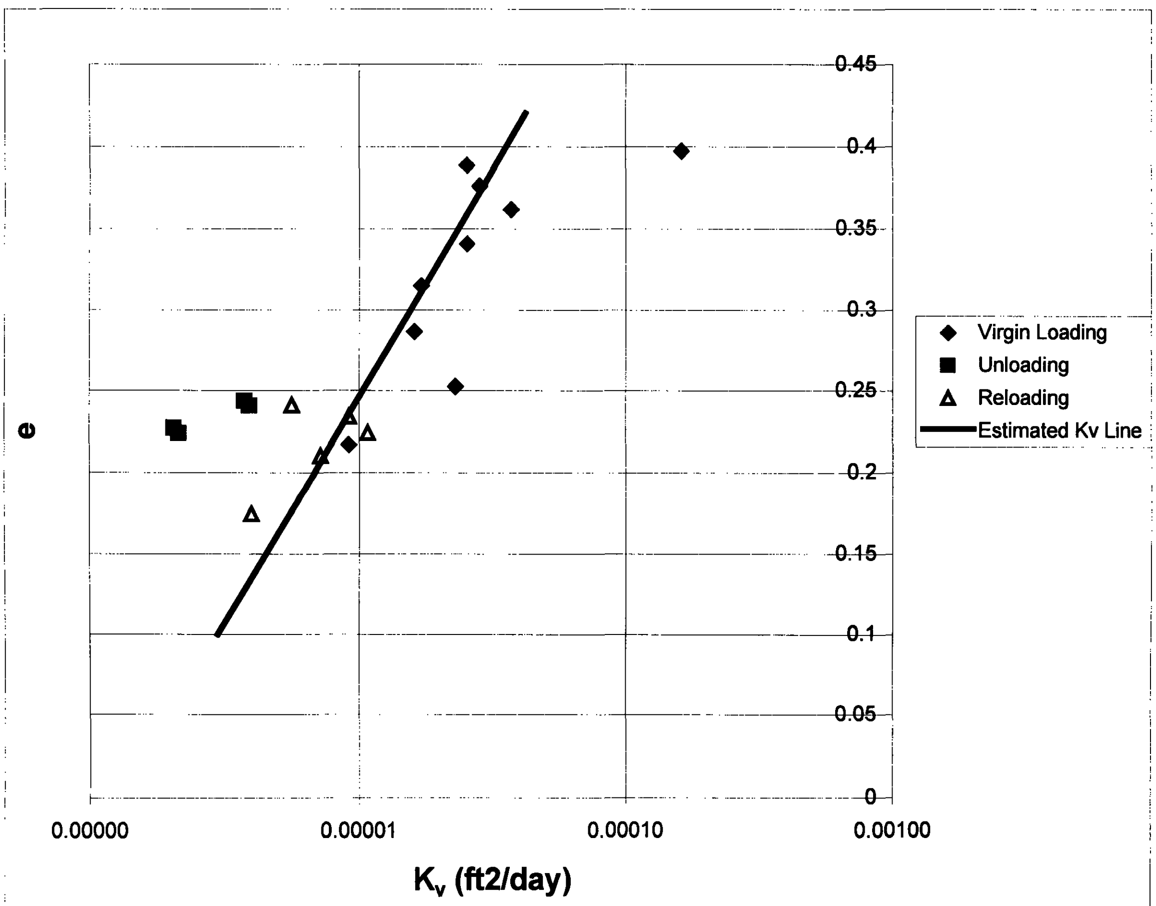

Performed by Woodward Clyde Consultants

Hammer: Automatic Trip Hammer (assume UK Pilcon)
Weight: 140 lb
Casing: 4 inch
Falling: 30 inch

$Depth_{MID}$ (ft)	$\sigma'_{v\,AVG}$ (ksf)	N	C_N (Skempton)	C_{ER}	C_{RL}	C_S	C_B	N_1	N_{60}	$N_{1\,60}$	Dr (fine sand)	ϕ' (DM7)	ϕ' (Sch, 1978)	ϕ' (De Mello)	ϕ' (Peck)	ϕ'_{AVG}
6	0.714	25	1.47	1.00	0.75	1.20	1.00	36.85	22.50	33.16	0.78	34	39	40	37	37.5
11	1.309	10	1.21	1.00	0.75	1.20	1.00	12.09	9.00	10.88	0.44	34	35.5	36	30.5	34
16	1.7038	30	1.08	1.00	0.85	1.20	1.00	32.40	30.60	33.05	0.78	34	39	40	37	37.5
21	1.9868	22	1.00	1.00	0.95	1.20	1.00	22.07	25.08	25.16	0.68	34	38.5	40	34.5	36.75
										Dr_{Avg}	**0.67**				$\phi'_{T\,AVG}$	36.4

Performed by STS Consultants Ltd.

Hammer: Automatic Safety Hammer (assume Standard Sampler)
Weight: 140 lb
Falling: 30 inch

$Depth_{MID}$ (ft)	$\sigma'_{v\,AVG}$ (ksf)	N	C_N (Skempton)	C_{ER}	C_{RL}	C_S	C_B	N_1	N_{60}	$N_{1\,60}$	Dr (fine sand)	ϕ' (DM7)	ϕ' (Sch, 1978)	ϕ' (De Mello)	ϕ' (Peck)	ϕ'_{AVG}
0.5	0.0595	18	1.94	0.90	0.75	1.00	1.00	34.96	12.15	23.60	0.66	34	38.5	40	33.5	36.5
2.5	0.2975	64	1.74	0.90	0.75	1.00	1.00	111.43	43.20	75.21	1.00	34	42.5	36	41	38.375
5.5	0.6545	49	1.51	0.90	0.75	1.00	1.00	73.84	33.08	49.84	0.95	34	42	40	41	39.25
8	0.952	29	1.36	0.90	0.75	1.00	1.00	39.30	19.58	26.52	0.69	34	39	40	35	37
10.5	1.2495	30	1.23	0.90	0.75	1.00	1.00	36.93	20.25	24.93	0.67	34	38.5	40	34.5	36.75
13	1.534	66	1.13	0.90	0.75	1.00	1.00	74.70	44.55	50.42	0.96	34	42	40	41	39.25
15.5	1.6755	72	1.09	0.90	0.85	1.00	1.00	78.36	55.08	59.94	1.00	34	42.5	40	41	39.375
18	1.817	52	1.05	0.90	0.85	1.00	1.00	54.49	39.78	41.69	0.87	34	41	40	39	38.5
20.5	1.9585	59	1.01	0.90	0.95	1.00	1.00	59.62	50.45	50.97	0.96	34	42	40	41	39.25
23	2.1	17	0.98	0.90	0.95	1.00	1.00	16.59	14.54	14.18	0.51	34	36	36	31.5	34.375
										Dr_{Avg}	**0.83**				$\phi'_{T\,AVG}$	37.9
															ϕ'_{design}	**37**

Appendix C

Pile Design Analysis for NGES at Northwestern University

Side Friction in Sand		
ϕ'_{Design}:	37	(degree)
Dr_{Design}:	75	(%)

Pipe Pile				H Pile 14*73					
Diameter	Length	Thickness	$E_{eq.}$	$Diameter_{eq}$	Length	T. Tip Area	width	depth	$E_{eq.}$
(ft)	(ft)	(ft)	(ksf)	(ft)	(ft)	(ft^2)	(ft)	(ft)	(ksf)
1.50	50.00	0.03	358333	1.50	50.00	0.15	1.22	1.13	363783

Poulos & Davis									
								Pipe or H pile	
Driven		Depth	$K_s\tan\delta'$	d/B	σ'_{vs}	fs	L	Area	Q_{sf}
ϕ'^*	d_c/B	(ft)			(ksf)	(ksf)	(ft)	(ft^2)	(kip)
(degree)		2.50	1.20	1.67	0.30	0.36	5.00	23.56	8.41
37.75	7.50	7.50	1.20	5.00	0.89	1.07	5.00	23.56	25.23
		12.50	1.20	8.33	1.34	1.61	5.00	23.56	37.85
		17.50	1.20	11.67	1.34	1.61	5.00	23.56	37.85
		21.50	1.20	14.33	1.34	1.61	3.00	14.14	22.71
								$Q_{sf\ subtotal}$	**132.06**

Design Curves (Vesic, 1970; Tomlinson, 1973)					
			Pipe or H pile		
Dr		fs	L	Area	Q_{sf}
(%)		(ksf)	(ft)	(ft_2)	**(kip)**
75.00		0.90	23.00	108.38	**97.55**

Skin Friction in Clay		
ϕ':	28	(degree)

Depth	σ'_{vo}	Su	PI	μ	$Su_{corrected}$	α	α	α	α	L_{embed}	β	β
(ft)	(ksf)	(ksf)	(%)		(ksf)	(Tomlinson)	(API)	(Peck)	(D&O, 1983	(ft)	(Meyerhof)	(Burland)
29.5	2.47	0.66	10	1.15	0.76	1	0.95	0.85	0.9	6.5	0.36	0.27
34.4	2.78	0.41	20	1.00	0.41	1	1	0.9	1	11.4	0.355	0.27
37.7	2.98	0.33	23	0.97	0.32	1	1	0.92	1	14.7	0.35	0.27
41	3.17	0.37	18	1.02	0.38	1	1	0.9	1	18	0.345	0.27
44.3	3.36	0.4	16	1.05	0.42	1	1	0.9	1	21.3	0.34	0.27
47.6	3.58	0.41	18	1.02	0.42	1	1	0.9	1	24.6	0.33	0.27
50.8	3.79	0.38	20	1.00	0.38	1	1	0.9	1	27.8	0.325	0.27

Depth	L	Area	α_{Avg}	fs	Q_{fs}	β_{AVG}	fs	Q_{fs}
Pipe or H pile				α Method	α Method		β Method	β Method
(ft)	(ft)	(ft^2)		(ksf)	(kip)		(ksf)	(kip)
29.5	6.5	30.63	0.93	0.70	21.51	0.32	0.78	23.87
34.4	4.9	23.09	0.98	0.40	9.23	0.31	0.87	20.07
37.7	3.3	15.55	0.98	0.31	4.88	0.31	0.92	14.36
41	3.3	15.55	0.98	0.37	5.74	0.31	0.98	15.17
44.3	3.3	15.55	0.98	0.41	6.36	0.31	1.03	15.95
47.6	3.3	15.55	0.98	0.41	6.36	0.30	1.07	16.71
50.8	2.4	11.31	0.98	0.37	4.19	0.30	1.13	12.76
				$Q_{fs\ tot\ \alpha}$	**58.27**		$Q_{fs\ tot\ \beta}$	**118.91**

	$Q_{fs\ low}$	$Q_{fs\ avg}$	$Q_{fs\ high}$
	(kip)	(kip)	(kip)
sand	97.55	114.80	132.06
clay	58.27	88.59	118.91
Total	155.81	203.39	250.97

Side Friction in Sand		
$\phi'_{Design:}$	37	(degree)
$Dr_{Design:}$	75	(%)

Drilled Pier		
Diameter (ft)	Length (ft)	E (ksf)
1.50	50.00	720000

Poulos & Davis

Drilled		Depth	$K_s\tan\delta'$	d/B	σ'_{vs}	fs	L	Pipe or H pile Area	Q_{sf}
ϕ'^*	d_c/B	(ft)			(ksf)	(ksf)	(ft)	(ft^2)	(kip)
(degree)		2.50	0.40	1.67	0.30	0.12	5.00	23.56	2.80
34.00	6.30	7.50	0.40	5.00	0.89	0.36	5.00	23.56	8.41
		12.50	0.40	8.33	1.12	0.45	5.00	23.56	10.60
		17.50	0.40	11.67	1.12	0.45	5.00	23.56	10.60
		21.50	0.40	14.33	1.12	0.45	3.00	14.14	6.36
								$Q_{sf\ subtotal}$	**38.77**

Design Curves
(Vesic, 1970; Tomlinson, 1973)

Dr		fs	L	Buried Pile Area	Q_{sf}
(%)		(ksf)	(ft)	(ft_2)	**(kip)**
75.00		0.50	23.00	108.38	**54.19**

Skin Friction in Clay		
ϕ':	28	(degree)
$L_{total\ Embed}$:	27	(ft)

Depth	σ'_{vo}	β_{AVG}	Depth	L	Area	β_{AVG}	fs	Q_{fs}
(ft)	(ksf)	(K&J)	Drilled Pile				β Method	β Method
			(ft)	(ft)	(ft^2)		(ksf)	(kip)
29.5	2.47	0.82	29.5	6.5	30.63	0.82	2.03	62.15
34.4	2.78	0.82	34.4	4.9	23.09	0.82	2.28	52.68
37.7	2.98	0.82	37.7	3.3	15.55	0.82	2.44	38.00
41	3.17	0.82	41	3.3	15.55	0.82	2.60	40.47
44.3	3.36	0.82	44.3	3.3	15.55	0.82	2.76	42.89
47.6	3.58	0.82	47.6	3.3	15.55	0.82	2.94	45.68
50.8	3.79	0.82	50.8	2.4	11.31	0.82	3.11	35.16
							$Q_{fs\ tot\ \beta}$	**317.01**

	$Q_{fs\ low}$ (kip)	$Q_{fs\ avg}$ (kip)	$Q_{fs\ high}$ (kip)
sand	38.77	46.48	54.19
clay	317.01	317.01	317.01
Total	355.79	363.50	371.21

		Double Layers Analysis																	
	L_{emb}	QT	ro	L_{sand}	L_{clay}	G_o	G_1	G_2	G_L	ξ_1	ξ_2	λ_1	λ_2	μL_1	μL_2	Qb1	w_{sand}	w_{clay}	w_{total}
	(ft)	(kip)	(ft)	(ft)	(ft)	(ksf)	(ksf)	(ksf)	(ksf)							(kip)	(in)	(in)	(in)
18" Pipe Pile	50	0	0.75	23.0	27.0	717	717	34	34	6.48	3.81	500	10539	0.76	0.25	0.00	0.000	0.000	0.000
	50	50	0.75	23.0	27.0	717	717	34	34	6.48	3.81	500	10539	0.76	0.25	0.57	0.022	0.004	0.026
	50	100	0.75	23.0	27.0	717	717	34	34	6.48	3.81	500	10539	0.76	0.25	1.14	0.044	0.008	0.052
	50	150	0.75	23.0	27.0	717	717	34	34	6.48	3.81	500	10539	0.76	0.25	1.72	0.065	0.012	0.078
	50	200	0.75	23.0	27.0	717	717	34	34	6.48	3.81	500	10539	0.76	0.25	2.29	0.087	0.016	0.103
	50	250	0.75	23.0	27.0	717	717	34	34	6.48	3.81	500	10539	0.76	0.25	2.86	0.109	0.021	0.129
	50	300	0.75	23.0	27.0	717	717	34	34	6.48	3.81	500	10539	0.76	0.25	3.43	0.131	0.025	0.155

		Double Layers Analysis																	
	L_{emb}	QT	ro	L_{sand}	L_{clay}	G_o	G_1	G_2	G_L	ξ_1	ξ_2	λ_1	λ_2	μL_1	μL_2	Qb1	w_{sand}	w_{clay}	w_{total}
	(ft)	(kip)	(ft)	(ft)	(ft)	(ksf)	(ksf)	(ksf)	(ksf)							(kip)	(in)	(in)	(in)
14*73 H Pile	50	0	0.75	23.0	27.0	717	717	34	34	6.48	3.81	507	10699	0.76	0.25	0.00	0.000	0.000	0.000
	50	25	0.75	23.0	27.0	717	717	34	34	6.48	3.81	507	10699	0.76	0.25	0.29	0.011	0.002	0.013
	50	75	0.75	23.0	27.0	717	717	34	34	6.48	3.81	507	10699	0.76	0.25	0.86	0.032	0.006	0.038
	50	125	0.75	23.0	27.0	717	717	34	34	6.48	3.81	507	10699	0.76	0.25	1.43	0.054	0.010	0.064
	50	175	0.75	23.0	27.0	717	717	34	34	6.48	3.81	507	10699	0.76	0.25	2.00	0.075	0.014	0.090
	50	225	0.75	23.0	27.0	717	717	34	34	6.48	3.81	507	10699	0.76	0.25	2.58	0.097	0.018	0.115
	50	275	0.75	23.0	27.0	717	717	34	34	6.48	3.81	507	10699	0.76	0.25	3.15	0.118	0.023	0.141

		Double Layers Analysis																	
	L_{emb}	QT	ro	L_{sand}	L_{clay}	G_o	G_1	G_2	G_L	ξ_1	ξ_2	λ_1	λ_2	μL_1	μL_2	Qb1	w_{sand}	w_{clay}	w_{total}
	(ft)	(kip)	(ft)	(ft)	(ft)	(ksf)	(ksf)	(ksf)	(ksf)							(kip)	(in)	(in)	(in)
18" Bored Pile (cased or slurry)	50	0	0.75	23.0	27.0	860	717	34	34	6.60	3.81	1004	21176	0.53	0.18	0.00	0.000	0.000	0.000
	50	50	0.75	23.0	27.0	860	717	34	34	6.60	3.81	1004	21176	0.53	0.18	0.56	0.014	0.004	0.018
	50	100	0.75	23.0	27.0	860	717	34	34	6.60	3.81	1004	21176	0.53	0.18	1.11	0.028	0.008	0.036
	50	150	0.75	23.0	27.0	860	717	34	34	6.60	3.81	1004	21176	0.53	0.18	1.67	0.042	0.012	0.054
	50	200	0.75	23.0	27.0	860	717	34	34	6.60	3.81	1004	21176	0.53	0.18	2.23	0.056	0.016	0.072
	50	250	0.75	23.0	27.0	860	717	34	34	6.60	3.81	1004	21176	0.53	0.18	2.78	0.070	0.020	0.090
	50	300	0.75	23.0	27.0	860	717	34	34	6.60	3.81	1004	21176	0.53	0.18	3.34	0.085	0.024	0.108
	50	350	0.75	23.0	27.0	860	717	34	34	6.60	3.81	1004	21176	0.53	0.18	3.90	0.099	0.028	0.126